Università degli Studi di Ferrara

DOTTORATO DI RICERCA IN
SCIENZE BIOMEDICHE

CICLO XXVII

COORDINATORE Prof. Capitani Silvano

Electrophysiological analysis of voltage-dependent currents in two types of periglomerular cells in the mouse olfactory bulb

Settore Scientifico Disciplinare BIO/09

Dottorando
Dott. Fogli Iseppe Alex

Tutore
Prof. Belluzzi Ottorino

Anni 2012/2014

Table of contents

INTRODUCTION

From the beginning, every life form necessitates to process information from the external environment in order to survive. For this purpose, chemical senses arose and, in the course of time, developed to be able to identify a very large range of different chemical molecules.

Olfaction is probably the most ancient member belonging to this group of senses. Its aim is to acquire the greatest number possible of data about the quantity and quality of external chemicals, termed odorants. Consequently, a great number of physiological responses can be elicited. Olfactory stimuli are involved in universal basic functions like feeding and reproduction. In addition, social behaviors, as clan or mother-infant recognition, are also influenced by sense of smell. Nonetheless, most of its fundamental processes are still unknown.

In mammals, the processing of olfactory information can be distinguished in a precise sequence of events occurring in distinct anatomical regions (Figure 1A).

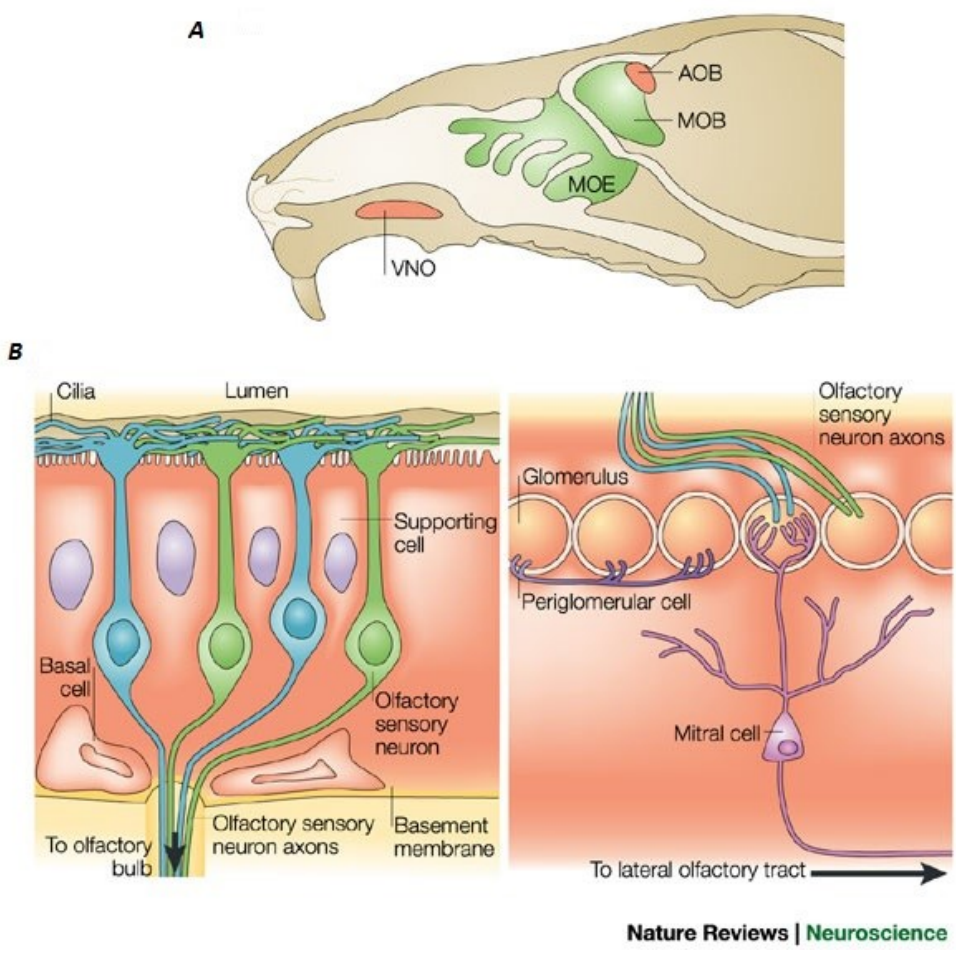

Figure 1 Mammalian olfactory system. A: Schematic representation of mouse head. From the main olfactory epithelium (MOE), axonal fibers of olfactory sensory neurons project to the main olfactory bulb (MOB). In addition, the vomeronasal organ (VNO) and the accessory olfactory bulb (AOB) are shown. B: Cross-section of the main olfactory epithelium on the left, and cross-section of the peripheral part of the main olfactory bulb on the right. Image adapted from (Mombaerts, 2004).

Initially, volatile odorants enter in the nasal cavity, which is lined in part by a layer of cells termed olfactory epithelium (Figure 1B). Within this layer, olfactory sensory neurons (OSNs) are responsible for the first phase of the transduction process. Neurons belonging to this class are bipolar cells with a long unmyelinated axon at its basal pole. On the contrary, at the apical surface is located a characteristic structure. This process consists of a unique dendrite generating a rounded prominence with microvilli. These elements, termed olfactory cilia, are submerged in a layer of mucus; interestingly, in the mucus are contained some odorant binding proteins or OBPs, which help hydrophobic odorants to pass through this fluid (Bignetti et al., 1985).

Odorant receptors, belonging to the G-protein-linked receptor class, represent the key player of this very versatile sensor system. Since their molecular cloning in 1991 (Buck and Axel, 1991), more than 1000 genes encoding for odorant receptors has been discovered, making their family the largest in the mammalian genome (Young et al., 2002; Zhang and Firestein, 2002). Moreover, odorant receptors have been identified in a great number of species, underlying their important role in survival. Interestingly, the percentage of functional genes in primates seems to decrease from monkey to hominoids. The reduction of olfactory abilities has been suggested to be related with this observation (Niimura and Nei, 2003, 2005, 2007).

The olfactory transduction starts when the binding between the odorant and the specific receptor (direct or OBP-mediated) occurs, activating a particular heterotrimeric G-proteins (G_{olf}) expressed by the receptor. This, in turn, induce a rise of cyclic adenosine monophosphate (cAMP) intracellular concentration by stimulation of type III adenylate cyclase. This event leads to the opening of cyclic nucleotide-gated (CNG) channels, which activate others membrane proteins and depolarize the apical region of the OSN. The membrane depolarization proceeds along apical dendrite and soma of the neuron and, when reaches the trigger zone of the axon in the basal pole, originates an action potential transmitted to the olfactory bulb (OB) (Firestein, 2001; Ronnett and Moon, 2002). This cascade was considered the only one acting in OSNs for long time. However, recent studies demonstrated that some minor pathways, involving different second messengers, are involved in the regulation of the main process mentioned above (Schild and Restrepo, 1998; Elsaesser et al., 2005; Liberles and Buck, 2006; Lin et al., 2007).

OSN axons leaving the olfactory epithelium gather to generate several fascicles, which in turn originate the olfactory nerve (ON). Axonal bundles are kept together by the ensheathing cells, a glial subpopulation probably involved in the synchronization of the olfactory transmission (Bokil et al., 2001). The bundles of the ON passes through the cribriform plate and contacts the ipsilateral olfactory bulb (Figure 1B). Synapsis between axonal terminals of the nerve and dendrites of bulbar neurons take place in spheroidal structures termed glomeruli. Interestingly, OSNs sharing the same odorant receptor converge on a specific pair of glomeruli in each bulb (Mombaerts, 1996, 1999), but each glomerulus reacts to different olfactory stimuli. This evidence endorses the thesis

of a peculiar glomerular pattern activation in response to the odorant detection in the olfactory epithelium. How the glomerular segregation occurs is still not completely understood, but it has been demonstrated that, unlike other sensory system, a spatial correlation between sensory neuron location in the olfactory epithelium and glomerulus position is absent (Yu et al., 2004a; Sakano, 2010; Mori and Sakano, 2011; Takeuchi and Sakano, 2014).

Axonal terminals of the OSNs contacts primary dendrites of mitral cells inside the glomeruli. This neuronal population represents the first projection neurons of the olfactory bulb. In addition, two different modulatory circuits have been identified in the OB. The former involves principally juxtaglomerular cells, which extend their processes in the glomeruli and synapse the mitral cells. The latter consists of granular cells, which create dendro-dendritic connections with mitral cells in the external plexiform layer. A second class of output neurons is composed by the tufted cells, located in different areas of the OB depending on their subtype.

Finally, axons of mitral cells and tufted cells leave the OB and merge to create the olfactory tracts. This bundle relays to the higher-order brain regions (olfactory tubercle, amygdala, entorhinal cortex, piriform cortex and, later, hippocampus, thalamus, hypothalamus, and orbitofrontal cortex), where all the physiological responses to odorant stimuli arise (Shipley and Ennis, 1996). Interestingly, olfaction is the only sensory system that does not project to neocortex directly through the thalamus. On the contrary, output neurons send their axons to the piriform cortex (belonging to the three-layered archicortex), which is considered a specific processing region of the olfactory signals (Purves, 2004).

Olfactory Bulb

Structure

Since Ramon y Cajal's pioneering anatomical descriptions (Ramon y Cajal, 1890, 1901, 1911), the anatomical structure of the main olfactory bulb can be described as a sequence of six concentric cell layers: olfactory nerve layer, glomerular layer, external plexiform layer, mitral cell layer, internal plexiform layer, and granule cell layer (Figure 2). Their properties are briefly illustrated below (for a complete review see Kosaka and Kosaka, 2009).

The most external layer is the olfactory nerve layer (ONL), composed by axonal fibers of the olfactory sensory neurons located in the olfactory epithelium. In addition, in this layer it is possible to identify ensheathing cells that keep together the axons.

The following layer is the glomerular layer (GL), which takes the name from the structure where the contact between OSN axonal terminals and apical dendrites of mitral cells occurs (Pinching and Powell, 1971a, 1971c; Kosaka et al., 1998; Kosaka and Kosaka, 2005). Furthermore, also neuronal processes of three types of interneurons contribute to generate the glomerular structure: periglomerular (PG) cells, external tufted (ET) cells and superficial short-axon (SSA) cells. These neurons are generally termed together as juxtaglomerular cells and are responsible for the glomerular microcircuit.

In the external plexiform layer (EPL) are located the middle and the deep tufted (MT and DT, respectively), which originate dendro-dendritic synapses with granular cells and some of their axons project to the brain (Jackowski et al., 1978; Macrides and Schneider, 1982; Schoenfeld et al., 1985).

Below the EPL resides the mitral cell layer (MCL). This thin layer mainly consists of mitral (M) cells, but also a small amount of deep short-axon (DSA) cells can be detected (Price and Powell, 1970a; Schneider and Macrides, 1978). Mitral cells can be distinguished in two group depending on the different morphology and abundance (Mori et al., 1983; Orona et al., 1984). Type 1 mitral cells represent the majority of mitral cells and extend their long dendrites in the deeper EPL. Conversely, type 2 cells are less numerous and show narrow dendritic processes.

Proceeding inside the olfactory bulb, the next layer is the internal plexiform layer (IPL). This region is occupied by axonal fibers of projection neurons, and only few cell bodies exist (Price and Powell, 1970a; Schneider and Macrides, 1978).

Finally, granule cell layer (GCL) is the innermost one. It takes its name by the granule (Gr) cells, small roundish interneurons without axonal processes (Price and Powell, 1970b, 1970c). Granule cells project their peripheral dendrites in the EPL and contact secondary dendrites of output neurons. Based on the position of their bodies in the GCL and on the arrangement of their

dendritic processes, granule cells can be discriminated in three subtypes (Price and Powell, 1970c; Schneider and Macrides, 1978).

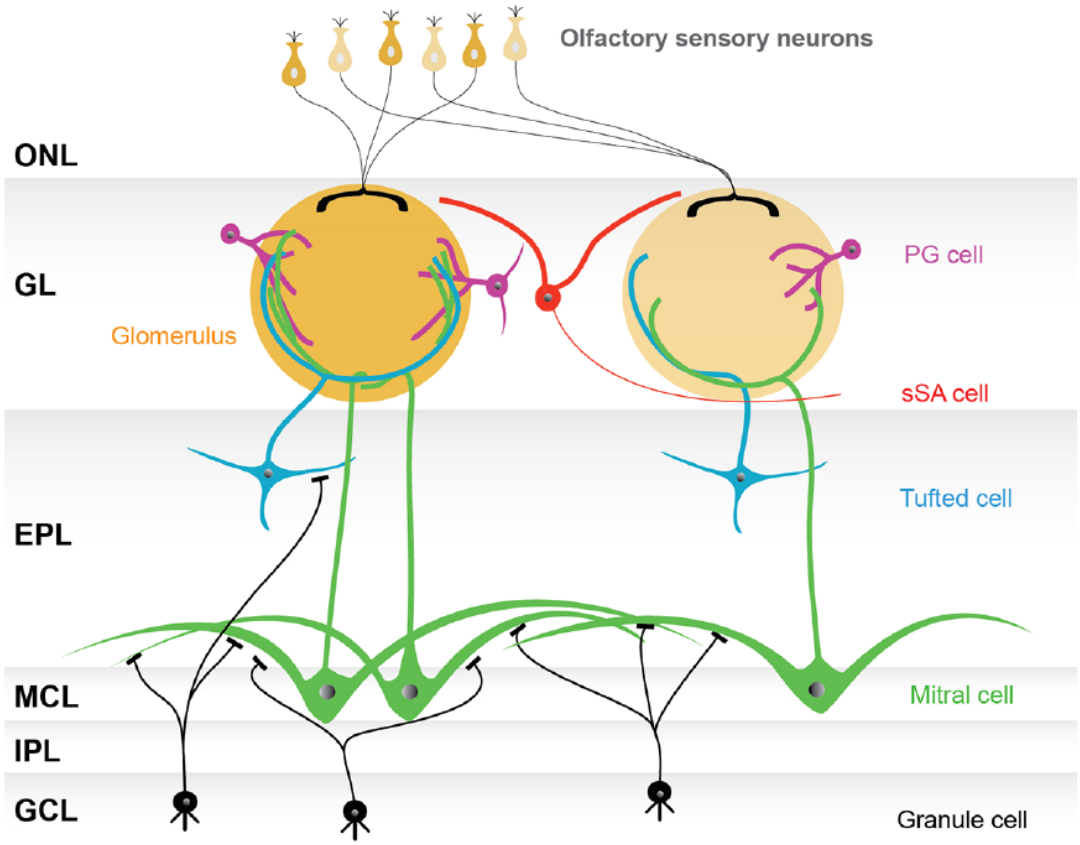

Figure 2 Basic model of the olfactory bulb network. The figure represents the conventional organization of the olfactory bulb network. The olfactory sensory neurons project in the glomerular layer (GL), consisting of spherical structures called glomeruli. Olfactory sensory neurons expressing the same type of odorant receptor converge their axons into only a few glomeruli. Neurons surrounding glomeruli in the GL are called juxtaglomerular cells (JG cells), consisting of three morphologically distinct cell types: periglomerular (PG) cells, external tufted (ET) cells (not shown), and superficial short-axon (sSA) cells. The mitral cells and the tufted cells, sending their axonal fiber to the olfactory cortex, constitute the projection neurons. Mitral cells are located in the mitral cell layer (MCL), while the tufted cells are scattered throughout the EPL. In the glomeruli, both mitral and tufted cells receive synaptic inputs from the axons of OSNs and make reciprocal synapses with the dendrites of PG cells. Secondary dendrites of mitral and tufted cells are arborized in the external plexiform layer (EPL), where reciprocal synapses are generated with granule cell dendrites. The internal plexiform layer (IPL), in which axons from mitral cells and axon collaterals of ET cells run, and the granule cell layer (GCL), which is largely composed of granule cells, both lie beneath the MCL. Granule cells are interneurons extending their dendritic processes apically into the EPL. Abbreviation: ONL, olfactory nerve layer.

Cellular heterogeneity in the glomerulus

The glomerulus represents the first processing center of the olfactory information. Since the beginning, as seen above, this structure was defined as a rough globe surrounded by neuronal and glial cell bodies (Ramon y Cajal, 1911). The inner volume, to the contrary, is a neuropil, originating from dendrites of both projection cells and juxtaglomerular cells and OSN axons. However, new details about its structure arose over the years, highlighting several new traits (Pinching and Powell, 1971b; Schoenfeld et al., 1985; Halász, 1990; Kosaka et al., 1998).

First, juxtaglomerular cells, originally thought as a unique population, could be distinguished on the basis of their properties in three distinct types: periglomerular cells, external tufted cells and superficial short-axon cells. Dendritic processes of PG cells and ET cells extend into the glomeruli; conversely, the dendrites of the last neuronal group are arborized in the GL but avoid entering in the glomerular structure (Kosaka and Kosaka, 2005). Moreover, every class of JG cells show heterogeneity in morphological, chemical, and functional features, and can be separated in additional subtypes (Macrides et al., 1985; Nagayama et al., 2004; Kiyokage et al., 2010; Kosaka and Kosaka, 2011). In particular, PG cells shows a wide range of properties.

Considering the synaptic organization, the intraglomerular space has been divided in two areas: the olfactory nerve zone (ON zone) and the non-olfactory nerve zone (non-ON zone) (Chao et al., 1997; Kosaka et al., 1997; Kasowski et al., 1999). The olfactory nerve, in fact, do not form synapses in every point of the internal glomerular volume, but is confined only in well delimited regions. Processes of bulbar neurons fill the remaining areas. Interestingly, different PG neurons show preferential dendritic projections to ON or non-ON zone (). Whereas type 1 PG cells contact indifferently both intraglomerular compartments, type 2 PG cells generate dendro-dendritic synapses with bulbar neurons, but are not linked to the OSNs (Kosaka et al., 1998).

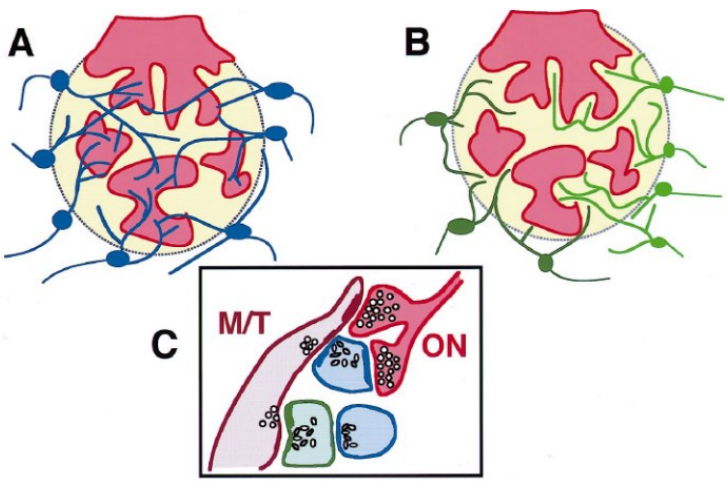

Figure 3 Types 1 and 2 periglomerular cells. A: Type 1 periglomerular cells send their intraglomerular dendrites into both the ON zone (red) and non-ON zone (yellow). B: Type 2 periglomerular cells send their intraglomerular dendrites only into the non-ON zone (yellow). C: Synaptic connections of types 1 and 2 periglomerular cells in the glomerulus. Olfactory nerves (ONs; red) terminate onto mitral/tufted cells (M/Ts; brown) and type 1 periglomerular cells (blue), but not type 2 periglomerular cells (green). Both type 1 (blue) and type 2 (green) periglomerular cells synapse apical dendrites of M/Ts (brown). Image adapted from (Kosaka et al., 1998).

Furthermore, PG cells are different also from the chemical point of view. Considering the high variability of results in literature and the purpose of this work, I will restrict my discussion to murine data. In mouse models, three main chemical markers have been found: tyrosine hydroxylase (TH), calbindin (CB) and calretinin (CR). Since the immunoreactivity for these compounds is largely mutually exclusive, these three cellular subtypes are virtually nonoverlapping (Kosaka and Kosaka, 2007; Parrish-Aungst et al., 2007). Moreover, it has been reported that all the PG cells synthesize γ-amino butyric acid (GABA) and express at least one of the two glutamic acid decarboxylase (GAD) isoforms, with the exception of a small percentage of CR-positive neurons (Kosaka and Kosaka, 2007). Several studies have also tried to calculate how many PG cells belong to the different groups. Results suggest that CR-positive cells are the most abundant, while the CB-positive cells the fewest, but the proportions depend on the method employed (Kosaka and Kosaka, 2007; Panzanelli et al., 2007; Parrish-Aungst et al., 2007; Whitman and Greer, 2007).

In addition, it has been observed that TH-positive cells belong to the type 1 PG cells, since they are directly contact by the olfactory nerve. On the other hand, CR- and CB- positive cells project to the non-ON zone and are classified as type 2 (Kosaka and Kosaka, 2007).

Finally, different PG subtypes have also distinct temporal patterns of neurogenesis during the lifetime. In fact, periglomerular cells, together with granular cells, represents two neuronal population that are produced also in the adult (Altman, 1962, 1969; Hinds, 1968a, 1968b). Addition of CB-positive neurons to the GL is sizable in the neonate and decreases in the course of time. Vice versa, production of CR-positive cells increases in the adult. Experiments on the age-dependent neurogenesis of TH-positive cells produced contrasting data (De Marchis et al., 2007; Batista-Brito et al., 2008; Lledo et al., 2008).

In the following chapters, the attention is focused on TH- and CR-positive PG interneurons, which represent the topic of my thesis.

TH-positive PG cells

In the forebrain, bulbar dopaminergic cells represent the major dopaminergic population (Baker and Farbman, 1993; Cave and Baker, 2009). These neurons are mainly located in the GL (Figure 4), where they represent 10-20% of all JG cells (De Marchis et al., 2007; Kosaka and Kosaka, 2007; Panzanelli et al., 2007; Parrish-Aungst et al., 2007; Whitman and Greer, 2007). The identification of the dopaminergic cells is carried out by the marker TH, a rate-limiting enzyme in the biosynthetic pathway of dopamine (DA) (Nagatsu et al., 1964; Joh et al., 1973). Considering the absence of cells synthesizing other cathecolamines in the OB, all the TH-positive neurons are accounted as dopaminergic cells (Baker et al., 1983).

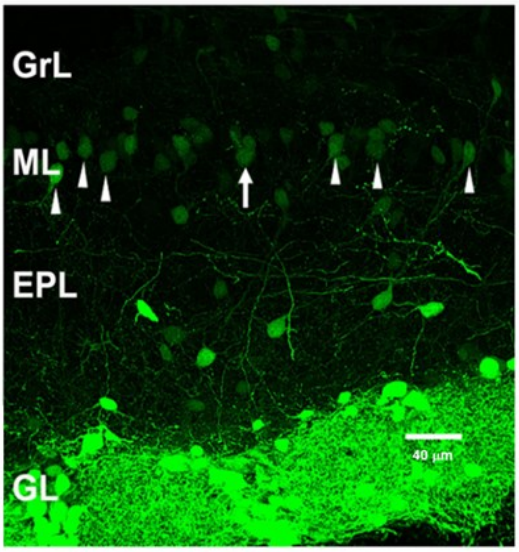

Figure 4 Dopaminergic periglomerular cells. Coronal section of the mouse olfactory bulb with dopaminergic cells expressing the GFP. Arrows indicate some dopaminergic cells faintly positive to the marker in the mitral layer.

With regard to their location and size, dopaminergic cells in the GL can be further grouped in two populations (Baker et al., 1983; Halász, 1990; Pignatelli et al., 2005; Kosaka and Kosaka, 2008), one including small PG cells with a soma diameter ranging from 5 to 10 µm, and another including larger neurons (10-15 µm in diameter), belonging to ET or SSA cell type (Cave and Baker, 2009; Nagayama et al., 2014). Nonetheless, both populations are GABAergic and share the same electrophysiological properties (Pignatelli et al., 2005; Kosaka and Kosaka, 2007).

The first part of this work is focused on the dopaminergic PG cells, which represent the first population. According with their classification as type 1 PG interneurons, these cells receive direct synaptic inputs from the ON and in turn create dendro-dendritic contacts with the projection neurons. This arrangement has several consequences. Firstly, TH-positive PG cells are influenced by the activity of OSNs in both direct and indirect ways. ON terminals, in fact, directly stimulate TH-positive PG cells via glutamate release; in addition, bulbar output neurons, activated by electrical activity coming from olfactory epithelium, stimulate dopaminergic PG interneurons (Ennis et al., 1996, 2001; Aroniadou-Anderjaska et al., 1997).

Dopaminergic PG cells influence the glomerular activity. Indeed, these neurons are able to release both DA and GABA, with several consequences on the activity of other components of glomerular circuits, namely OSNs, mitral cells, and JG cells (Hsia et al., 1999; Berkowicz and Trombley, 2000; Ennis et al., 2001). Interestingly, in the OB, DA release can also alter cellular sensitivity to GABA, underling a peculiar modulatory mechanism (Brünig et al., 1999).

From the electrophysiological point of view, a first description of dopaminergic PG cells has been provided by our group in 2005 (Pignatelli et al., 2005). In this study, the spontaneous activity in the absence of synaptic inputs, common feature of several dopaminergic populations (Grace and Onn, 1989; Hainsworth et al., 1991; Yung et al., 1991; Feigenspan et al., 1998; Neuhoff et al., 2002), has been proved to characterize also the bulbar dopaminergic neurons in GL. Furthermore, five different depolarization-activated conductances have been identified in these cells. A non-inactivating potassium current and a fast transient sodium current represent the two more sizable currents. In addition, one persistent sodium conductance and two different types of calcium conductances (L-type and T-type) have been pharmacologically isolated. Remarkably, only persistent sodium current and T-type calcium current are required to generate the autorhythmicity.

In more recent years two small conductances activated by hyperpolarization have also been described. The former is a fast-activating inward rectifier potassium current blocked by Ba^{2+} (Borin et al., 2014). The characterization of the latter, a mixed-cation conductance sustained by HCN channels important in the determination of the resting membrane potential, and thereby of the cell excitability profile, constitutes the first part of my thesis.

CR-positive PG cells

Calretinin is a very common marker of several neuronal types (Jacobowitz and Winsky, 1991; Miettinen et al., 1992; Resibois and Rogers, 1992; Rogers and Résibois, 1992; Schurmans et al., 1997; Huberman et al., 2008; Barinka and Druga, 2010). This protein, together with parvalbumin, secretagogin, and calbindin, belongs to the calcium-binding family (reviewed in Schwaller, 2014). It shows a hexa-EF-hand structure, with five helix-loop-helix domains able to bind Ca^{2+} ions. However, complex chemical interactions characterize binding sites of CR, conferring peculiar kinetic properties to this protein (Schwaller et al., 1997; Stevens and Rogers, 1997; Palczewska et al., 2003; Faas et al., 2007).

In the cell, CR acts mainly as a calcium buffer, regulating the intracellular level of this ion and, consequently, the different physiological signaling cascades. Besides, additional roles have been confirmed in specific neuronal types. In the cerebellum of mice lacking CR, for instance, modifications in the firing properties of granule cell have been observed, presumably due to increased intracellular free Ca^{2+} concentration; remarkably, addition of the exogenous fast-calcium buffer BAPTA (1,2-bis(o-aminophenoxy)ethane-N,N,N',N'-tetraacetic acid) brings back the firing to the normal condition (Gall et al., 2003). Furthermore, a direct binding site for CR has been identified in the sequence of the voltage-gated calcium channel 2.1; the interaction modulates ionic flux through the channel, leading to an altered cellular excitability (Christel et al., 2012).

Many neuronal populations are also positive for the CR staining in several OB layers (Figure 5); only the ONL, in fact, lacks positivity to this marker (Parrish-Aungst et al., 2007). In the GL, CR-positive cells account for 28-44% of all JG cells (Kosaka and Kosaka, 2007; Panzanelli et al., 2007; Parrish-Aungst et al., 2007; Whitman and Greer, 2007). Dimensionally, this neuronal group is the smallest among PG cells, with a soma diameter varying from 6 to 8 µm (Kosaka and Kosaka, 2007; Parrish-Aungst et al., 2007; Batista-Brito et al., 2008). Furthermore, CR-positive cells do not express cholinergic markers and, contrary to all other PG subtypes, only some of them are GABAergic, suggesting the existence of at least two populations (Kosaka and Kosaka, 2007; Parrish-Aungst et al., 2007; Krosnowski et al., 2012).

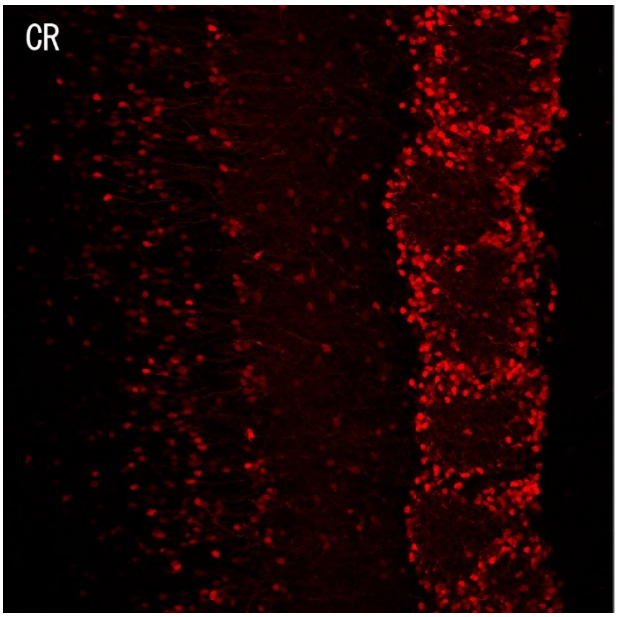

Figure 5 Calretinin-positive periglomerular cells. Coronal section of the mouse olfactory bulb with CR-positive cells in red.

CR neurons, together with CB-positive cells, constitute type 2 PG cells. They create contacts with other bulbar cells, but are not directly in contact with the ON axons. Activation of CR-positive neurons, consequently, is elicited by inputs from projection neurons (Kosaka and Kosaka, 2007). Interestingly, in the neocortex and hippocampus some CR-positive cells have been proved to synapse especially GABAergic interneurons, in order to modulate their inhibitory contribution to the neuronal network (Freund and Buzsáki, 1996; Gonchar and Burkhalter, 1999). This observation can highlight a possible parallelism with bulbar dopaminergic PG cells. Moreover, some studies reported that the amount of neo-generated CR-positive cells increases postnatally (De Marchis et al., 2007; Batista-Brito et al., 2008), suggesting an involvement in the adaptive adjustment of bulbar circuitry to external stimuli.

The exact role of CR-positive type II PG cells in the glomerular circuits is still unknown - more data on the electrical properties of CR-positive PG could help to find it; nevertheless, an electrophysiological characterization is still absent in the literature. The second part of my thesis is aimed at filling this gap.

h-current

Historical notes

The hyperpolarization-activated current was described for the first time in the rabbit sinoatrial node myocytes in 1976 (Noma and Irisawa, 1976), and in other cell types over the following years (Bader et al., 1979; Halliwell and Adams, 1982). Furthermore, in the early 1980s DiFrancesco provided the first accurate descriptions of this conductance in the sinoatrial node (Brown and DiFrancesco, 1980; DiFrancesco, 1981b, 1982). The experimental data revealed that the current under study begins to activate around -50 mV, raises in amplitude as hyperpolarized voltage steps increase and is carried by a mixed flux of K^+ and Na^+ ions. Because of its unusual properties, primarily activation by membrane hyperpolarization, DiFrancesco decided to name it "*funny*" current.

In the CNS, an equivalent current was initially termed "*queer*" current by Halliwell and Adams in 1982, during their studies in the hippocampus (Halliwell and Adams, 1982). In the last years, this name has been mainly replaced by the term h-current, or I_h, to indicate the hyperpolarization-activated current in the brain areas. To avoid any misunderstanding, I will use only the latter denomination in my thesis.

Since the beginning, it was clear that the hyperpolarization-activated current plays important roles in several physiological processes, still largely unidentified. This conductance, indeed, participates in the generation of the heartbeat (Yanagihara and Irisawa, 1980; DiFrancesco, 1981a), in the processing of visual signals (Attwell and Wilson, 1980; Bader et al., 1982; Demontis et al., 1999; Lee and Ishida, 2007), in the regulation of rhythmic activity in thalamic circuits (McCormick and Pape, 1990b; Soltesz et al., 1991), as well as in other basic neuronal mechanisms (Doan and Kunze, 1999; Beaumont and Zucker, 2000; Lupica et al., 2001). In addition, dysregulations of h-current have been also related to numerous pathologies, from Parkinson's disease (PD) to epilepsy (Shin et al., 2008; Jung et al., 2010; Chan et al., 2011).

HCN channels

The ionic channels underlying I_h are also called Hyperpolarization-activated Cyclic Nucleotide-gated or HCN channels for their dual mechanism of activation (Clapham, 1998), influenced by both membrane hyperpolarization and intracellular concentration of cyclic nucleotides.

These channels belong to the group of the cyclic nucleotide-regulated cation channels, including Eag-like K^+ and CNG channels too (Yu et al., 2005; Craven and Zagotta, 2006).

Structure

In their structure, HCN channels are polymeric complexes with four subunits organized around a central pore (Figure 6), an arrangement shared with many other voltage-gated pore loop channels (Doyle, 1998; Yu and Catterall, 2003). As well as in vertebrates, genes encoding for HCN subunits have been found also in some invertebrates, but are absent in prokaryotes and yeast (Gauss et al., 1998; Krieger et al., 1999; Marx et al., 1999). In mammals, four different HCN subunits, encoded by the *HCN1-4* gene family, have been identified (Robinson and Siegelbaum, 2003).

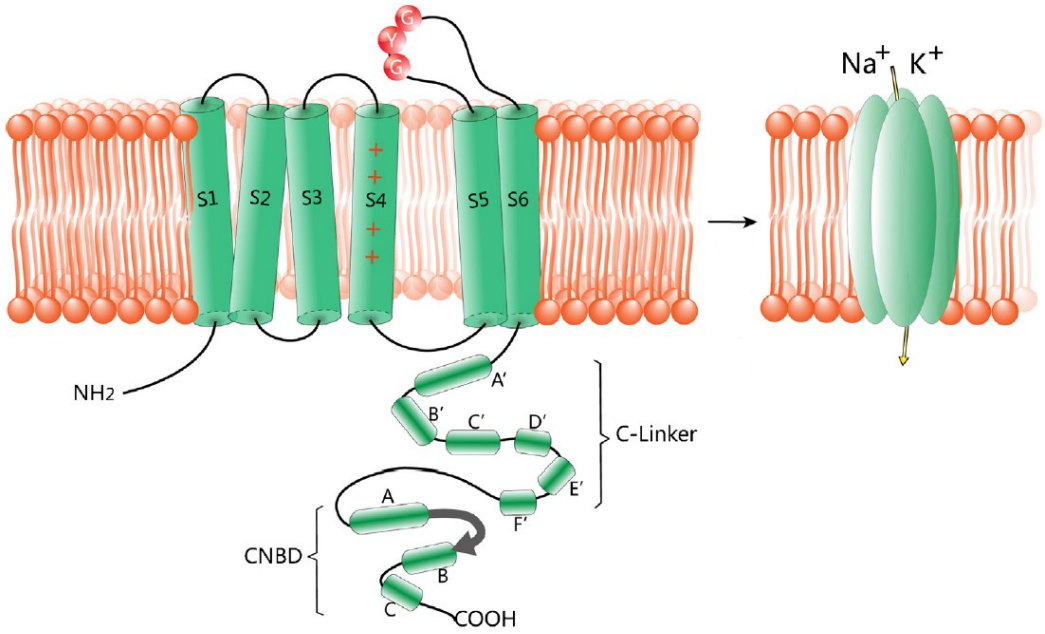

Figure 6 Structure of HCN channels. Each subunit consists of six transmembrane segments (S1–S6), with the positive charged voltage sensor (S4) and the pore region carrying the GYG motif between S5 and S6. The C-terminal of HCN channels is composed of the C-linker and the cyclic nucleotide-binding domain (CNBD), which mediates their responses to cAMP. The C-linker consists of six α-helices: A' to F'. The CNBD follows the C-linker domain and consists of three α-helices and eight-stranded antiparallel β-rolls. The four subunits assemble in tetrameric configurations in vivo. Image adapted from (He et al., 2014).

HCN subunits could generate both homotetramers and heterotetramers, due their high level of similarity in the amino acidic sequence (Figure 6). Peculiar biophysical properties characterizing different combination of subunits have been reported in several studies (Santoro et al., 1998; Ishii et al., 1999; Ulens and Tytgat, 2001; Altomare et al., 2003; Much et al., 2003; Whitaker et al., 2007).

Functionally, it is possible to recognize in each subunit two main structures with different roles: the transmembrane core and the intracellular C-terminal domain. Both of them are characterized by highly conserved sequence in all the members of the HCN family. On the contrary, intracellular N-terminal domains show very variable traits (Baruscotti et al., 2005).

Transmembrane domain

The transmembrane domain consists of six amino acidic chains (S1-S6) crossing the cellular membrane, commonly termed 6 transmembrane or 6TM architecture. In particular, S5-S6 loop and S4 helix play fundamental roles in the activity of the channel.

The complex of S5 segment, S6 segment, and reentrant loop between them of each subunit contribute to generate the ion-conducting pore of HCN channels. Also, in this structure has been found the amino acidic sequence C-IGYG, forming the selectivity filter of this channel (Macri et al., 2012). Interestingly, this sequence is nearly the same of the filter sequence that exclusively allows the permeation of the K^+ ions through the potassium channels (Shealy et al., 2003), although h-current is a mixed (Na^+-K^+) cation current (Ho et al., 1994; Yu et al., 2004b). This property is probably related to a more flexible organization of the residues (Wahl-Schott and Biel, 2009). Cysteine at position 400 contained in selectivity filter sequence is located deeply in the membrane. The cysteines of the four subunits channel create a ring that actively contribute to the pore selectivity of the HCN channel (Macri et al., 2012). Finally, asparagine at position 380 is not implied in the pore formation, but its glycosylation is essential for the correct channel positioning in the cell membrane (Much et al., 2003).

The S4 helix, as in many other voltage-gated ion channels (Yu and Catterall, 2004), represents the voltage sensor of HCN channel and consists of nine positive charged amino acids (mainly arginine and lysine) (Chen et al., 2000). In response to a hyperpolarization, S4 segments undergoes an inward movement through the membrane. This movements, which in normal voltage-dependent channels lead to the channel closing, opens the HCN channel (Männikkö et al., 2002). The reason of this behavior is still unknown, although it has been proposed an involvement of intracellular S4-S5 loops (Decher et al., 2004; Prole and Yellen, 2006).

C-terminal domain

The two main components of the carboxy-terminal domain are the cyclic nucleotide-binding domain (CNBD) and the C-linker, together termed the cAMP-sensing domain (CSD) (Figure 7). Indeed, those structures are responsible for the regulation of the HCN channel by cyclic nucleotides, which accelerate the opening kinetics and shift the activation curves to more positive membrane potentials) (DiFrancesco and Tortora, 1991; Flynn et al., 2007).

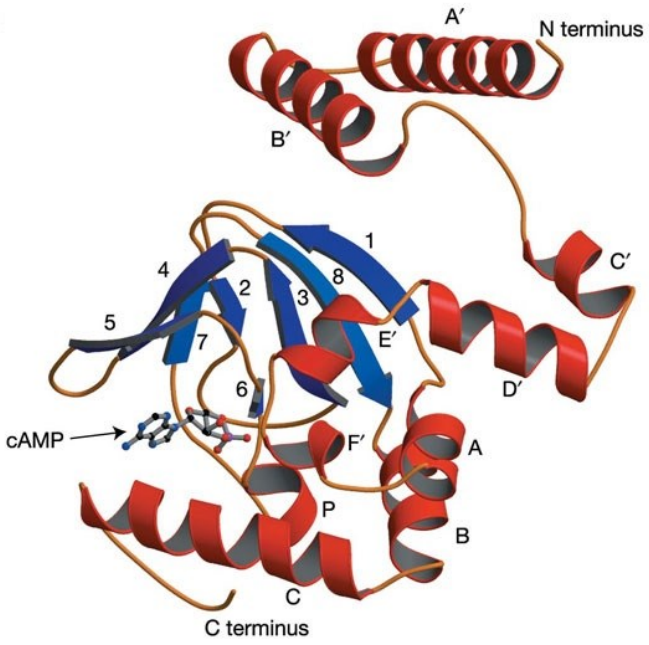

Figure 7 Structure of the mouse HCN2 C-linker and CNBD construct bound to cAMP. Ribbon representation of the C-linker, consisting of six α-helices (A'-F', in red), and of the CNBD, consisting of three α-helices (A, B, and C, in red) and eight-stranded antiparallel β-rolls (1-8, in blue). A molecule of cAMP is shown in the binding site of the structure. Image adapted from (Zagotta et al., 2003).

The CNBD is a 120 amino acid-long highly conserved complex composed by three α-helices (A, B, and C) and eight-stranded antiparallel β-rolls (β1-β8). The spatial organization of those elements, clarified at an atomic resolution in 2003 (Zagotta et al., 2003), generates a binding pocket for cyclic nucleotides (Figure 7). Only seven residues directly bind the cyclic nucleotides inside the pocket: four belong to C-helix and three to the β-roll. In more detail, the arginine at position 632 plays the lead role in the improvement of the pore opening (Zhou and Siegelbaum, 2007). Finally, a sequence of 80 residues arranged in 6 α-helices, termed C-linker, connects the CNBD to the S6 segment.

It has been observed that cAMP and cGMP (cyclic guanidine monophosphate) bind the HCN channels in the same way, determining the resulting CNBD conformation (Zagotta et al., 2003). However, HCN channels show a preferential binding for the cAMP compared with the cGMP. The molecular basis of this behavior is still unknown, even though some possible causes are supposed to be the different hydration energies of the two cyclic nucleotides or the specificity of the link with the amino acid residues (Zhou and Siegelbaum, 2007, 2008).

In recent years, a model auto inhibition has been proposed by various researchers to explain the modulation of the HCN channels by the cAMP (Craven and Zagotta, 2006; Wicks et al., 2011; Chow et al., 2012). The model predicts that the channel voltage-dependent activation is inhibited by the unbound CSD, limiting the S6 segment movements. This assumption is in agreement with previous studies suggesting that when cAMP binds the CNBD, conformational changes in the CSD sequence, relieving the inhibitory effect on the channel and promoting its activation (Wainger et al., 2001)..

Basic biophysical properties

Generally, all the HCN channels share some basic biophysical properties. First, their activation kinetics is very slow until -50 mV and they do not show any type of voltage-dependent inactivation. Moreover, if carefully analyzed, two different components can be recognized in the current evoked by hyperpolarization: a small, fast instantaneous current (I_{ins}) and a large steady-state current (I_{ss}). The former reaches a complete activation in few milliseconds, the latter requires tens milliseconds to several seconds. Furthermore, if the nature of I_{ss} is well characterized, the origin of the small I_{ins} is not completely clear (Proenza et al., 2002; Macri and Accili, 2004).

Several studies in different cell populations have revealed that I_h currents can be fitted by either a single or double exponential function (Attwell and Wilson, 1980; DiFrancesco and Noble, 1985; Edman et al., 1987; Kamondi and Reiner, 1991; Ulrich, 2002). In addition, important kinetic parameters have also been observed to diverge importantly in different works. For example, activation time constants range from tens of milliseconds to seconds (Attwell and Wilson, 1980; Pape, 1996). Half-maximal activation potentials (V_{50}), obtained from the activation curves fitted by the Boltzmann equation, also show a high variability (DiFrancesco and Tromba, 1988; Farès et al., 1998).

These diversities are supposed to originate from intrinsic (cellular types, HCN subunits, etc.), and extrinsic variables (experimental conditions), (Biel et al., 2009). In particular, temperature affects many biophysical properties of HCN channels, as demonstrated for other types of ion channels (Allen and Mikala, 1998; Rodríguez et al., 1998; Yanagida et al., 2000; Voets et al., 2004).

Ion selectivity

As mentioned above, HCN and K^+ voltage-gated channels share a very similar selectivity filter, but the firsts sustain a mixed cation current (Ho et al., 1994; Yu et al., 2004b; Macri et al., 2012). In fact, both K^+ and Na^+ ions can permeate HCN channel, with a ratio ranging between 3:1

and 5:1. Accordingly, the normal reversal potential for this current vary from -25 to -40 mV, so that I_h results to be a depolarizing inward current at rest (DiFrancesco, 1981a; Edman et al., 1987; Ho et al., 1994; Travagli and Gillis, 1994; Mercuri et al., 1995; Ludwig et al., 1998; Robinson and Siegelbaum, 2003). In addition, it has been reported a small flux of Ca^{2+} ions through HCN channels, suggesting an involvement in the process of secretion (Yu et al., 2004, 2007).

Interestingly, extracellular K^+ concentration has been proved to exert an important influence in channel permeation ratio and, consequently, in current amplitude (Frace et al., 1992; Wollmuth and Hille, 1992; Ludwig et al., 1998). In fact, if the external $[K^+]$ is raised, the current amplitude increases significantly and selectivity for K^+ over Na^+ is reduced. On the contrary, in the absence of potassium, HCN channel conductivity is nearly extinguished.

Modulation by cAMP

A hallmark of HCN channels is their modulation by cyclic nucleotides, in particular cAMP. This molecule is capable of speeding the opening kinetics, and shifting the activation curve of HCN channels to more depolarized voltages (DiFrancesco and Tortora, 1991; Wainger et al., 2001). V_{50} shifts caused by cAMP in different cell types are highly variable, since HCN channel isoforms have different sensitivity to the cyclic nucleotide (Santoro et al., 1998; Chen et al., 2001; Craven and Zagotta, 2006; Wicks et al., 2011).

HCN channel modulation by cAMP is important to explain many effects of neurotransmitters. Indeed, the majority of neurochemical compounds is able to modify the intracellular concentration of cAMP. Consequently, neurotransmitters that upregulate cAMP enhance HCN channels activation, and vice versa (Brown et al., 1979; DiFrancesco and Tromba, 1988; McCormick and Pape, 1990a; Garratt et al., 1993; Larkman and Kelly, 1997).

Pharmacology

HCN channels are sensitive to millimolar concentrations of Cs^+ (Fain et al., 1978; DiFrancesco, 1982; Ludwig et al., 1998). On the contrary, they are not blocked by millimolar concentrations of external Ba^{2+}, 4-aminopyridine (4-AP) and tetraethylammonium (TEA), common blockers of voltage-gated K^+ channels (Ludwig et al., 1998).

Anyway, for their key role in heartbeat generation, HCN channels have been the object of several studies. The first class of compounds discovered to act selectively on the HCN channels was alinidine, an analogue of the α_2-adrenoceptor agonist clonidine (Kobinger et al., 1979; Traunecker and Walland, 1980). However, this drug and its derivatives were quickly rejected for

their CNS side effects. Later, also some analogues of the L-type Ca^{2+} channel blocker verapamil have been proved to have bradycardic effect (Van Bogaert and Pittoors, 2003).

The HCN channels blocker more used is ZD7288. This molecule blocks the channel from the inside: two specific amino acids of the HCN2 subunit S6 segment are responsible for the high-affinity binding (Shin et al., 2001; Cheng et al., 2007).á ZD7288 block is not use-dependent and leads to an alteration of the biophysical properties of the channel (BoSmith et al., 1993; Aponte et al., 2006). Furthermore, this drug has been reported to block also other types of voltage-dependent conductances, like T-type Ca-channels (Sánchez-Alonso et al., 2008).

More recently, Laboratoires Servier have synthesized the first blocker of HCN channels approved for therapeutic use (ivabradine or S16257) (Thollon et al., 1994). This molecule is able to decrease HCN channels conductance without altering their biophysical properties (e.g. voltage dependence) (Bois et al., 1996). Ivabradine acts on HCN channel at micromolar concentrations, blocking it from the intracellular side. This effect has been demonstrated to be both current- and use-dependent (Bucchi et al., 2002, 2006; Thollon et al., 2007).

Functional properties of I_h

Due to their biophysical properties, a portion of the HCN channels is open at the resting membrane potential. This event has important outcomes on the physiology of excitable cells (Aponte et al., 2006; Rodrigues and Oertel, 2006; Nolan et al., 2007). Some of those consequences are discussed below.

Resting membrane potential control

Since a fraction of HCN channels is open at rest, this current maintains the cell membrane in a depolarized state in physiological conditions. The tonic activation of these channels also stabilizes the RMP and prevents its oscillation through different mechanisms (Maccaferri et al., 1993; Ludwig et al., 2003; Nolan et al., 2007). Since this conductance contributes to a decrease of the input resistance, an input current elicits a smaller variation in membrane potential. Furthermore, h-current restricts membrane potential variations through the singular relationship between its reversal potential and activation (Solomon and Nerbonne, 1993; Bayliss et al., 1994; Nolan et al., 2007). When a hyperpolarizing stimulus opens HCN channels, in fact, the elicited h-current produces a depolarization. Vice versa, reduction of Ih, as it can be produced by a depolarization, has a hyperpolarizing effect.

Dendritic integration

It has been proposed that HCN channels play a role in the dendritic integration of excitatory postsynaptic potentials (EPSPs) (Magee, 1998, 1999; Williams and Stuart, 2000; Berger et al., 2001). Generally, rising and decaying times of EPSPs depend on the passive properties of the dendrites. However, during the rising phase of EPSP, deactivation of HCN channels occurs, producing a hyperpolarization. Consequently, the time required for the decay of EPSP is reduced. Moreover, the resulting attenuation of EPSPs can be modulated by the expression level of these channels in distinct dendrites.

Spontaneous activity

The depolarizing effect of HCN channels brings the RMP close to firing threshold, contributing in several ways to spontaneous activity. This mechanism has been studied extensively in different cells (Jahnsen et al., 1984; McCormick and Pape, 1990b; Williams et al., 2002; Kocsis and Li, 2004; Atkinson et al., 2011; Kopp-Scheinpflug et al., 2011). In thalamocortical relay neurons, for example, HCN channels are directly involved in the pacemaking mechanism. In the

absence of external stimuli, these neurons show periodic bursts of action potential produced by T-type Ca^{2+} current and h-current: I_h depolarizes the membrane and activates the calcium current, which generates the bursts. During the spike depolarization, HCN channels are deactivated, leading to a hyperpolarization at the end of the burst. This event activates again the Ih, and the sequence can restart (Jahnsen et al., 1984; McCormick and Pape, 1990b). In other cases, HCN channels are not directly implicated in autorhythmicity, but are capable to modulate the currents that act as pacemakers (Williams et al., 2002).

Synaptic transmission

In the axon terminals of several neurons has been reported the presence of HCN channels, exerting opposite effects.

In the murine *globus pallidus*, the steady depolarization of the cell membrane produced by the h-current maintains in the inactivated state a significant portion of T-type Ca^{2+} channels. Therefore, during the action potential, a smaller amount of Ca^{2+} enters, and synaptic release of neurotransmitter results impaired (Boyes et al., 2007; Huang et al., 2011).

On the contrary, in other preparations, the HCN channels have been reported to enhance the transmitter release through the stimulation of P/Q-type Ca^{2+} channels as in the calyx of Held (Awatramani et al., 2005). Yet in other preparations, it has been reported a facilitating mechanism produced by I_h activation. The molecular basis of this mechanism is still unknown, but it has been proposed a cAMP-dependent increase in the pool size of releasable vesicles (Beaumont et al., 2002).

MATERIALS AND METHODS

Animals

For this thesis, depending on the purpose of the experiment, two transgenic mice strains have been employed.

Experiments on dopaminergic neurons are performed using the transgenic strain "TH-GFP/21-31", which carries the eGFP transgene under the control of the TH promoter. Precisely, the transgene construct contains the 9.0 kb 5'-flanking region of the rat TH gene, the second intron of the rabbit β-globin gene, cDNA encoding eGFP, and polyadenylation signals of the rabbit β-globin and simian virus 40 early genes (Sawamoto et al., 2001; Matsushita et al., 2002). Identification of transgenic mice is realized, within postnatal day 4, looking at the fluorescence of the olfactory bulbs trans-illuminated with a light source (FBL/Basic-B & N-01; BLS, Hungary; FHS/F-01) and observed with an emission filter (FHS/EF-2G2; BLS, Budapest, Hungary).

In the second part of the thesis the properties of the CR-positive neurons were studied using the transgenic strain "Tg(Calb2-EGFP)CM104Gsat/Mmmh". The genotype of this strain is modified to contain multiple copies of a modified BAC, in which eGFP is inserted immediately upstream of the coding sequence of the CR gene (Gong et al., 2003). Transgenic mice were identified through the genotyping protocol supplied by the Mutant Mouse Regional Resource Centers (MMRRC).

The two strains were maintained as heterozygous by breeding with wild-type inbred mice.

Ethical statement

The experimental process was designed to minimize animal number and suffering of the animals used. The protocols adopted were designed according to European Council Directives (609/1986 and 63/2010) and Italian laws (DL 116/92 and D.Lgsl. 26/2014) on the protection of animals used for scientific purposes. The experimental procedures were approved by the Ethical Committee for Animal Experiments of the Ferrara University (CEASA), by the Directorate-General for Animal Health of the Ministry of Health, and supervised by the Campus Veterinarian of the University of Ferrara.

Surgical procedures

Mice between 25 and 60 days have been used in the experiments. Once isolated by beheading, the head was submerged in refrigerated and oxygenated high sucrose artificial cerebrospinal fluid (ACSF) solution (see Solutions). In this solution, sodium chloride was

substituted with an equiosmolar quantity of sucrose to limit the excitotoxic damage. The whole brain was then removed from the cranium and the olfactory bulbs are dissected.

To obtain isolated neurons, an enzymatic and mechanical dissociation was executed. Olfactory bulbs were separated in small pieces and moved in a flask, containing 3% protease type XXIII dissolved in a dissecting medium (see Solutions). The enzymatic digestion was realized at 37 °C. After 30-45 min, the medium containing the protease was removed and replaced with a solution containing dissecting medium, 1% bovine serum albumin and 1% trypsin inhibitor to stop enzymatic activity (10 min at 37 °C). Later, bulbar pieces were moved into a new flask containing Tyrode's solution (see Solutions). A suspension of olfactory bulb neurons was obtained forcing the pieces through home-made fire-polished Pasteur pipettes of varying gauges. Isolated cells were plated on glass coverslips previously coated with concanavalin A (1 mg/ml) to facilitate adhesion and kept in incubator. After 12 hours, bulbar neurons could be used for the experiment. This protocol is a modified version of the procedure described by Gustincich (Gustincich et al., 1997).

To obtain slices, isolated olfactory bulbs were included in a cube-shaped block of low gelling temperature agarose. The block was then fixed to the slicing chamber of the vibroslicer using cyanoacrylate glue, and submerged in refrigerated and oxygenated ACSF. Low temperature and agar inclusion contributed to the mechanical stability of the tissue. Olfactory bulbs were then cut in the frontal plane obtaining slices with a thickness of 100-150 µm.

Recording conditions

During the experiment, the 1-ml recording chamber was constantly perfused with an approximately 2 ml/min flux of solution. The temperature in the chamber was regulated with a couple of 39.7 Peltier devices (RS Components) and measured with a high-precision, low mass thermocouple (RS Components). Slices were covered by a homemade grid in inert material to avoid vibrations and folding of the preparation during the recordings (*Figure* 8). The upright microscope used in the experiments was the Olympus BX50WI, equipped with Nomarski DIC (Differential Interference Contrast) optics. The microscope was equipped with epifluorescence, in order to identify eGFP-expressing cells in the preparation.

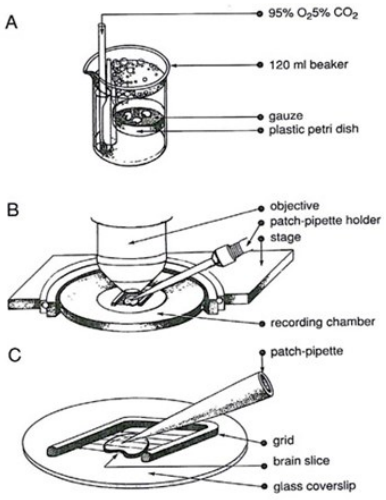

Figure 8 Slice preparation and recording conditions. A: After sectioning, slices are kept in a carbogenated high sucrose ACSF where they remain until use. B: recording chamber under the water immersion objective of the microscope. C: a grid is used to fix the slice.

The 5 cm long pipettes used in the experiments were produced with a P-97 puller (Sutter Instruments) starting from 10 cm long borosilicate glass capillaries (1.5 outer diameter, 0.87 inner diameter, with filament). The electrical resistance measured when the pipettes were filled with intracellular solution and immersed in the bath solution ranged from 4 to 7 MΩ.

The experimental setup included a remote-controlled micromanipulator PatchMan (Eppendorf), a microelectrode amplifier Axopatch 200B (Molecular Devices) and a 12 bit A/D-D/A converter Digidata 1320A (Molecular Devices). Finally, an air pressure controller MCPU-3 (MPI, Lorenz Meβgerätebau) was used to regulate the pipette inside pressure and the fluid level in the recording chamber.

Patch clamp technique

The patch clamp is a powerful electrophysiological technique that allows recording of single-channel currents and whole cell recordings also from very small cells, inaccessible to classical sharp electrodes. This technique, introduced by the Nobel prize laureates Neher and Sakmann (Neher and Sakmann, 1976), utilizes large-bore pipettes to contact the cell and electrically isolate a membrane patch, which is tightly sealed to the tip of the pipette (Hamill et al., 1981).

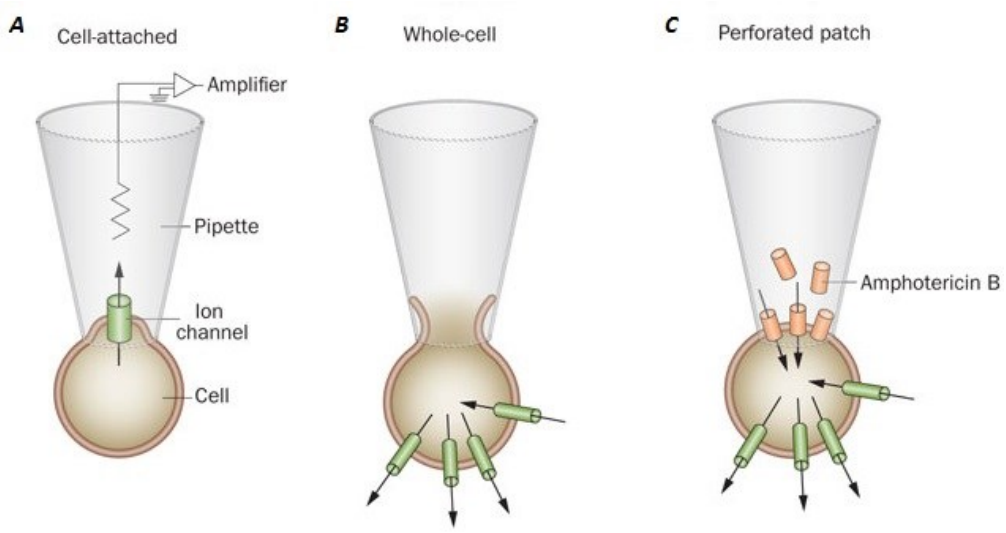

Figure 9 Patch clamp configurations. A: In the cell-attached configuration, the patch electrode is sealed to the surface of an intact cell, allowing channel activity in the patch of membrane under the electrode tip to be studied under physiological conditions. B: The standard whole-cell configuration is obtained by forming a cell-attached patch and then destroying the patch membrane with strong suction to gain electrical access to the cell interior. The intracellular solution then dialyses with that in the patch. C: The perforated patch configuration preserves cellular metabolism and intracellular second messenger systems by using a pore-forming antibiotic (such as amphotericin B) to provide electrical access to the cell interior. Image adapted from (Ashcroft and Rorsman, 2013).

If the rupture of the membrane patch through a negative pressure follows the seal formation, it is possible to record ionic currents that flows through the entire cell membrane. In addition, as for conventional intracellular recordings, it is possible to obtain information about the passive properties of the cell, such as membrane capacitance and resistance. This technical configuration is called whole cell configuration (Figure 9). An important consequence of the whole cell configuration is that the cytosol is rapidly replaced by the intracellular solution contained in the micropipette. In some experiments, this feature can be an advantage, as it can be exploited for the application of specific drugs, but in many cases the wash out of the intracellular components is a problem, as for studies of currents sensitive to intracellular signaling molecules . In order to circumvent this problem, the perforated patch configuration has been developed (Figure 9). After the seal formation, a perforating agent (usually an antibiotic) contained in the micropipette filling solution creates pores on the membrane patch, allowing the electrical communication with the cytosol. Generally, these pores permit the transit of monovalent ions, but avoid the dilution of larger intracellular soluble chemicals, like second messenger molecules. Both these configurations have been used in my thesis, depending on the goal of each experiment.

In my investigation two different methods of the patch clamp technique have been employed: voltage clamp and current clamp. The first method allows the control of membrane potential of the cell, recording the currents that flow through the cell membrane. This result is achieved by an electronic feedback system, which enables a differential amplifier to detect any variation of the membrane potential with respect to the potential established by the experimenter and correct it instantaneously. On the contrary, using the current clamp method it is possible to control the current injected into the cell, leaving the membrane potential to follow. In this way, the variations of membrane potential can be monitored.

Solutions

Depending on the distinct purpose of each experiment, different solutions have been used. All the composition listed below are expressed in mM.

For the dissection and slice preparation the solution used was:

- *High sucrose ACSF solution*: 215 sucrose, 3 KCl, 21 $NaHCO_3$, 1.25 NaH_2PO_4, 1.6 $CaCl_2$, 2 $MgCl_2$, and 10 glucose.

Two solutions were utilized in the dissociation protocol. The pH of these solutions is adjusted to 7.4 with NaOH and they are continuously bubbled with 100% O_2.

- *Dissecting medium*: 82 Na_2SO_4, 30 K_2SO_4, 10 HEPES (4-(2-hydroxyethyl)-1-piperazineethanesulfonic acid), 5 $MgCl_2$, 10 glucose, and 0.001% phenol red indicator.
- *Tyrode's solution*: 137 NaCl, 5.4 KCl, 1.8 $CaCl_2$, 1 $MgCl_2$, 5 HEPES, 20 glucose.

During the electrophysiological experiments, several extracellular solutions (EC) have been employed to characterize the different conductances under study.

- EC1, *standard ACSF extracellular solution*: 125 NaCl, 2.5 KCl, 26 $NaHCO_3$, 1.25 NaH_2PO_4, 2 $CaCl_2$, 1 $MgCl_2$, and 15 glucose.
- EC2, *normal K^+ plus TEA EC solution*: 100 NaCl, 2.5 KCl, 26 $NaHCO_3$, 1.25 NaH_2PO_4, 2 $CaCl_2$, 1 $MgCl_2$, 20 TEA, and 10 glucose.
- EC3, *high K^+ plus TEA EC solution*: 70 NaCl, 32.5 KCl, 26 $NaHCO_3$, 1.25 NaH_2PO_4, 2 $CaCl_2$, 1 $MgCl_2$, 20 TEA, and glucose.
- EC4, *no Na^+ plus TEA EC solution*: 110 CholineCl, 2.5 KCl, 26 $NaHCO_3$, 1.25 NaH_2PO_4, 2 $CaCl_2$, 1 $MgCl_2$, 20 TEA, and 10 glucose.

The osmolarity of all the solutions without HEPES was adjusted at 305 mOsm with glucose. EC solutions are continuously bubbled with 95% O_2 and 5% CO_2 during the experiment. In all the recordings in slices, kinurenic acid (1 mM) and bicuculline (10 µM) have been added to the EC to abolish glutamatergic and GABAergic synaptic activity.

The standard pipette-filling intracellular solution used contained (in mM): 120 KCl, 10 NaCl, 2 $MgCl_2$, 0.5 $CaCl_2$, 5 EGTA (ethylene glycol tetraacetic acid), 10 HEPES, 2 Na-ATP, and 10 glucose. The osmolarity of IC solution was adjusted to 295 mOsm with glucose, and the pH to 7.2 with KOH. The free calcium concentration with this internal solution was calculated to be 16 nM.

In perforated patch configuration, the perforating agent added to the intracellular solution in the recording pipette was amphotericin B (200 mg/ml, plus 300 mg pluronic F-127). To avoid unmonitored spontaneous transformation from perforated patch to whole cell configuration, the calcium chloride concentration in the recording pipette was increased to 3 mM and EGTA was absent.

Data analysis

Offline analysis was performed using version 10.3 of pClamp (Molecular Devices) and version 9.0 of Origin (OriginLab Corporation). Unless otherwise indicated, data are presented as means ± s.e.m. When used, box charts represent the mean (the central line, the S.E. (the box), the min-max values (the whiskers) of the data. Statistical significance of the results was calculated with Student's t test, one-way or two-way analysis of variance (ANOVA), as indicated. D'Agostino & Pearson omnibus normality test was used. A P value of <0.05 is considered significant.

RESULTS

PART I

h-current in dopaminergic PG cells

The topic of the first part of my thesis is the characterization of the h-current, one of the two hyperpolarization-activated conductance in the dopaminergic periglomerular neurons of the olfactory bulb.

These cells belong to the first type of PG neurons, which extends its dendrites in both ON and non-ON zone and represents a fundamental component of the glomerular circuitry. In the laboratory where I conducted my Ph.D. experience, the electrophysiological properties of the dopaminergic cells in the bulbar glomerular layer have been already analyzed (Pignatelli et al., 2005). Five depolarization-activated currents have been detected in these cells. The two main conductances are a fast transient sodium current and a non-inactivating potassium current; two different types of calcium conductances (L-type and T-type) and a persistent sodium current have been also characterized.

The transgenic mouse strain used in the experiments described below carries the reporter protein GFP under the control of the TH promoter, and represents a reliable animal model for the study of dopaminergic cells in the murine CNS (Saino-Saito et al., 2004; Maher and Westbrook, 2008; Pignatelli et al., 2009).

In this study, the recordings have been obtained from 285 TH-positive cells. During the experiments, periglomerular cells have been distinguished from the other types of juxtaglomerular cells not only for the presence of the reporter protein but also for their morphology (location in the GL, soma shape, dendritic arborization, etc.) and biophysical properties: input resistance (915.69 ± 31.31 MΩ, n=248), membrane capacitance (8.54 ± 0.21 pF, n=285) and regular firing.

Identification

In perforated patch configuration and voltage clamp mode, application of hyperpolarizing voltage commands from -50 mV to -130 mV (10 mV increments, 10 s interval) elicits a small current at room temperature both in slices and dissociated cells (Figure 10A), current which was mistaken for leakage conductances in the first experiments. To record larger h-currents, it is preferable to increase the external potassium concentration (EC3, $[K^+]_o$ = 32.5 mM), (Figure 10B). In addition, to isolate the I_h, 0.5 mM Ba^{2+} is added in the bath to suppress the K_{ir} current component, which is activated in the same range of potentials (Figure 10C). The residual current can be blocked by 1 mM Cs^+ (Figure 10D) or 30 µM ZD7288 (Figure 10E-F), a non-selective and a selective blocker of HCN channels, respectively (DiFrancesco and Ojeda, 1980; BoSmith et al., 1993).

Furthermore, under current clamp conditions in EC2 solution, the injection of a negative current (-60 pA) provokes the appearance of a sag, a hallmark of the I_h presence in the cells. The sag is enhanced by increasing the external potassium concentration (Figure 10G) and suppressed in presence of 1 mM Cs^+ (Figure 10H).

The dependence of the current amplitude on external potassium concentration, the slow kinetics of activation, and the distinctive pharmacology, confirm that the conductance under study is an h-current.

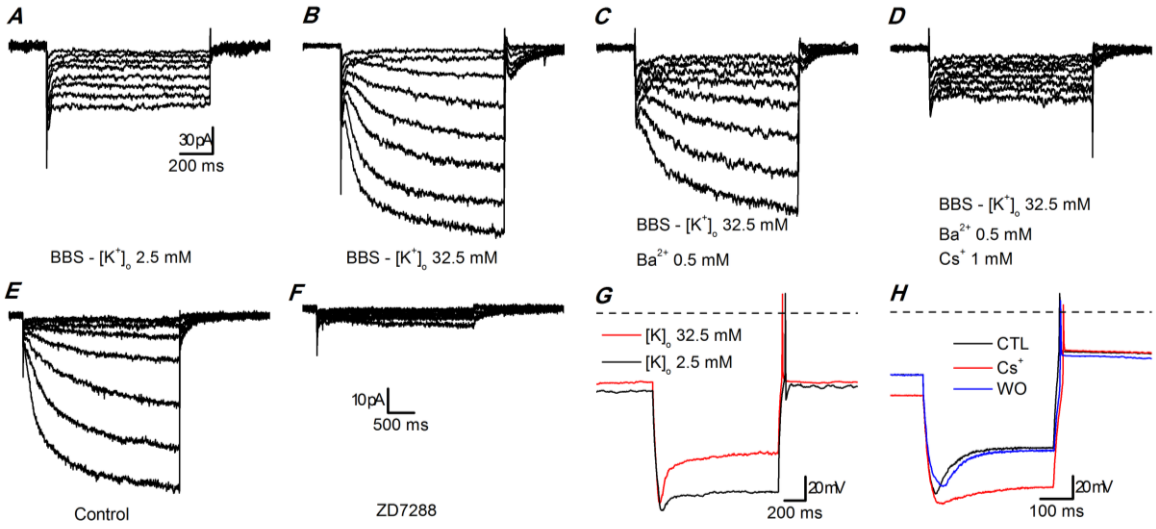

Figure 10 ***Hyperpolarization-activated currents in slices****.*
A-D: currents activated by hyperpolarizing steps. A - Standard EC saline (EC1, with 0.6 µM TTX, 100 µM Cd^{2+}); B - High K^+ EC saline (EC3, with 0.6 µM TTX, 100 µM Cd^{2+}); C - Same as B plus 0.5 mM Ba^{2+} to block the Kir current; D - Same as C after addition of a blocker of the h-current (1 mM Cs^+). The recordings have been taken after 5 min at any change of the bathing conditions. All the recordings of this group have been performed with synaptic blockers in the bath; perforated patch in slice at 34 °C.
E-F: effect of 7 min application of 30 µM ZD7288; perforated patch in slice; EC3 saline with 0.6 µM TTX, 100 µM Cd^{2+}, 0.5 mM Ba^{2+}; RT.
G - Current clamp responses to the injection of a hyperpolarizing current step (-60 pA) in a dopaminergic cell; black trace recorded in normal $[K^+]_o$ (EC2), red trace recorded in high $[K^+]_o$ (EC3); resting potential was -64.9 and -57.8 mV in normal and high K^+, respectively; both recordings have been performed with synaptic blockers, perforated patch in slice at 26 °C.
H - Current clamp responses to the injection of a hyperpolarizing current step (-56 pA) in a dopaminergic cell; all traces have been recorded in high $[K^+]_o$ (EC3) plus synaptic blockers; the red trace has been recorded in the same saline plus 1 mM Cs^+; resting potential was -55.8, -73.2 and -55.3 mV in control, Cs^+ and washout, respectively; current-clamp recording; perforated patch in slice at 37 °C.

Basic properties

The kinetics of the h-current has been investigated under voltage clamp conditions. In order to suppress the other currents, a mixture of blockers has been always added to the extracellular solutions: 0.6 µM TTX for sodium currents, 0.1 mM Cd^{2+} for calcium currents, and 0.5 mM Ba^{2+} for K_{ir} current.

The two-step protocol applied to study the activation kinetics consists of hyperpolarizing voltages ranging from -60 to -130 mV (10 mV increments, 10 s interval), from an holding potential of -40 mV; at the end of this first step, followed by a second hyperpolarizing pulse to -130 mV, in order to completely activate the I_h (Kamondi and Reiner, 1991). An example of the currents evoked by this protocol in a dopaminergic PG neuron is shown in Figure 11A. It is possible to observe that the h-current manifests a slow activation, and rises in amplitude as the hyperpolarization is prolonged. Inactivation is not detected.

As explained in the introduction, two different components can be distinguished in the I_h: an instantaneous current (I_{ins}) and a steady-state current (I_{ss}). The first, detected at the onset of the step, has been observed to be virtually linear along the applied voltage; the second, on contrary, has been measured at the end of the voltage command and increases in amplitude as the membrane potential becomes more negative.

The I_h amplitude is calculated as the difference between the I_{ss} and the I_{ins}; the latter is measured fitting the h-current with a double exponential equation and extrapolating the value at the time of the onset of the hyperpolarizing command. The I/V relationships of I_h in different conditions are illustrated in Figure 11B. Firstly, it should be noted that the current amplitude measured in dissociated cells (n=11) is 30.7 ± 1.2 % smaller than in slices (n=14). Moreover, amplitude of this current is also strongly sensitive to temperature. This aspect will be further discussed. Consequently, most of the experiments have been made under controlled temperature in slices, in order to standardize the recording conditions.

To create the activation curves of h-current, I_h tail currents (recorded in response to the -130 mV pulse of the two-step protocol) have been normalized on the maximal amplitude and plotted as a function of the voltage. Then, curves have been fitted by the following Boltzmann equation (Eq. 1):

$$\frac{I_{tail}}{I_{tailmax}} = \left\{1 + exp\left[\left(v_m - V_{50}\right)/k\right]\right\}^{-1}$$

where:

- I_{tail} is the amplitude of the tail recorded at -130 mV;
- $I_{tailmax}$ is the maximal amplitude of the tails;
- V_m is the membrane potential;

- V_{50} is the half-maximal activation potential, the voltage for which half of the channels are open;
- k is the slope factor, representing the dependence of the opening of channels by the change of potential.

The dependence of the V_{50} from the duration of the conditioning step has been evaluated changing the length of the first command in the two-step protocol. Durations of 1, 2, and 4 s have been tested. Longer durations cause the shift of the steady-state activation curve to more positive potentials (Figure 11C). Average data, obtained from 9 cell at 37 °C, show that V_{50} changes from -94.1 ± 2.0 mV for 1 s stimuli to -84.5 ± 1.2 mV for 4 s stimuli.

Finally, the deactivation time constant τ has been analyzed using a double-pulse protocol: from a holding potential of -40 mV, two hyperpolarizing steps to -130 mV (4 s) have been applied, separated by a voltage command to -40 mV of variable duration (Figure 12A). Deactivation of h-current at -40 mV and the envelope of reactivation records at -130 mV share a similar exponential time course, as illustrated in Figure 12B. Amplitudes of the tail currents elicited in the second hyperpolarizing pulse have been normalized and plotted as a function of the length of the repolarizing pulse applied. It is possible to fit the experimental values through the following exponential function (Eq. 2):

$$f(t) = \sum_{i=1}^{n} A_i e^{-\frac{t}{\tau_i}} + C$$

where *f(t)* is the normalized current amplitude at time t, and τ_i is the deactivation time constant at the indicated potential.

A last series of experiments in this part of the study has been carried out in order to analyze the reversal potential of the h-current. A specific protocol has been utilized: a fixed hyperpolarized potential of -120 mV is imposed to the cell membrane, followed by commands to various voltages (Figure 14A-B). It has been observed that the reversal potential depends on potassium and sodium ion concentrations. In figure 5, the dependence on $[K^+]_o$ has been analyzed: on average, the reversal potential of the current is -20.18 ± 1.67 mV (n=9) in EC3, and -43.95 ± 1.51 mV in EC2 (n=7).

Effect of temperature

Several studies in different preparations have reported that the temperature at which electrophysiological experiments are carried out critically influence the kinetics of h-current (Hart, 1983; Yanagida et al., 2000; Pena et al., 2006). In this study, it has been observed that the amplitude of I_h increases as the temperature rises (Figure 11B, 13B). Current amplitude evoked at -130 mV, in fact, is -139.02 ± 16.73 pA at 22 °C (n=14), and increases to -462.51 ± 85.84 pA at 37 °C (n=7). In addition, a variation of the maximal conductance has been confirmed, from 0.93 nS at 22 °C to 3.08 nS at 37 °C.

To quantify the effect of the temperature on the biological systems, the temperature coefficient Q_{10} is commonly used. It represents the fold change of the rate under study for every 10 °C variation, and is defined as:

$$Q_{10} = \left(\frac{rate(T_2)}{rate(T_1)} \right)^{\frac{10}{T_2 - T_1}}$$

For the h-current amplitude, the average value of Q_{10} between -100 and -130 mV is 2.87 ± 0.38. To explain this observation, a temperature-induced shift in the voltage dependence of the I_h can be proposed. Indeed, also V_{50} value is affected by the thermic conditions. Repeating the activation protocol described above at different temperatures (27, 32 and 37 °C), a shift of the steady-state activation curve have been observed (Figure 11D): from -95.4 ± 2.3 mV at 27 °C (n=13) to -84.2 ± 1.3 mV at 37 °C (n=18) ($p < 0.0001$, two-tailed Student t-test for unpaired data). No significant changes have been calculated in the slope factor k.

Temperature also affects the activation kinetics of the h-current in other two aspects. First, the current tracings at 22 °C can be carefully fitted only using a double exponential (Figure 13A), whereas a single exponential is sufficient to fit the current at temperatures above 32 °C (Figure 13C). Second, the rate of development of the current is increased. However, considering the distinct fitting required at different temperatures, a comparison of the time courses is possible only comparing the 10–90% rise time.

Since the steady state is not always reached due to the instability of the membrane at the more negative potentials, the following equations have been used, obtained solving Eq. 2 for y=10 and y=100 after normalization of the total amplitude to 100:

- <u>for a single exponential</u>: $t_{90} = \tau \ln(100/10)$ and $t_{10} = \tau \ln(100/90)$, where t_{10} and t_{90} are the times at which the current is developed for the corresponding percentage, and τ is the time constant;

- <u>for a double exponential</u>:
    - first the amplitudes of the two exponentials (A_1 and A_2) have been normalized so that their sum is 100;
    - then, Eq.2 have been solved numerically for t using standard numerical methods, solving Eq. 2 for *f(t)* = 90 and 10, thereby obtaining t_{10} and t_{90}, respectively.

In Figure 13D the comparison of the t_{10} - t_{90} times at 22 and 32 °C is graphically represented. Setting *rate* as (t_{90} - t_{10}) in Eqn. 3, in the range between -90 and -130 mV the corresponding Q_{10} is 4.72. Finally, thermic conditions have been verified to influence also the deactivation time constant, which decreases as the temperature rises. Average results, obtained from five cells, are illustrated in Figure 12C.

Blockers

Low concentrations of Cs^+ (1-2 mM) are able to suppress the h-current (DiFrancesco and Ojeda, 1980), as well as ZD7288 and S-16257 (ivabradine), two organic compounds that block selectively the HCN channels (BoSmith et al., 1993; Bucchi et al., 2002, 2006). In our preparation, I_h is effectively blocked by 1 mM Cs^+ (Figure 10D-H). However, the action of this ion is voltage-dependent: in the negative region of the I/V curve, cesium induces the suppression of the current, whereas is ineffective at more positive potentials. More selective and completely voltage-independent blockages can be achieved with 30 µM ZD7288 (Figure 10F) and 10 µM ivabradine (not shown).

Role in autorhythmicity

The presence of the h-current is frequently related to the pacemaking process in the autorhythmic cells (for a review, see Wahl-Schott and Biel, 2009). Therefore, its role in autorhythmicity has been investigated also in our preparation. Under perforated patch configuration and current clamp conditions at 37 °C, the addition of any HCN channel blocker in the bath provokes a hyperpolarization (Figure 15A). Starting from -58.76 ± 0.90 mV, the membrane potential is hyperpolarized to -65.17 ± 1.64 mV by 1 mM Cs^+ (n=5), to -65.50 ± 1.31 mV by 30 µM ZD7288 (n=5), and to -64.64 ± 1.81 mV by 10 µM ivabradine (n=8) ($p < 0.01$, two-tailed Student t-test for unpaired data). The effect is rapid and reversible with Cs^+ and ivabradine, slower and often irreversible with ZD7288.

Notably, the hyperpolarization have been observed to cause the interruption of the spontaneous activity in the dopaminergic PG cells. In order to clarify if this blockade represents the evidence of a direct role played by the h-current in the pacemaking mechanism, or just the consequence of the hyperpolarization, a depolarizing current has been injected in presence of ivabradine. When the positive current restored the resting potential to the value preceding the I_h block (grey arrowhead in Figure 15B), spontaneous activity resumed reproducibly and immediately (Figure 15C).

These observations confirm that the h-current is not directly involved in the pacemaker mechanism, but also demonstrate that I_h plays a relevant role in determining the resting membrane potential of this class of bulbar periglomerular neurons.

Modulation by intracellular cAMP

As already mentioned, the h-current is dually regulated by the hyperpolarization and by cAMP, which interacts with the CNBD in the C-terminal segment (DiFrancesco and Tortora, 1991; Wainger et al., 2001). Therefore, the modulatory effect of cAMP on the I_h has been analyzed. In order to minimize the perturbations of the intracellular medium, the perforated patch configuration adopted in this series of recording is of particular importance. Under current clamp conditions and in EC1, 10 µM forskolin, a classical activator of adenylyl cyclase (Seamon and Daly, 1981), and 0.1 mM 3-isobutyl-1-methylxanthine (IBMX), a phosphodiesterase inhibitor (Beavo et al., 1970), have been added to the extracellular solution to increase the intracellular levels of cAMP. The resulting effect, measured in six cells, is a large depolarization of 20.53 ± 4.21 mV (n=6, $P < 0.005$, two-tailed Student t-test for paired data) (Figure 16A). In addition, the effect becomes more evident at more negative membrane potentials (Figure 16B), as expected due to the increasing importance of the h-current at more hyperpolarized membrane levels.

Furthermore, under voltage-clamp condition and in EC2, the h-current amplitude is increased by applying 10 µM forskolin and 0.1 mM IBMX in the bath (Figure 16C). At the potential of -130 mV, the current amplitude is -93.8 ± 4.0 pA in control conditions (n=5), and -139.5 ± 20.4 pA in the presence of the drugs (n=5); for each tested potential, the increase in current amplitude was statistically significant ($p < 0.005$, ANOVA). Later, the shift of the steady-state activation curve in the depolarizing direction induced by forskolin has been evaluated. In EC2, it has been observed a variation of V_{50} from -82.44 ± 1.57 mV to -77.11 ± 1.33 mV (n=4, $p < 0.005$), but the effect is more evident in high $[K^+]_o$ saline (EC3). In this condition, V_{50} shifts from -85.26 ± 1.96 to -75.77 ± 2.41 mV (n=7, $p < 0.002$, ANOVA), as illustrated in Figure 16D. The experiment, repeated in the same testing conditions but increasing the intracellular cAMP concentration with 10 mM 8Br-cAMP, gave results largely superimposable: from -85.36 ± 2.32 to -78.99 ± 3.59 mV (n=7, $p < 0.05$, ANOVA). In both cases, the slope was insensitive to the treatment.

In a last series of experiments, carried out in EC3, we evaluated the sensitivity of the activation time course of h-current onset to $[cAMP]_i$. It has been verified that both forskolin and 8Br-cAMP are able to reduce the activation time constant. In particular, this parameter decreased from 141.75 ± 13.81 to 95.58 ± 17.94 ms with forskolin (n=7, $p < 0.02$, ANOVA), and from 130.27 ± 26.16 to 103.21 ± 23.48 ms with 8Br-cAMP (n=7, $p < 0.02$, ANOVA).

Modulation by neurotransmitters

The final part of the study of h-current was focused on the modulation by neurotransmitters. Many neurotransmitters, in fact, are able to modify the intracellular concentration of cAMP. Therefore, they may have a modulatory effect on the I_h.

Under voltage clamp conditions, effects of several compounds have been tested on the h-current amplitude: 5-HT (50 µM), dopamine (100 µM, plus 1mM ascorbic acid), quinpirole (D2 agonist, 30 µM), noradrenaline (100 µM, plus 1 mM ascorbic acid), phenylephrine (α1 agonist, 10 µM), clonidine (α2 agonist, 10 µM), histamine (10 µM), oxotremorine (muscarinic agonist, 10 µM) and baclofen ($GABA_B$ agonist, 10 µM). The results are illustrated in Figure 17: only NA has proved to affect the h-current, with an inhibition that, after 10 min of application, reached 50% of the control level (Figure 17A), whereas all the other neurotransmitters are ineffective (Figure 17B). Interestingly, the effect of noradrenaline is reproduced almost exactly by the α2 agonist clonidine, both in amplitude and time course (Figure 17A), whereas the α1 agonist phenylephrine was completely ineffective (Figure 17B). Finally, both NA (not shown) and clonidine have been observed to induce an evident hyperpolarization of the cell membrane when tested in current clamp conditions (Figure 17C).

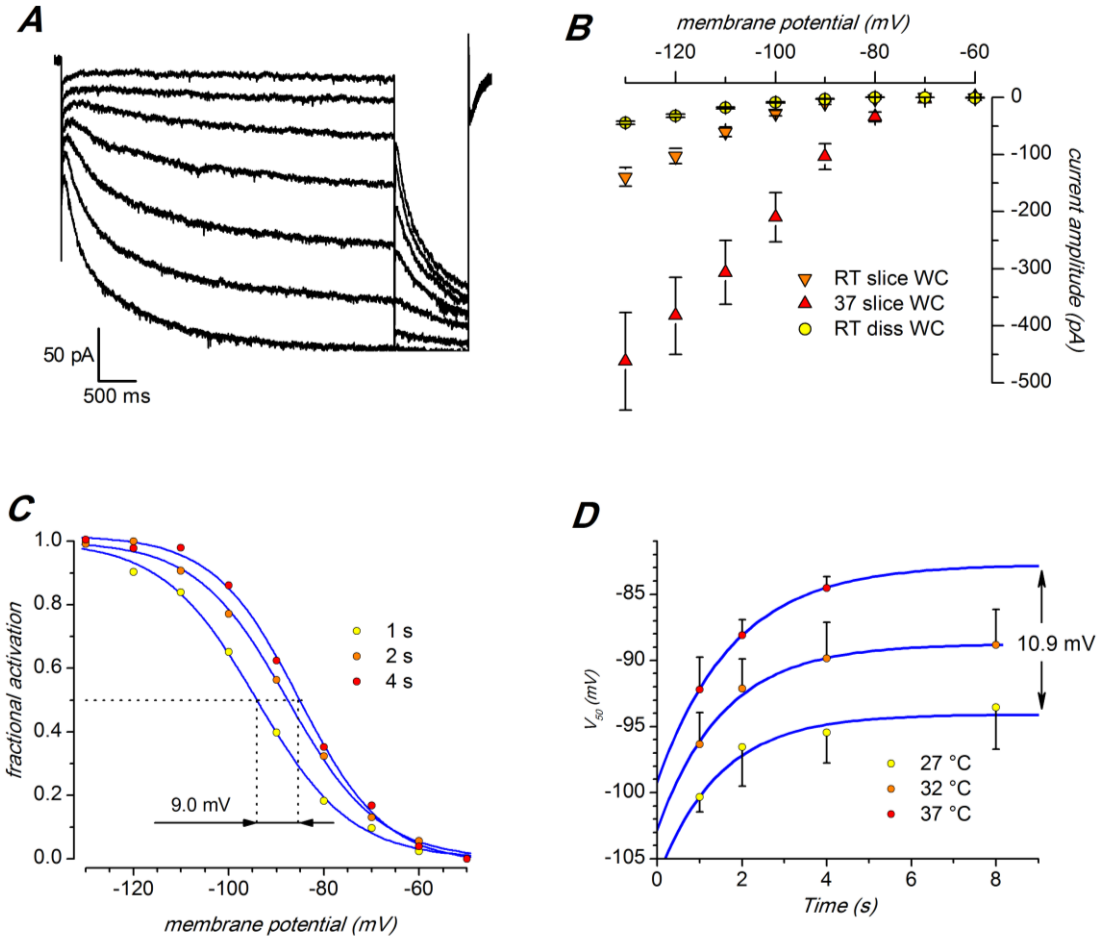

Figure 11 ***Activation kinetics****.*

A - Representative current traces for the analysis of activation. The membrane has been held at -40 mV and then hyperpolarized to test voltages from -60 to -130 mV in 10 mV increments, 10 s interval. I_h tails have been elicited in response to a second pulse to −130 mV, following test voltages. EC solution: EC3, plus synaptic blockers, 0.6 µM TTX, 100 µM Cd^{2+}, 0.5 mM Ba^{2+}; 37°C; slice; perforated patch.

B - Whole cell I/V relationship of the h-current in different experimental conditions: dissociated cells at RT (○, n=11); slice at RT (▽, n=14); slice at 37 °C (△, n=7); mean values ± S.E. EC solution was EC3 plus 0.6 µM TTX, 100 µM Cd^{2+}, 0.5 mM Ba^{2+} in all cases, with the further addition of synaptic blockers in slice preparation. C - Fractional activation of the h-current as in a group of 9 cells as a function of voltage using the protocol shown in A, and with the indicated duration of the hyperpolarizing step (see text for explanation). EC solution: EC3, plus synaptic blockers, 0.6 µM TTX, 100 µM Cd^{2+}, 0.5 mM Ba^{2+}; perforated patch in slice at 37 °C. D - Effect of temperature and of the variable duration of the hyperpolarizing step on the midpoint of the h-current. Notice that the change from room temperature (22 ± 1 °C) to 37 °C entails a shift of 10.9 mV of the V50. EC solution: EC3, plus synaptic blockers, 0.6 µM TTX, 100 µM Cd^{2+}, 0.5 mM Ba^{2+}; slice; perforated patch.

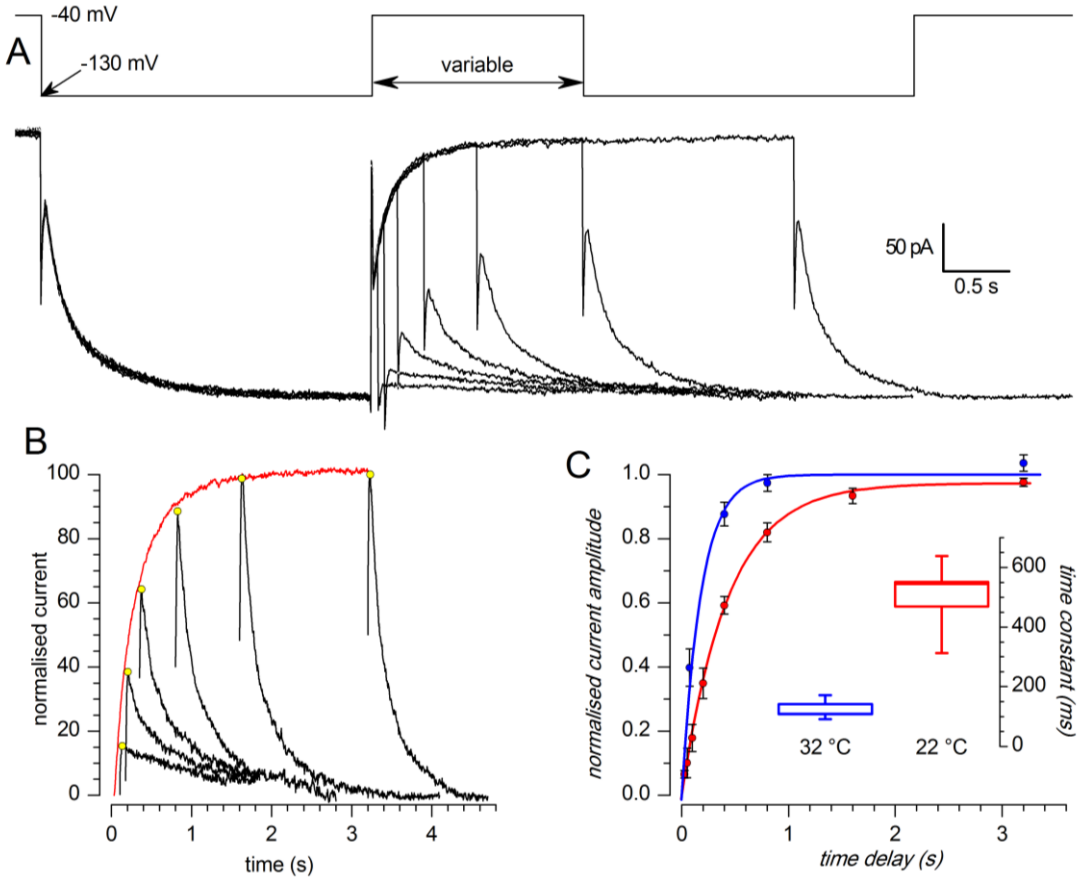

Figure 12 ***Deactivation kinetics****.*
A - Envelope test during deactivation at -40 mV. After current activation at -130 mV, pulses to -40 mV of variable duration have been followed by re-activating steps to -130 mV (see protocol in the top panel). Recording temperature 24 °C.
B - The tail at -40 mV have been also re-plotted after appropriate scaling (red trace) to better compare its time course with that of the re-activation records envelope shown in panel A.
C - Analysis of the deactivation time constant for a group of five cells at 32 (blue) and 22 °C (red); the average time dependence was fitted with the equation I(t) = 1 - exp(-t/τ) (continuous lines).
C - inset: box chart of deactivation time constants at 22 and 32 °C.
All recordings shown in this figure have been made in slice, perforated patches, EC3 saline plus synaptic blockers, 0.6 µM TTX, 100 µM Cd^{2+}, 0.5 mM Ba^{2+}, at the indicated temperatures.

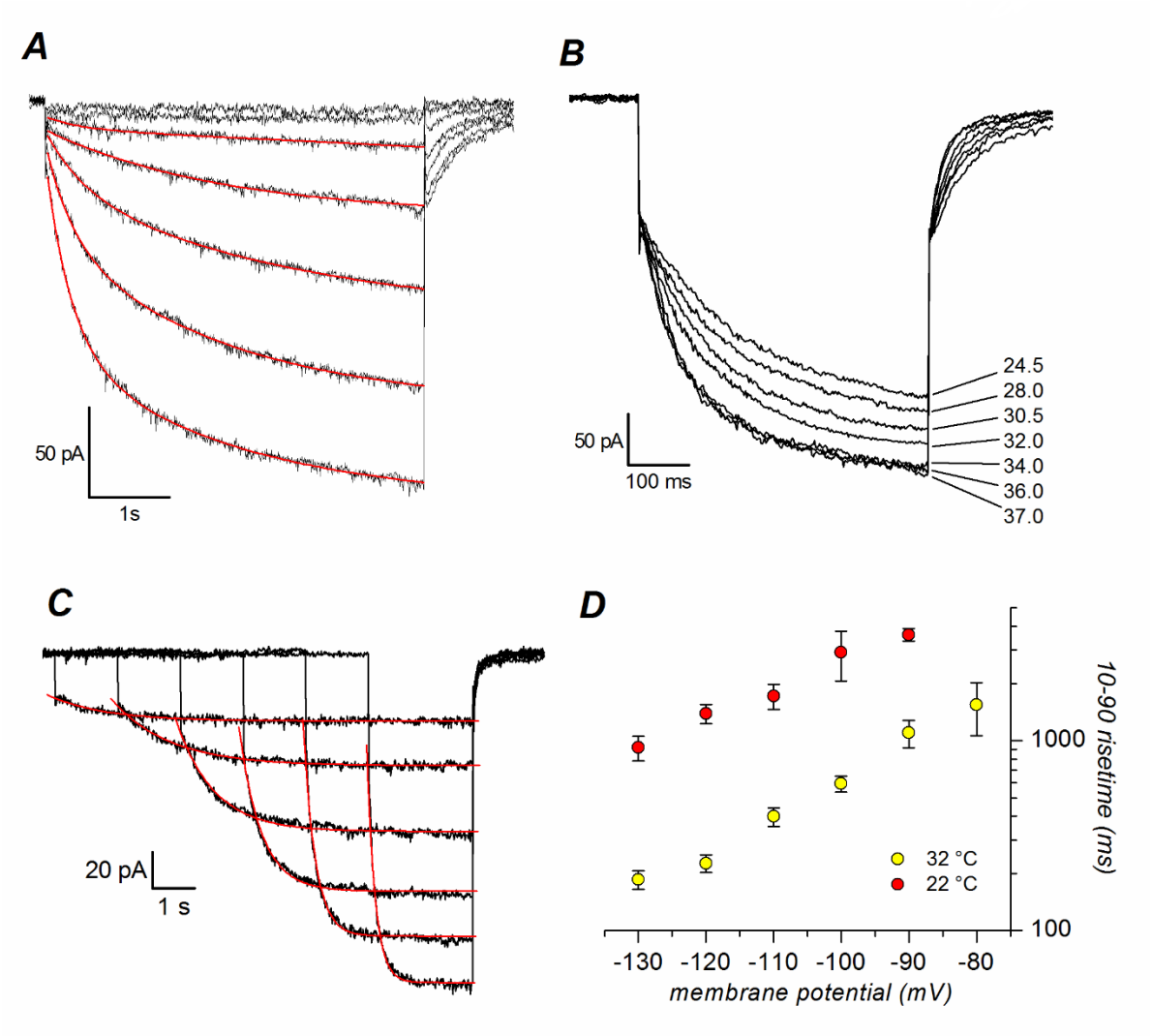

Figure 13 ***Analysis of time constants****.*
A - Activation at 22 °C: family of current tracings recorded in a single cell in response to hyperpolarizing pulses ranging from -70 to -130 mV from a holding potential of -40 mV; the red line represents the best fit with a double exponential.
B - Family of current tracings recorded in a single cell in response to hyperpolarizing pulses from -40 to -130 mV, repeated at the temperatures indicated.
C - Activation at 32 °C, using a different protocol minimizing the stress of the membrane at the more negative potentials.
D - Comparison of the 10-90 rise time at the two temperatures.
All the records shown in this figure were made in slice, perforated patch configuration, EC3 saline plus synaptic blockers, 0.6 µM TTX, 100 µM Cd^{2+}, 0.5 mM Ba^{2+}, at the indicated temperatures.

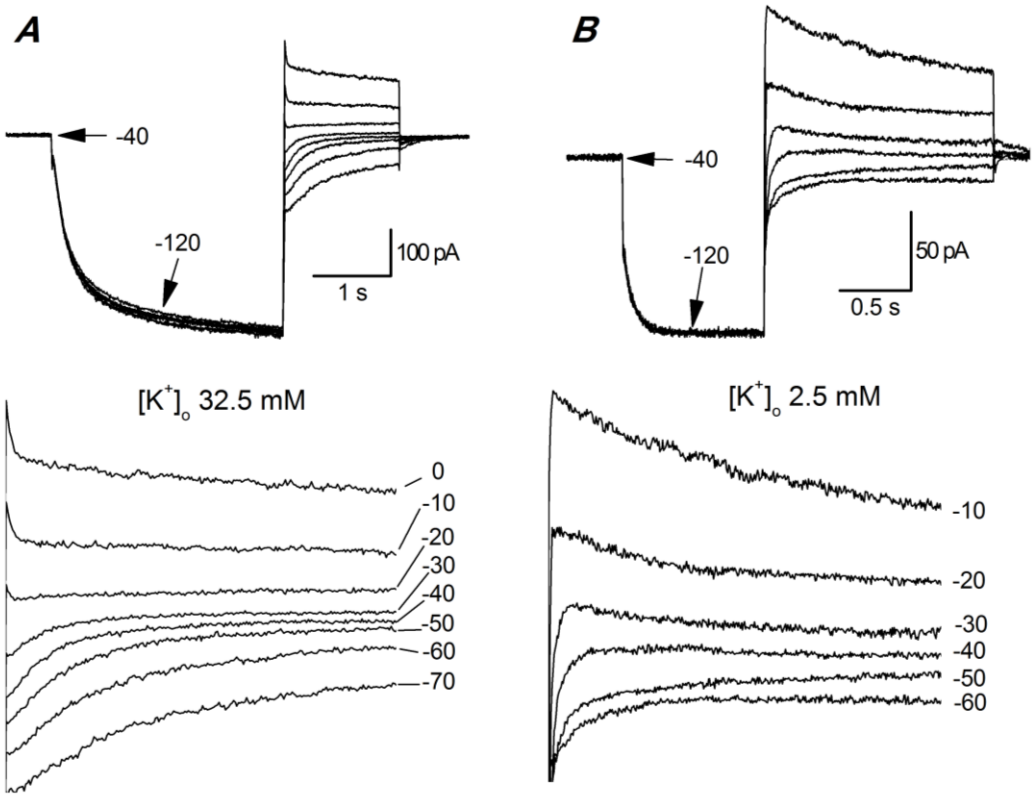

Figure 14 ***Reversal potential****.*
A, B - Measure of I_h reversal potentials; following activation, I_h was deactivated by 1.4 s depolarizing steps to various voltage levels, as indicated in the bottom panels. The expanded decay tails, plotted in the bottom panels, show that the I_h reversal potential is around -20 mV in A, and around -40 mV in B. The reversal potentials do not change with temperature (not shown).
Recording conditions: A: EC 3 plus synaptic blockers, 0.6 µM TTX, 100 µM Cd^{2+}, 0.5 mM Ba^{2+}, RT; B: EC 2 plus synaptic blockers, 0.6 µM TTX, 100 µM Cd^{2+}, 0.5 mM Ba^{2+}, 37 °C; both recordings have been made in slice using perforated patch configuration.

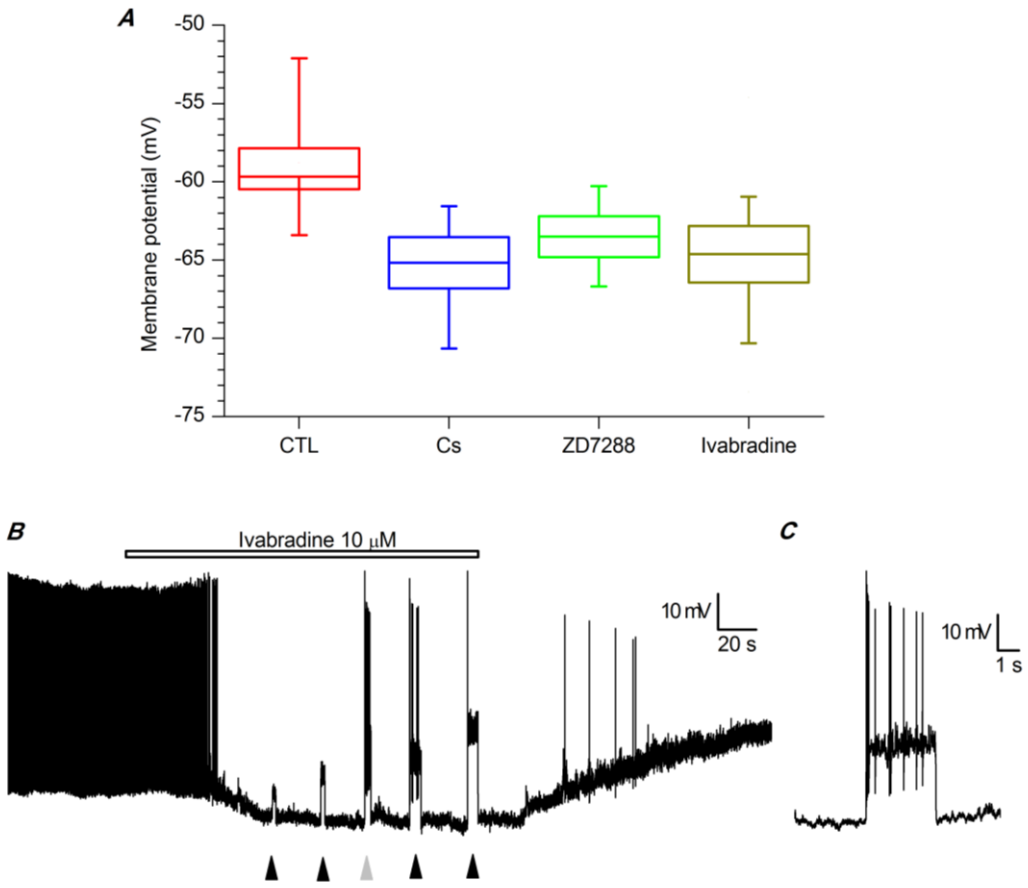

Figure 15 ***Effect of blockers of HCN channels on membrane potential and spontaneous firing***.
A - Box charts showing the effect of HCN channels blockers on resting membrane potential; the recording condition for the experiments represented in this figure were: perforated patch in slice at 37 °C; all differences were significant at the 0.01 level with Student t-test paired data analysis.
B – Ivabradine (10 μM, bar) block of spontaneous activity. At the times indicated by arrowheads, depolarizing currents of increasing amplitudes (+15, +30, +40, +50, +70 pA, in the order) have been delivered.
C - Enlargement of the response to the third injection of depolarizing current (grey arrowhead) to show that the block of the h-current does not impair the spontaneous activity, as indicated by the restoration of firing upon forcing the membrane back to resting values.
All the experiments shown in this figure were performed using standard saline (EC1) plus synaptic blockers; perforated patch in slice at 37 °C.

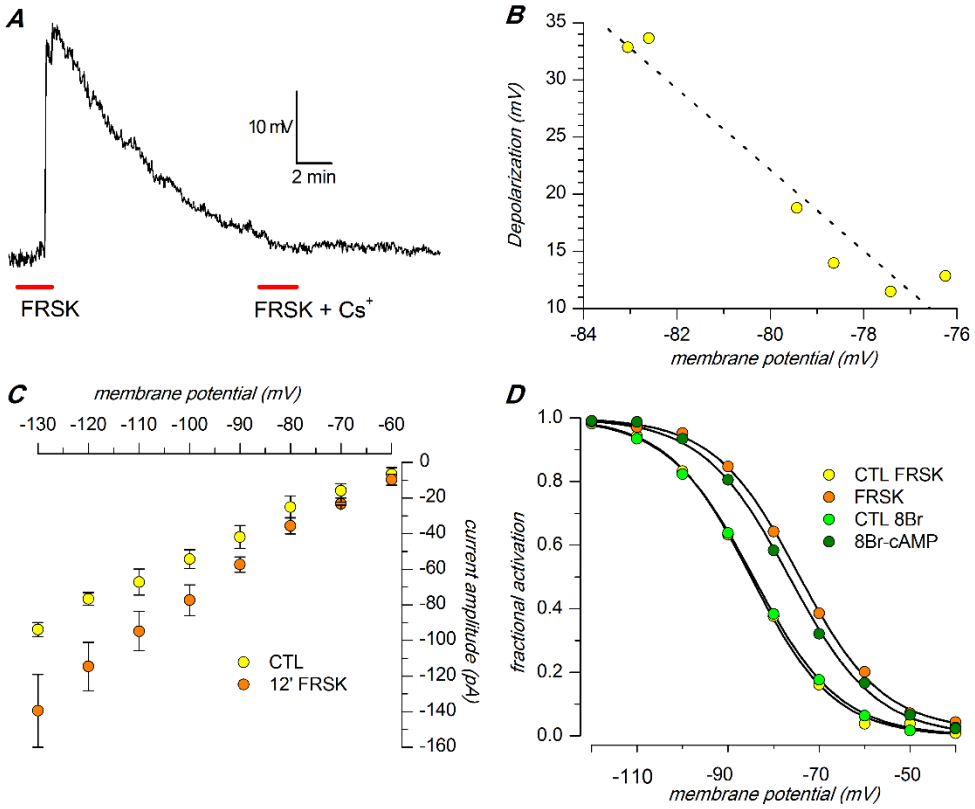

Figure 16 ***Effect of forskolin****.*
A - Focal application of forskolin (10 µM) and IBMX (0.1 mM) alone and in the presence of 1 mM Cs^+ at the times indicated by the red bars in current clamp conditions. Extracellular saline was EC1 plus synaptic blockers.
B - Voltage-dependence of the effect of forskolin on the membrane potential, showing that the depolarization increases at more negative potentials; the cell membrane has been manually hyperpolarized before the application of the drug to circumvent spontaneous activity; recording conditions as in A.
C - Modification in h-current amplitude after 10' perfusion with forskolin (10 µM) and 8Br-cAMP (10 µM). Extracellular saline was EC2 plus synaptic blockers, 0.6 µM TTX, 100 µM Cd^{2+}, 0.5 mM Ba^{2+}.
D - Shift in h-current activation curve following perfusion with forskolin; following treatment with the drug the midpoint is depolarized of 4.4 mV, and the slope becomes faster (from 7.6 to 5.2 mV); recording conditions as in C.
All the experiments illustrated in this figure were performed in slice, perforated patch at 37 °C .

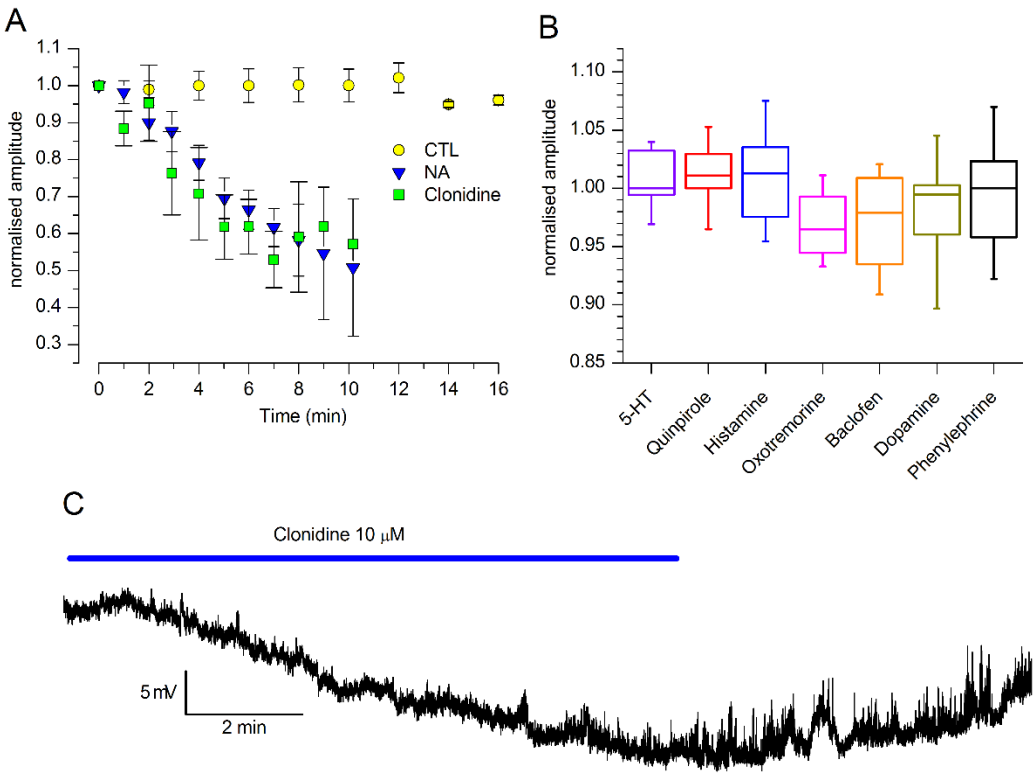

Figure 17 ***Effect of different neurotransmitters on the h-current****.*
A - Effect of NA (100 µM, + 1 mM ascorbic acid); the amplitudes at different time points are normalized with respect to the amplitude at time zero; n = 16 (controls) 11 (NA), 6 (clonidine).
B - Box charts showing the lack of effect of the indicated neurotransmitters; 5-HT (50 µM, n=7), quinpirole (30 µM, n=14), histamine (10 µM, n=11), oxotremorine (10 µM, n=7), baclofen (10 µM, n=4) and dopamine (100 µM, + 1 mM ascorbic acid; n=8).
C - Effect of clonidine (α2 agonist, 10 µM) on the resting membrane potential. The membrane has been hyperpolarized to -74 mV (by injecting -45 pA) in order to prevent spontaneous firing.
All recordings shown in this figure have been performed in slice, perforated patch at 37 °C; external saline was EC3 plus synaptic blockers, 0.6 µM TTX, 100 µM Cd^{2+}, 0.5 mM Ba^{2+} for experiments shown in A and B, EC 1 plus synaptic blockers for the experiment shown in C.

PART II

The second part of my thesis is focused on the electrophysiological properties of the CR-positive periglomerular cells of the olfactory bulb.

These neurons, in fact, are involved in the processing of olfactory information, but our knowledge about these cells is very poor. In particular, electrophysiological papers describing their features are absent in literature. This study is designed to fill this gap, in order to contribute to understand the functional role of the CR-positive periglomerular population.

The animal model used for this investigation is a transgenic mouse strain carrying the eGFP transgene under the calretinin promoter. The data presented have been obtained from 59 cells recorded in slices; all of them expressed the eGFP and were located in the glomerular layer. The membrane capacitance and the membrane resistance values of these neurons are 3.9 ± 0.4 pF and 2186 ± 151 MΩ, respectively. The low variability in their electric properties contribute to identify the CR-positive periglomerular cells as a unique neuronal population.

A first series of recordings, performed in voltage clamp mode, have been carried out in order to identify the conductances of the CR-positive periglomerular cells. For this purpose, using the EC1 solution, depolarizing steps from the holding potential (V_h) of -100 mV to potentials ranging from -80 to +40 mV (with 10 mV increments) have been applied (Figure 18). This protocol evokes two distinct main currents: a transient outward K^+ current and a fast transient Na^+ current. Moreover, analyzing the recordings at the end of the depolarizing steps, a small persistent inward current sustained by Ca^{2+} ions is identified. All these conductances have been isolated with specific blockers and ionic substitution in order to analyze their basic properties.

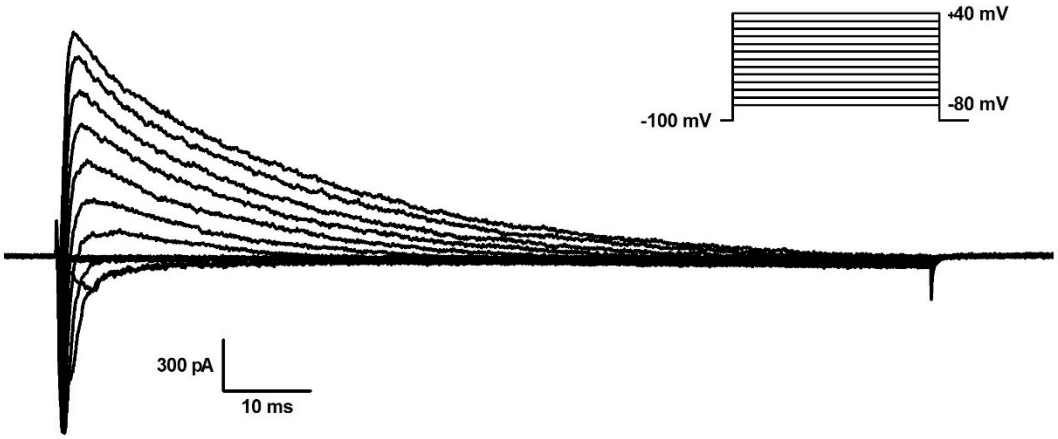

Figure 18 Responses of CR-positive PG neurons in thin slices to depolarizing voltage steps. Currents activated by depolarizing steps ranging from -80 to +40 mV; holding potential was -100 mV; external saline was EC1 plus synaptic blockers.

Fast transient sodium current in CR-positive PG cells

The fast transient sodium current, or $I_{Na(F)}$, has been isolated by applying in the external solution 20 mM TEA and 100 µM Cd^{2+} in order to block potassium and calcium current, respectively; all voltage clamp experiments on the sodium conductance have been carried out under these conditions. A precise control of the membrane potential resulted difficult to obtain; this is probably related to a prevalent expression of Na^{+} channels on the processes of these cells. Consequently, only when the compensation applied was acceptable, the neurons have been recorded.

Activation

To evaluate both the amplitude of the fast sodium current and its activation kinetics, the same activation protocol above-mentioned has been applied. It consisted of thirteen depolarizing steps, from -80 to +40 mV, lasting 20 ms. This short time, in fact, was enough to evoke this fast-activating current. Importantly, the holding potential of the protocol was set to -100 mV, to ensure that the fraction of sodium inactivated channels was negligible. At potentials more positive than -50 mV, the sodium current is evoked and increases up to -20 mV, when it reaches the maximum amplitude in less than 2 ms (Figure 19).

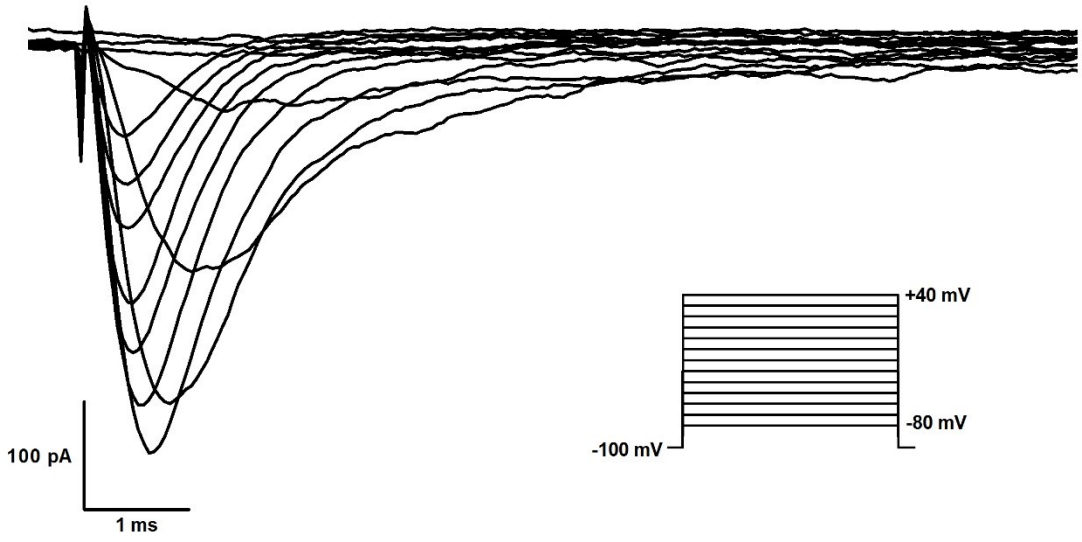

Figure 19 Fast transient sodium current activation. Sodium currents recorded in response to depolarizing voltage steps ranging from -80 to +40 mV (10 mV increments), from a holding potential of -100 mV; external saline was EC1 plus synaptic blockers, 20 mM TEA, 100 µM Cd^{2+}.

The I/V relationship of the Na^+ current has been obtained in a group of 19 neurons. For this analysis, the theoretical amplitude of the current evoked at the beginning of the depolarizing pulse has been used; this value was calculated by extrapolating to zero time the best fit of the decaying phase of the current.

Observing the I/V relationship (Figure 20), it may be observed that the Na^+ current peaks at -20 mV, when it reaches an amplitude of -943.70 ± 113.19 pA (n=19).

In addition, the sodium equilibrium potential, measured indirectly from the extrapolation of the I/V plot to the x-axis, can be estimated between +60 and +70 mV, a good approximation of the theoretical reversal potential predicted by Nernst equation.

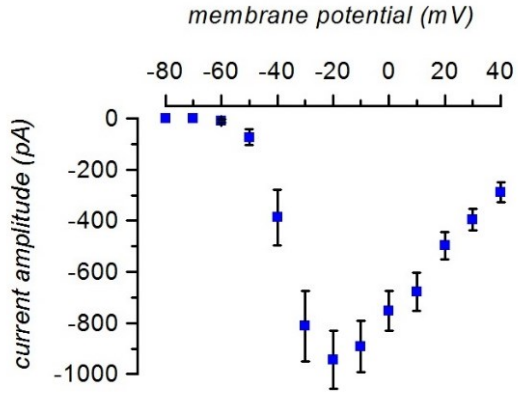

Figure 20 I/V relationship of fast transient sodium currents. Average data obtained from 19 neurons in thin slices; external saline was EC1 plus synaptic blockers, 20 mM TEA, 100 µM Cd^{2+}.

Inactivation

To study the voltage-dependent inactivation characterizing the fast transient sodium current in the CR-positive PG cells, a classical voltage clamp protocol has been used (Figure 21A). A first step (conditioning pulse) was imposed at voltages ranging from -120 to -20 mV for 100 ms to let the channel inactivation to reach its steady-state value. Next, the cell membrane was depolarized to the fixed test potential of 0 mV in order to measure the fraction of non-inactivated $I_{Na(F)}$ for each conditioning potential (Hodgkin and Huxley, 1952).

In the subsequent off-line analysis, the currents evoked were normalized to the maximum current elicited at 0 mV, and plotted as a function of the voltage command applied in the preconditioning pulse. Average data, obtained in 9 neurons, show a sigmoidal dependence on voltage (Figure 21C). Moreover, the resulting steady-state inactivation curve can be described by the Boltzmann equation (Eq. 1). In our preparation, the half-maximal inactivation potential V_{50} of the fast transient sodium current is -69.77 mV and the slope factor k is 9.78 mV. Interestingly, when the current elicited reaches the maximum amplitude, the fraction of inactivated sodium current is virtually abolished.

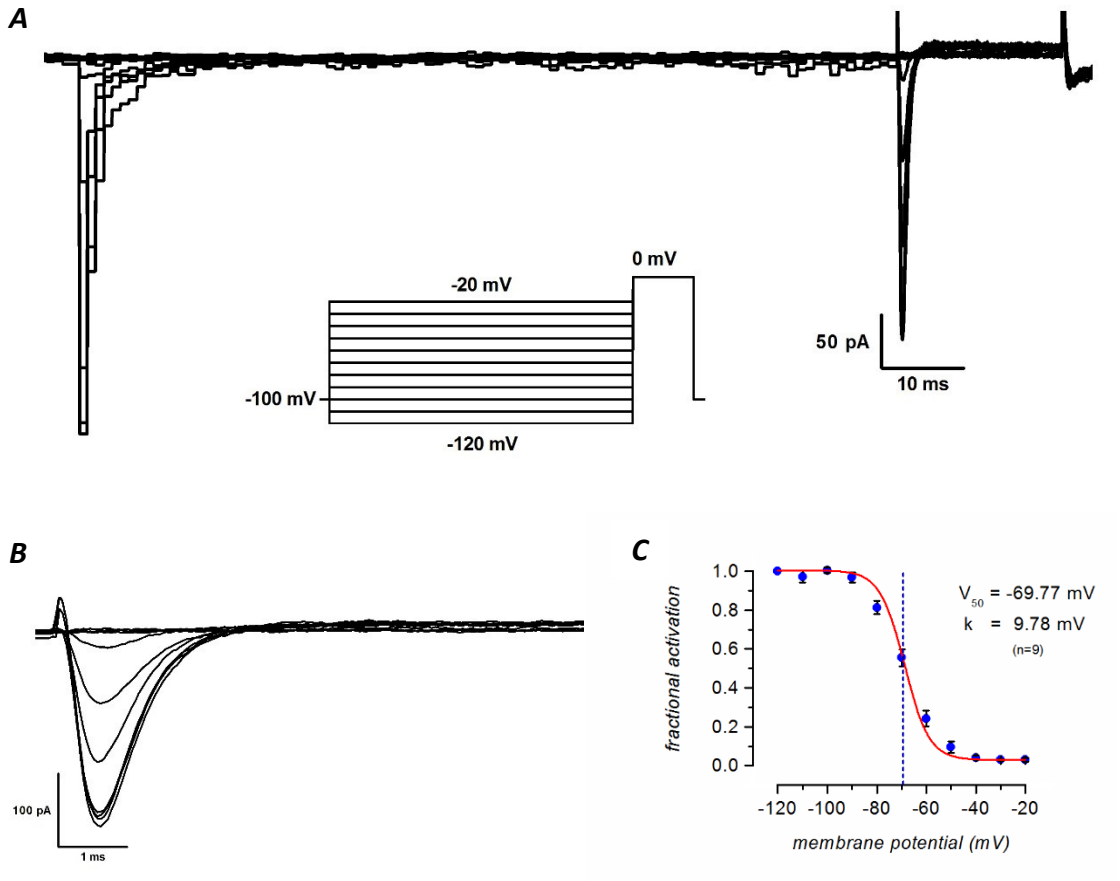

Figure 21 Fast transient sodium current inactivation. A: representative current traces for the analysis of inactivation. The membrane have been held at -100 mV and then depolarized to test voltages from -120 to -20 mV in 10 mV increments. Sodium current has been fully activated in response to a second pulse to 0 mV, following test voltages (see protocol in the panel below); external saline was EC1 plus synaptic blockers, 20 mM TEA, 100 µM Cd2+. B: magnification of the currents elicited during the second pulse to 0 mV in the panel A. C: Fractional activation of the sodium current in a group of 9 neurons as a function of voltage using the protocol shown in A. The continuous curve is the Boltzmann fit, with V50 at -69.77 mV and k at 9.78 mV.

Deactivation

Finally, the recovery of the fast transient sodium current from inactivation has been evaluated using the double-pulse protocol shown in Figure 22.

From the holding potential of -70 mV, the membrane potential is commanded to a first depolarizing potential to 0 mV for 100 ms to completely inactivate the sodium conductance; next, a second pulse to -20 mV (the potential at which the largest current is observed) is delivered after an interval of variable duration during which the membrane is commanded to -110 mV; depending on the duration of the interval, different fractions of the sodium conductance recovers from inactivation. The behavior of a CR-positive PG neuron in response to the described protocol can be observed in Figure 22: The current amplitudes progressively increased as a function of the length of the hyperpolarizing pulse applied, and the peak amplitudes could be fitted with a single exponential function (Eq.2). The value of the deactivation time constant τ in our cells was 11.75 ± 1.07 ms (n=15).

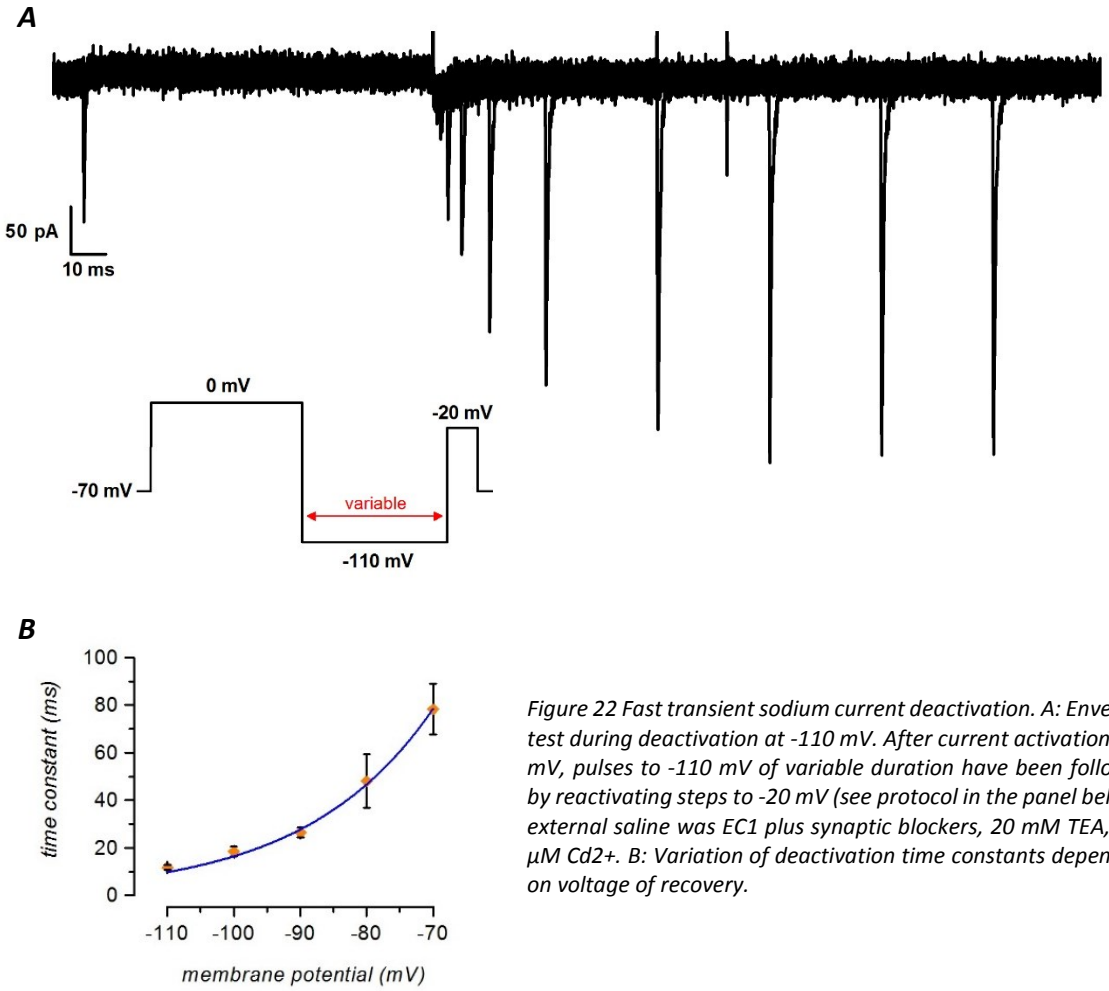

Figure 22 Fast transient sodium current deactivation. A: Envelope test during deactivation at -110 mV. After current activation at 0 mV, pulses to -110 mV of variable duration have been followed by reactivating steps to -20 mV (see protocol in the panel below); external saline was EC1 plus synaptic blockers, 20 mM TEA, 100 µM Cd2+. B: Variation of deactivation time constants depending on voltage of recovery.

The rate of recovery from inactivation is closely related to the potential to which the membrane is commanded during the hyperpolarizing pulse. To evaluate this relation, the protocol described has been repeated using different hyperpolarizing potentials; as expected from the Hodgkin-Huxley model, the recovery rate decreases as the potential become more positive (Figure 22):

- τ_{-70mV} = 78.30 ± 10.56 ms, n=15;
- τ_{-80mV} = 48.06 ± 11.29 ms, n=5;
- τ_{-90mV} = 26.35 ± 2.05 ms, n=16;
- τ_{-100mV} = 18.45 ± 2.07 ms; n=6.

A-type potassium current in CR-positive PG cells

The transient outward current has been recognized as an A-type potassium current (I_A). This current, TEA-insensitive, is involved in several physiological roles, like the control of the RMP or the regulation of the pacemaker activity (for a review, see Birnbaum et al., 2004). To characterize this conductance, voltage clamp experiments have been performed. In order to eliminate the sodium current, 0.6 µM TTX has been added to the external solutions.

Activation

The A-type potassium current has been analyzed by means of the activation protocol already described for the $I_{Na(F)}$: from a holding potential of -100 mV, depolarizing pulses between -80 to +40 mV in 10 mV steps were applied to evoke the currents (Figure 23). The I_A activates rapidly, reaching the peak in about 10 ms, whereas more than 100 ms are required to inactivate completely.

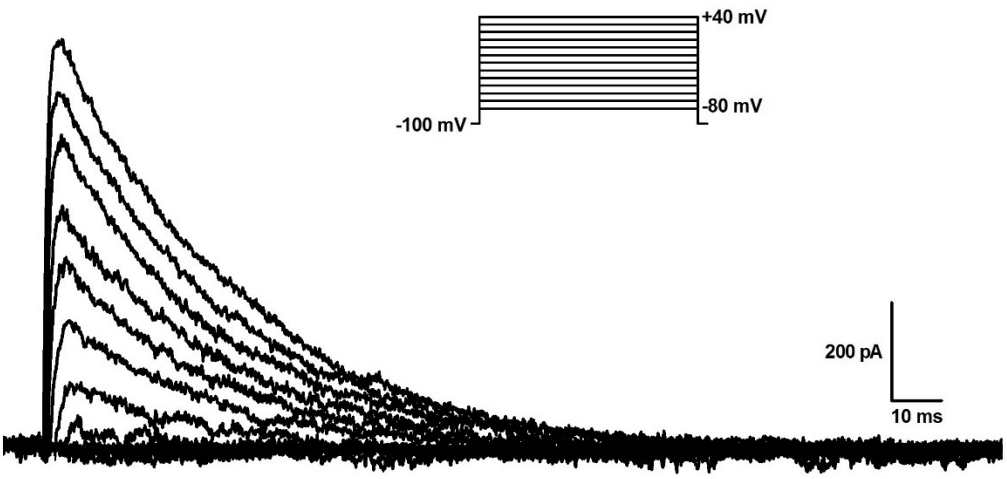

Figure 23 A-type potassium current activation. Transient potassium currents recorded in response to depolarizing voltage steps ranging from -80 to +40 mV (10 mV increments), from a holding potential of -100 mV; external saline was EC1 plus synaptic blockers, 0.6 µM TTX.

The I/V relationship of the A-type current has been obtained averaging the currents recorded in 20 cells (Figure 24). As already explained for the sodium conductance, the current amplitudes used in the analysis have been calculated by extrapolating the exponential fitting the decaying phase to time of the onset of the depolarizing pulse. The I_A in the CR-positive PG cells can be elicited at potentials positive to -30 mV and grows in amplitude as the membrane potential becomes more positive. At the maximal depolarizing potential tested (+40 mV), a current amplitude of 1188.33 ± 148.86 pA has been measured (n=20).

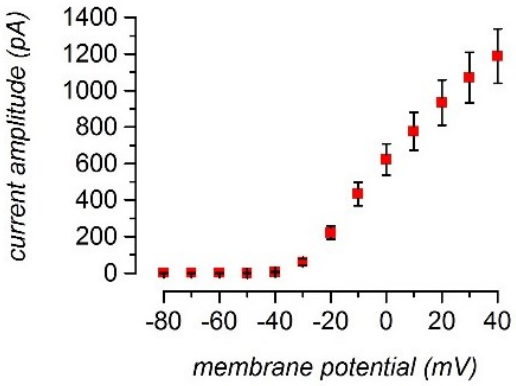

Figure 24 I/V relationship of A-type potassium currents. Average data obtained from 20 neurons in thin slices; external saline was EC1 plus synaptic blockers, 0.6 µM TTX.

Inactivation

Next, the steady-state voltage dependence of the A-type current inactivation has been studied. Under voltage clamp conditions, the cell membrane is preconditioned to potentials extending from -110 to +10 mV (in order to inactivate different fractions of the channels), and subsequently depolarized to the test voltage of 0 mV. This protocol is similar to that used for the sodium current inactivation. Nevertheless, it should be noted that the I_A inactivation requires a longer pre-pulse duration (200 ms vs 100 ms) to reach the steady-state. An exemplifying recording is illustrated in Figure 25.

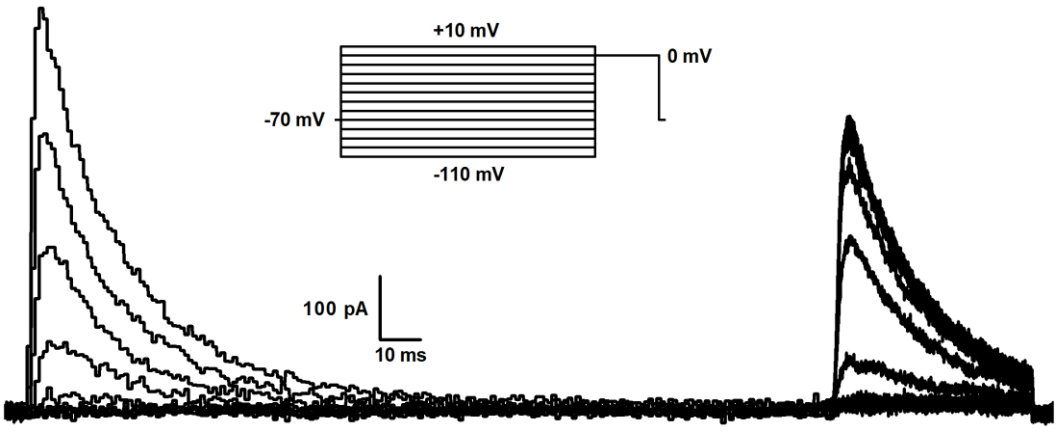

Figure 25 A-type potassium current inactivation. Representative current traces for the analysis of inactivation. The membrane have been held at -100 mV and then depolarized to test voltages from -110 to +10 mV in 10 mV increments. Potassium current has been fully activated in response to a second pulse to 0 mV, following test voltages (see protocol in the panel below); external saline was EC1 plus synaptic blockers, 0.6 µM TTX.

Again, the normalized transient potassium currents evoked at the test pulse (analyzed as described for $I_{Na(F)}$) are plotted as a function of the membrane potential set in the preconditioning command. Average data, displayed in Figure 26, are obtained from a sample of 12 CR-positive PG cells. The curve is described using the Boltzmann equation (Eq. 1), where the half-maximal inactivation potential V_{50} and the slope factor k are -53.25 mV and 7.52 mV, respectively.

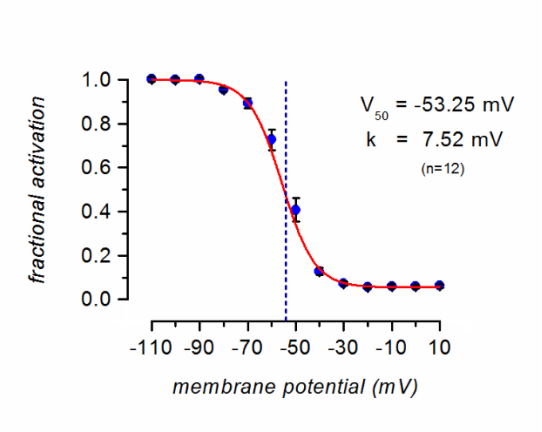

Figure 26 Fractional activation of the potassium current in a group of 12 neurons as a function of voltage using the protocol shown in figure 17. The continuous curve is the Boltzmann fit, with V50 at -53.25 mV and k at 7.52 mV; external saline was EC1 plus synaptic blockers, 0.6 µM TTX.

Deactivation

The last series of experiments regarding the I_A study were aimed at describing the rate of recovery from steady-state inactivation. Neurons, starting from -70 mV, have been depolarized to +20 mV two times: the first to inactivate the potassium current, the second to evaluate the recovery. Between them, a hyperpolarizing voltage command variable in duration has been applied (Figure 27A). Recovery curves originated from double-pulse experiments followed a single-exponential time course (Eq. 2), and permit to calculate the different deactivation time constants τ related to each recovery potential tested. The following results are graphed in Figure 27B:

- τ_{-70mV} = 41.88 ± 5.43 ms, n=7;
- τ_{-80mV} = 27.79 ± 4.27 ms, n=6;
- τ_{-90mV} = 20.46 ± 2.22 ms, n=7;
- τ_{-100mV} = 15.05 ± 2.63 ms; n=5;
- τ_{-110mV} = 14.08 ± 1.77 ms; n=7;
- τ_{-120mV} = 13.62 ± 3.09 ms; n=4.

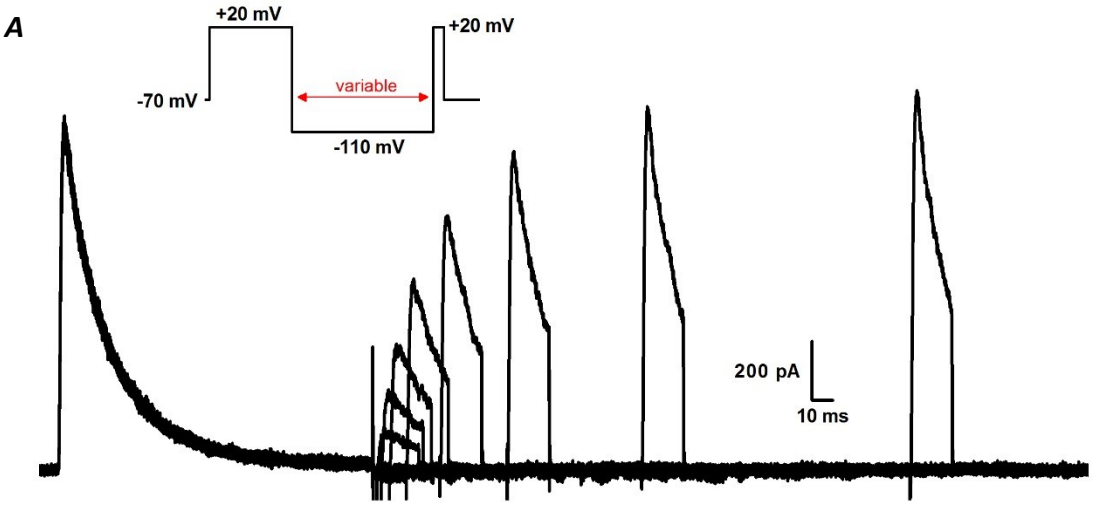

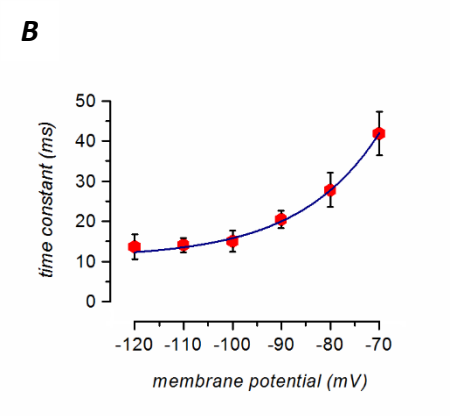

Figure 27 A-type potassium current deactivation. A: Envelope test during deactivation at -110 mV. After current activation at +20 mV, pulses to -110 mV of variable duration have been followed by reactivating steps to +20 mV (see protocol in the panel above); external saline was EC1 plus synaptic blockers, 0.6 µM TTX. B: Variation of deactivation time constants of A-type potassium current, depending on voltage of recovery.

L-type calcium current in CR-positive PG cells

For its biophysical properties, the persistent inward current, detected during prolonged depolarizing pulses, has been identified as a L-type calcium current ($I_{Ca(L)}$).

For the voltage clamp experiments shown below, the extracellular solution EC4 has been utilized (see Solutions). In this saline, extracellular sodium was substituted for by an equimolar amount of choline chloride, in order to suppress the $I_{Na(F)}$. In addition, the block of the I_A has been achieved with the simultaneous addition of 20 mM TEA and replacement of K^+ with Cs^+ in the intracellular solution. The protocol applied to evoke the current presented voltage commands ranging from -80 to +40 mV, starting from a holding potential of -70 mV (Figure 28) Current amplitudes in all the analysis have been measured averaging the last 10 ms at the end of each step.

The Figure 28, shown below, represents a typical recording of the L-type calcium current in response to the protocol under the experimental conditions described.

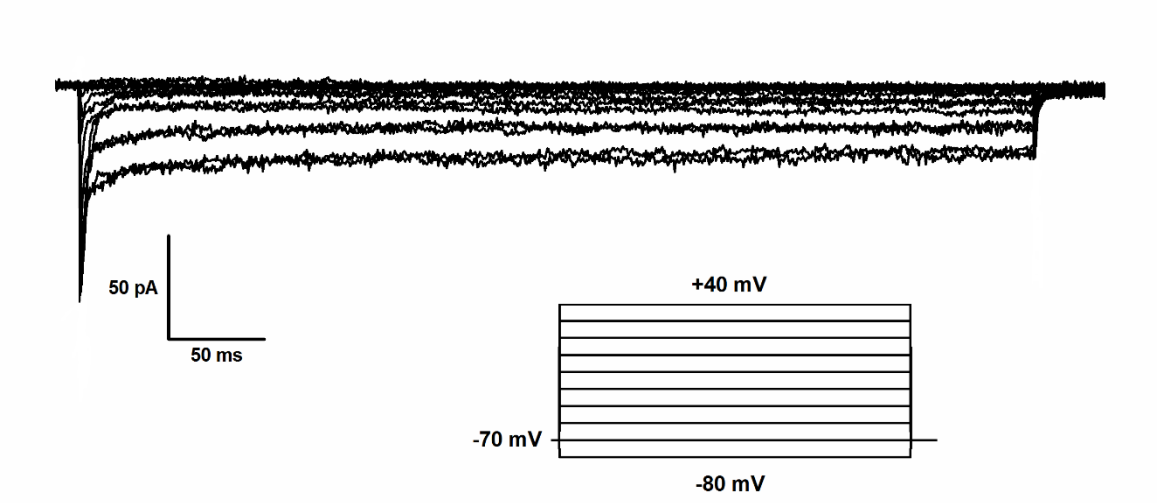

Figure 28 L-type calcium current activation. Persistent calcium currents recorded in response to depolarizing voltage steps ranging from -80 to +40 mV (10 mV increments), from a holding potential of -70 mV; tracings recorded in the presence of 0.6 µM TTX, 20 mM TEA in the extracellular solution, and with Cs^+ as a substitute for K^+ ions in the intracellular solution.

The I/V relationship of the $I_{Ca(L)}$, illustrated in Figure 30, has been obtained from 14 CR-positive PG neurons. In this sample, the current has been observed to reach a maximum amplitude of -26.37 ± 4.71 pA at 0 mV (n=14).

Barium substitution

Barium ions are known to permeate the L-type calcium channels more easily than the calcium ions (Hille, 1992). When calcium was substituted for by 4 mM Ba^{2+} in the extracellular solution, we observed an increase of the current amplitudes (figure 29) : barium currents through L-type channels were about twice as large as calcium currents, reaching an amplitude of -42.58 ± 7.03 pA at the peak (n=10).

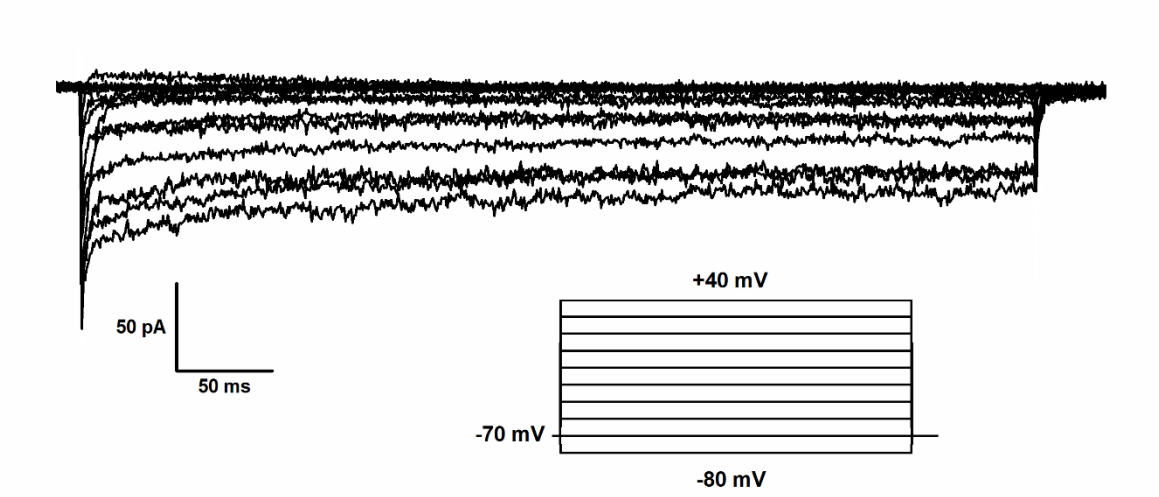

Figure 29 Barium current activation. Currents recorded in the same conditions described in figure 20, after replacement of extracellular Ca^{2+} with 4 mM Ba^{2+}.

Interestingly, in the I/V relationships calculated from 10 cells and plotted in Figure 30, it should be noted that barium substitution provokes a change in the voltage dependence of the channel, shifting the current peak from 0 to -10 mV.

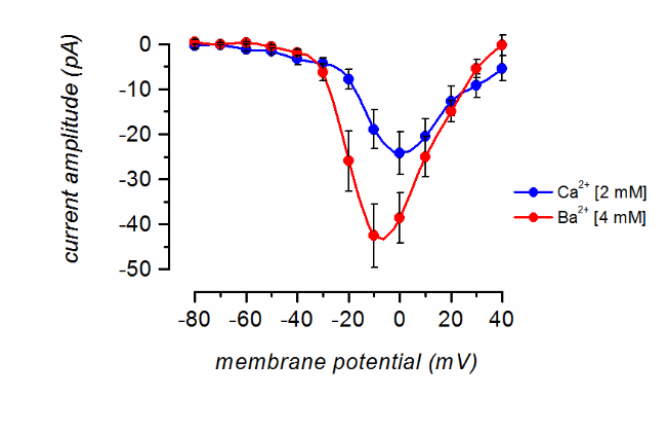

Figure 30 I/V relationship of Ca^{2+} and Ba^{2+} currents. Voltage dependence of calcium (blue) and barium (red) currents from 14/10 neurons in thin slices; tracings recorded in the presence of 0.6 µM TTX, 20 mM TEA in the extracellular solution, and with Cs^{+} as a substitute for K^{+} ions in the intracellular solution.

Cadmium block

Cadmium is a common blocker of several types of calcium channel (Hille, 1992). In our analysis, the effect of 100 µM Cd^{2+} on the current sustained by barium ions have been assessed in 3 CR-positive cells (Figure 31). On average, cadmium has been proved to block 89.45 ± 19.57 % (n=3) of the barium current measured at its peak (-10 mV).

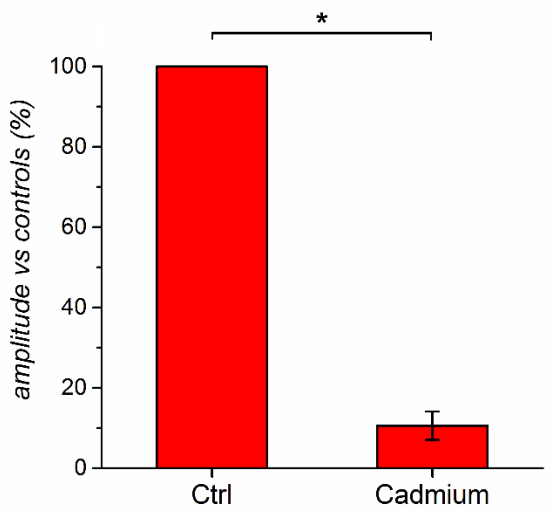

Figure 31 Histogram showing the effect of 100 µM Cd^{2+} measured at -10 mV in 3 cells.

Nifedipine block

The last series of experiments was aimed at investigating the suppression of the barium current by 20 µM nifedipine. This drug is a selective blocker of the L-type calcium channels (McCleskey et al., 1986). In our preparation, nifedipine suppresses the 81.60 ± 14.81 % (n=4) of the barium current at -10 mV, the point of its maximal amplitude (Figure 32).

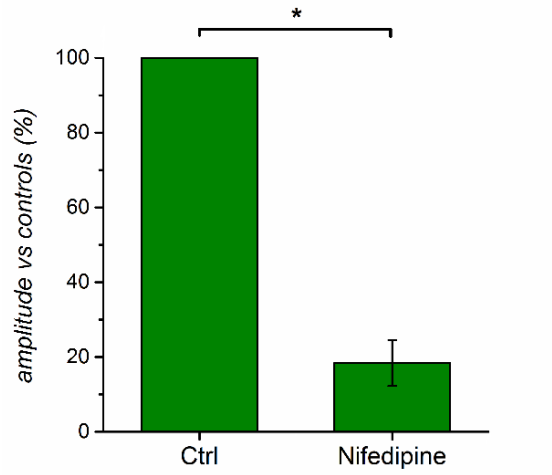

Figure 32 Histogram showing the effect of 20 µM Nifedipine measured at -10 mV in 4 cells.

DISCUSSION

The olfaction represents a fundamental sense for every life form: its role is to obtain the greatest number of information from the external environment, in order to evoke the appropriate physiological response to each situation. In particular, in the olfactory system, the olfactory bulb is an interesting structure for its unique features.

First, this region is the first center processing the olfactory information coming from the olfactory epithelium. Second, some neuronal classes in the olfactory bulb are continuously replaced also in the postnatal period. Therefore, this structure constitutes a model for several studies, aimed to clarify the mechanisms underlying the processing of the information in our brain or the adult neurogenesis.

My research has been focused on the characterization of the electrophysiological properties of two types of bulbar neurons: dopaminergic and calretinin-positive periglomerular cells. Both these neurons belong to the periglomerular class, which is located in the glomerular layer and contributes to generate the microcircuitry into the glomeruli. Periglomerular interneurons involved in the modulation of the signals from the olfactory sensory neurons to the bulbar projection neurons can be distinguished in type 1 and type 2, according as they expand their dendritic arborization in both the ON zone and the non-ON zone or only in the latter. Dopaminergic neurons are type 1 periglomerular cells, whereas calretinin-positive cells belong to the type 2. The two types are supposed to play different roles in the glomerular circuitry.

Dopaminergic periglomerular cells

The first part of my thesis was aimed at completing the electrophysiological characterizations of the dopaminergic periglomerular cells already initiated by our group (Pignatelli et al., 2005). Dopaminergic PG cells are characterized by spontaneous activity, which persists also in absence of external stimuli, as it can be seen in dissociated cells. Five depolarization-activated conductances have been isolated and analyzed. A non-inactivating potassium current and a fast transient sodium current represent the two larger currents. In addition, a persistent sodium conductance and two different types of calcium conductances (L-type and T-type) have been identified. Of these conductances, only the persistent sodium current and the T-type calcium current have been demonstrated to give a significant contribution to the pacemaker mechanisms.

Two hyperpolarization-activated currents with inward rectifying properties have been also detected in the dopaminergic periglomerular neurons. The first has been identified as a classical potassium inward rectifier (K_{ir}) current for its fast kinetics, selective permeability to K^+ ions, suppression by extracellular Ba^{2+} and Cs^+, and voltage-dependence dependent on extracellular K^+ concentration. The electrophysiological description of this conductance has been illustrated in a recent work of our group (Borin et al., 2014).

The h-current, the second type of hyperpolarization-activated current, represents the object of my investigation. This mixed cation current displays a reversal potential substantially positive to E_K, a relatively slow activation kinetics, is relatively insensitive to Ba^{2+}, and does not show a voltage sensitivity dependent on $[K^+]_o$ (Hibino et al., 2010). In addition, this current is sensitive to drugs very selective for HCN channels. like ivabradine or ZD7288.

It is still not clear which type of HCN channels is expressed in the olfactory bulb.. As already mentioned, the HCN gene family consists of four members, which are able to generate both homo- and heterotetrameric channels (Wahl-Schott and Biel, 2009). In the Allen Brain Atlas, only the expression of HCN4 subunit is found in the olfactory bulb, whereas other studies detect both HCN2 and HCN4 subunits (Santoro et al., 2000). To further complicate the picture, almost all the family members are detected through in situ hybridization methods (Moosmang et al., 1999; Monteggia et al., 2000). Using immunohistochemical techniques, high expression levels of HCN3 subunit has been reported in the GL (Notomi and Shigemoto, 2004; Mistrik et al., 2005). In a more recent study, it has been reported the expression of all four HCN subunits in the majority of the bulbar cell populations, with at least 17 different combinations of staining patterns (Fried et al., 2010). Anyway, no HCN subunit has been detected in the soma of dopaminergic periglomerular cells. The explanation of this result is unclear, but certainly, as it can be inferred from the analysis of the electrophysiological recordings, low levels of expression in these cells are expected, probably with a preferential localization in the dendritic compartment, which, extending into the glomerular neuropil, cannot be easily assigned to a specific cell type.

A first observation was that in dissociated cells the h-current is rather small, whereas in slices its amplitude is more than three times larger. This observation could suggest that the HCN channels are mainly expressed in the dendrites (largely lost in the dissociation procedure), or that these channels are damaged by the enzymatic treatment. In spite of the prevalent dendritic localization of h-channels, suggesting a role in the modulation of synaptic input, and despite its small amplitude, the h-current also importantly contributes to the RMP.

A series of experiments have been carried out to investigate the kinetics of the h-current. At 37 °C and using 1 s hyperpolarizing pulses, a half-maximal activation potential V_{50} of -94.1 ± 2.0 mV with a slope factor k of 9.88 ± 0.28 mV have been found. It should be noted that, on the basis of the activation curve obtained from our data, at rest (-65 mV) only 5% of the HCN channels would be open in our cells. Furthermore, The V_{50} has been shown to depend on the length of the first step of the protocol used, resulting -94.1 ± 2.0 mV for 1 s stimuli and -84.5 ± 1.2 mV for 4 s stimuli. Therefore, longer durations provoke the shift of the steady-state activation curve to more positive potentials. The functional implication of this shift becomes more evident considering that, assuming an approximate slope factor of 9 (the slope displays only a modest increase with change in conditioning step), at rest about 12.7% HCN channels are open. The fraction is small but, since

the input resistance of these cells is 915.69 ± 31.31 MΩ (n=248), the current sustained is sufficient to provide a significant depolarizing contribution to the resting membrane potential.

A further observation concerned the effects of the temperature. The h-current, in fact, has been reported to be critically influenced by thermic conditions in several papers (Hart, 1983; Yanagida et al., 2000; Pena et al., 2006). Our experiments confirmed this effect also in the dopaminergic periglomerular cells. Change of temperature has been demonstrated to affect the amplitude of the h-current (the Q_{10} between -100 and -130 mV has been calculated around 2.87 ± 0.38). In addition, also the maximal conductance (from 0.93 nS at 22 °C to 3.08 nS at 37 °C), the half-maximal activation potential (from -95.4 ± 2.3 mV at 27 °C to -84.2 ± 1.3 mV at 37 °C), the rate of development (the Q_{10} between -100 and -130 mV is 4.72), and the deactivation time constant resulted sensitive to the thermic conditions. Consequently, the temperature is a critical parameter during the experiments on the h-current, requiring a careful control.

Next, the role of the h-current in the autorhythmicity has been investigated under current clamp conditions.

The pharmacological block of the h-current with Cs^+, ivabradine or ZD7288, has been observed to induce a mean hyperpolarization of 7 mV, enough to stop the spontaneous firing. Considering that the spontaneous activity can easily disappear by changes of few millivolts of the RMP (Pignatelli et al., 2005), this observation is not unexpected. Further experiments demonstrated that the I_h is not directly involved in the pacemaker mechanism, but plays a relevant role in defining the resting membrane potential of the dopaminergic PG cells.

Notably, these results are different to those observed by Puopolo (Puopolo et al., 2005), who did not observe any effect on spontaneous firing and RMP using ZD7288. This inconsistency could be explained in several ways. First, our experiments are carried out in perforated patch and not in whole cell configuration. Second, the blocker used in our experiments is ivabradine: its effect is fast and reversible, whereas ZD is slow, and in the cited paper was applied only for a minute. Lastly, the data were obtained at different thermic conditions.

The last part of the study is focused on the modulation of the h-current. HCN channels are known to be directly activated by cAMP (DiFrancesco and Tortora, 1991). Accordingly, application of 10 µM forskolin and 0.1 mM IBMX in the bath have been observed to cause a 48.7% increase of the I_h. This effect is at least in part sustained by a positive shift of the steady-state activation curve. The increase of the intracellular levels of cAMP in our preparation, in fact, has been verified to provoke a V_{50} shift from -85.26 ± 1.96 to -75.77 ± 2.41 mV. In addition, an enhanced concentration of cAMP induces a depolarization of the membrane positively correlated with the resting membrane potential. This effect is justified by the higher degree of activation (and hence by the greater importance) of the h-current at more negative potentials. Notably, the increase of the intracellular levels cAMP has been observed to have an opposite effect on the K_{ir} current

amplitude in these cells (Borin et al., 2014). This evidence suggests the existence of common modulatory mechanisms of the two hyperpolarization-activated current in the dopaminergic PG cells.

A final group of experiments has been made to evaluate the effects of the neurotransmitters on the h-current. Indeed, many neurotransmitters, capable to interact with the cAMP pathway, are released on the dopaminergic periglomerular cells. In our experiments, several compounds have been tested: monoamine (dopamine, serotonin, histamine), and metabotropic cholinergic and GABAergic agonists (oxotremorine and baclofen). All these neurotransmitters have been observed to influence the excitability profile of the neurons under study, but none of them displayed any effect on the amplitude of the h-current. The only significant effect detected on the I_h is elicited by the noradrenaline, producing a decrease of the amplitude. Examining the effect of different selective noradrenergic agonists, we have shown that NA inhibition can be mimicked by clonidine (α2 agonist). A similar effect of the noradrenaline has been reported also in other preparations, as dorsal ganglion neurons and midbrain (Yagi and Sumino, 1998; Cathala and Paupardin-Tritsch, 1999; Inyushin et al., 2010). On the contrary, in other areas the application of noradrenaline has been associated to an amplitude increase of the h-current (Pape and McCormick, 1989; Maccaferri and McBain, 1996).

All the noradrenergic projections to the olfactory bulb originate from the pontine nucleus and the *locus cœruleus*, which contain the largest collection of NA-containing cells in the brain (Záborszky et al., 1986; McLean et al., 1989). NA fibers preferentially target the internal plexiform layer and the granule cell layer, and, to a lesser extent, the mitral cell layer and the external plexiform layer (McLean et al., 1989). The functional role of NA in adult rodent olfactory bulb has been accurately reviewed (Linster et al., 2011): converging data from electrophysiological studies of OB neurons cellular-membrane properties and behavioral assays of perception indicate that NA affects the olfactory bulb network improving odor detection and discrimination. Most of the available electrophysiological data concerning the NA effect in different cell types of the olfactory bulb are limited to the granule and mitral cell layer. As for the glomerular layer, despite the fact that all NA receptor types have been localized in this region (Young and Kuhar, 1980; Day et al., 1997; Domyancic and Morilak, 1997; Winzer-Serhan et al., 1997), no data concerning possible modulation roles of NA inputs are available. Our observation, therefore, represents the first report of NA action in a specific subpopulation of glomerular cells, and is well in line with the general effect of NA: dopamine released by glomerular dopaminergic cells is known to inhibit glutamate release from olfactory nerve terminals (Ennis et al., 2001). Consequently, an inhibition of the h-current, with its hyperpolarizing effect, would decrease the DA-mediated tonic inhibition of olfactory nerve terminals, in line with the general positive influence of NA on odor detection and discrimination.

CR-positive periglomerular cells

The second part of my thesis has been focused on the CR-positive periglomerular cells. These neurons, belonging to the type-2 PG cells, do not directly interact with the ON axons, but are in contact only with bulbar neurons. CR-positive cells are one of the bulbar interneuron subtypes undergoing adult neurogenesis (De Marchis et al., 2007; Batista-Brito et al., 2008), suggesting a possible role in the adaptive capability of glomerular circuitry to external stimuli.

This study represents the first analysis of the functional properties of CR-positive cells of the OB. For this study, we used a transgenic mouse strain in which the GFP transgene is under the calretinin promoter. All recordings have been made in whole cell configuration.

A first observation is that the CR-positive cells show a low variability in their passive properties (membrane capacitance and input resistance), indicating that these neurons belong to a single cellular population.

Under voltage clamp conditions, depolarizing steps applied in normal saline evoke three different currents: a fast transient sodium current, a persistent calcium current and a transient potassium current. Each of these conductances has been pharmacologically isolated and described in its basic properties. The two larger currents have been identified as the classical sodium current and the A-type potassium current. A fast inactivation process characterizes both these conductances.

The $I_{Na(F)}$ in these neurons shows a classical kinetics, reaching its maximal amplitude (-943.70 ± 113.19 pA) at -20 mV. The steady-state inactivation curve of this current has presents a midpoint of -69.77 mV, and a slope factor of 9.78 mV. The analysis of the A-type potassium current followed similar experimental protocols. The I/V relationship of the I_A display a conventional voltage dependence, in which the current is evoked at potentials positive to -30 mV and its amplitude increases as the membrane potential becomes more positive (1188.33 ± 148.86 pA at +40 mV). From the analysis of I_A inactivation kinetics, the values of V_{50} and k resulted -53.25 mV and 7.52 mV, respectively. The smaller of the voltage-dependent conductances present in these cells is represented by the L-type calcium current. To analyze this conductance, pharmacological blocks have been used to eliminate any contamination from the other currents. The suppression of the current with Cd^{2+} demonstrated that it is carried by Ca^{2+} ions (Hille, 1992), whereas the channel subtype has been identified by applying nifedipine, a selective blocker of L-type calcium channels (McCleskey et al., 1986). This calcium current displays a typical I/V relationship, with an average maximal amplitude of -26.37 ± 4.71 pA at 0 mV. Interestingly, substitution of the calcium with 4 mM Ba^{2+} provokes not only an increase of the current sustained by the L-type calcium channels, but also a negative shift of the voltage dependence. In Ba^{2+}, we found a maximal amplitude of -42.58 ± 7.03 pA at -10 mV.

CONCLUSION

Periglomerular cells in the olfactory bulb participate in the generation of the glomerular microcircuitry, and are involved in the processing of the olfactory information originating from the olfactory epithelium. Despite their physiological role, the role of neurons in the processing of olfactory information within the OB is still largely unknown. In my thesis, some property of two distinct subpopulations of periglomerular cells have been investigated by patch clamp technique.

The first part of my work consisted in the analysis of the h-current in the dopaminergic periglomerular neurons. The h-current has been thoroughly investigated , using voltage clamp and current clamp protocols, in both whole cell and perforated patch configuration. Several series of experiments on this current revealed its biophysical properties, pharmacology, modulation, and role in autorhythmicity. The results of this study, already published (Pignatelli et al., 2013), is part of a more general project aimed at obtaining a complete characterization of the electrophysiological properties of these cells in order to understand their role in the bulbar circuitry. Dopaminergic periglomerular neurons, indeed, have been demonstrated to influence significantly the activity of the other components of the glomerular network, thus participating to the processing of olfactory information before the signal is transmitted to other brain areas.

The second part of my thesis was focused on the study of the calretinin-positive periglomerular cells. The function of these cells is even more elusive, since descriptions of their features are entirely absent in literature. In this work, basic properties of the calretinin-positive neurons have been characterized. In addition, under voltage clamp conditions, the three main conductances of these cells have been isolated and analyzed. All the results collected represent the first electrophysiological description of calretinin-positive periglomerular cells. Although these information are not sufficient to clarify how these interneurons operates, this study allows a first analysis of their electrical properties, and gives the bases to identify their role in the glomerular circuitry.

Abbreviations

4-AP	*4-aminopyridine*
cAMP	C*yclic adenosine monophosphate*
BAPTA	*1,2-bis(o-aminophenoxy)ethane-N,N,N',N'-tetraacetic acid*
CB	*Calbindin*
CC	*Current clamp*
CR	*Calretinin*
cGMP	C*yclic guanosine monophosphate*
CNBD	*Cyclic nucleotide-binding domain*
CNG	*Cyclic nucleotide-gated*
CNS	*Central nervous system*
CSD	*Cyclic AMP-sensing domain*
DA	*Dopamine*
EC	*Extracellular solution*
EGTA	E*thylene glycol tetraacetic acid*
EPL	*External plexiform layer*
EPSP	*Excitatory postsynaptic potential*
ET	*External tufted*
GABA	*γ-amino butyric acid*
GAD	*Glutamic acid decarboxylase*
GL	*Glomerular layer*
GCL	*Granule cell layer*
HCN	*Hyperpolarization-activated Cyclic Nucleotide-gated*
HEPES	*4-(2-hydroxyethyl)-1-piperazineethanesulfonic acid*
I_A	*A-type potassium current*
IBMX	*3-isobutyl-1-methylxanthine*
$I_{Ca(L)}$	*L-type calcium current*
I_h	*Hyperpolarization-activated current*
I_{ins}	*I_h instantaneous component*
$I_{Na(F)}$	*Fast transient sodium current*
I_{ss}	*I_h steady-state component*
IPL	*Internal plexiform layer*
JG	*Juxtaglomerular*

K_{ir}	*Potassium inward rectifier*
MCL	*Mitral cell layer*
NA	*Noradrenaline*
OB	*Olfactory bulb*
ON	*Olfactory nerve*
OSN	*Olfactory sensory neuron*
PG	*Periglomerular*
Q_{10}	*Temperature coefficient*
RMP	*Resting membrane potential*
TEA	*Tetraethylammonium*
TH	*Tyrosine hydroxylase*
TTX	*Tetrodotoxin*
V_{50}	*Half-maximal activation potential*
VC	*Voltage clamp*
V_h	*Holding potential*

References

Allen, T.J., and Mikala, G. 1998. Effects of temperature on human L-type cardiac Ca2+ channels expressed in Xenopus oocytes. Pflugers Arch. 436:238–247.

Altman, J. 1962. Are new neurons formed in the brains of adult mammals?. Science. 135:1127–1128.

Altman, J. 1969. Autoradiographic and histological studies of postnatal neurogenesis. IV. Cell proliferation and migration in the anterior forebrain, with special reference to persisting neurogenesis in the olfactory bulb. J Comp Neurol. 137:433–457.

Altomare, C., Terragni, B., Brioschi, C., Milanesi, R., Pagliuca, C., Viscomi, C., Moroni, A., Baruscotti, M., and DiFrancesco, D. 2003. Heteromeric HCN1-HCN4 channels: a comparison with native pacemaker channels from the rabbit sinoatrial node. J Physiol. 549:347–59.

Aponte, Y., Lien, C.-C., Reisinger, E., and Jonas, P. 2006. Hyperpolarization-activated cation channels in fast-spiking interneurons of rat hippocampus. J Physiol. 574:229–243.

Aroniadou-Anderjaska, V., Ennis, M., and Shipley, M.T. 1997. Glomerular synaptic responses to olfactory nerve input in rat olfactory bulb slices. Neuroscience. 79:425–434.

Ashcroft, F.M., and Rorsman, P. 2013. K(ATP) channels and islet hormone secretion: new insights and controversies. Nat Rev Endocrinol. 9:660–9.

Atkinson, S.E., Maywood, E.S., Chesham, J.E., Wozny, C., Colwell, C.S., Hastings, M.H., and Williams, S.R. 2011. Cyclic AMP signaling control of action potential firing rate and molecular circadian pacemaking in the suprachiasmatic nucleus. J Biol Rhythms. 26:210–220.

Attwell, D., and Wilson, M. 1980. Behaviour of the rod network in the tiger salamander retina mediated by membrane properties of individual rods. J Physiol. 309:287–315.

Awatramani, G.B., Price, G.D., and Trussell, L.O. 2005. Modulation of transmitter release by presynaptic resting potential and background calcium levels. Neuron. 48:109–121.

Bader, C.R., Bertrand, D., and Schwartz, E.A. 1982. Voltage-activated and calcium-activated currents studied in solitary rod inner segments from the salamander retina. J Physiol. 331:253-84:253–284.

Bader, C.R., Macleish, P.R., and Schwartz, E.A. 1979. A voltage-clamp study of the light response in solitary rods of the tiger salamander. J Physiol. 296:1–26.

Baker, H., and Farbman, A.I. 1993. Olfactory afferent regulation of the dopamine phenotype in the fetal rat olfactory system. Neuroscience. 52:115–134.

Baker, H., Kawano, T., Margolis, F.L., and Joh, T.H. 1983. Transneuronal regulation of tyrosine hydroxylase expression in olfactory bulb of mouse and rat. J Neurosci. 3:69–78.

Barinka, F., and Druga, R. 2010. Calretinin expression in the mammalian neocortex: a review. Physiol Res. 59:665–77.

Baruscotti, M., Bucchi, A., and DiFrancesco, D. 2005. Physiology and pharmacology of the cardiac pacemaker (“funny”) current. Pharmacol Ther. 107:59–79.

Batista-Brito, R., Close, J., Machold, R., and Fishell, G. 2008. The distinct temporal origins of olfactory bulb interneuron subtypes. J Neurosci. 28:3966–3975.

Bayliss, D.A., Viana, F., Bellingham, M.C., and Berger, A.J. 1994. Characteristics and postnatal development of a hyperpolarization-activated inward current in rat hypoglossal motoneurons in vitro. J Neurophysiol. 71:119–128.

Beaumont, V., Zhong, N., Froemke, R.C., Ball, R.W., and Zucker, R.S. 2002. Temporal synaptic tagging by Ih activation and actin: Involvement in long-term facilitation and cAMP-induced synaptic enhancement. Neuron. 33:601–613.

Beaumont, V., and Zucker, R.S. 2000. Enhancement of synaptic transmission by cyclic AMP modulation of presynaptic Ih channels. Nat Neurosci. 3:133–141.

Beavo, J.A., Rogers, N.L., Crofford, O.B., Hardman, J.G., Sutherland, E.W., and Newman, E. V. 1970. Effects of xanthine derivatives on lipolysis and on adenosine 3’,5'-monophosphate phosphodiesterase activity. Mol Pharmacol. 6:597–603.

Berger, T., Larkum, M.E., and Lüscher, H.R. 2001. High I(h) channel density in the distal apical dendrite of layer V pyramidal cells increases bidirectional attenuation of EPSPs. J Neurophysiol. 85:855–868.

Berkowicz, D.A., and Trombley, P.Q. 2000. Dopaminergic modulation at the olfactory nerve synapse. Brain Res. 855:90–99.

Biel, M., Wahl-Schott, C., Michalakis, S., and Zong, X. 2009. Hyperpolarization-activated cation channels: from genes to function. Physiol Rev. 89:847–85.

Bignetti, E., Cavaggioni, A., Pelosi, P., Persaud, K.C., Sorbi, R.T., and Tirindelli, R. 1985. Purification and characterisation of an odorant-binding protein from cow nasal tissue. Eur J Biochem. 149:227–231.

Birnbaum, S.G., Varga, A.W., Yuan, L.-L., Anderson, A.E., Sweatt, J.D., and Schrader, L.A. 2004. Structure and function of Kv4-family transient potassium channels. Physiol Rev. 84:803–833.

Bogaert, P.P. Van, and Pittoors, F. 2003. Use-dependent blockade of cardiac pacemaker current (If) by cilobradine and zatebradine. Eur J Pharmacol. 478:161–171.

Bois, P., Bescond, J., Renaudon, B., and Lenfant, J. 1996. Mode of action of bradycardic agent, S 16257, on ionic currents of rabbit sinoatrial node cells. Br J Pharmacol. 118:1051–1057.

Bokil, H., Laaris, N., Blinder, K., Ennis, M., and Keller, A. 2001. Ephaptic interactions in the mammalian olfactory system. J Neurosci. 21:RC173.

Borin, M., Fogli Iseppe, A., Pignatelli, A., and Belluzzi, O. 2014. Inward rectifier potassium (Kir) current in dopaminergic periglomerular neurons of the mouse olfactory bulb. Front Cell Neurosci. 8:223.

BoSmith, R.E., Briggs, I., and Sturgess, N.C. 1993. Inhibitory actions of ZENECA ZD7288 on whole-cell hyperpolarization activated inward current (If) in guinea-pig dissociated sinoatrial node cells. Br J Pharmacol. 110:343–349.

Boyes, J., Bolam, J.P., Shigemoto, R., and Stanford, I.M. 2007. Functional presynaptic HCN channels in the rat globus pallidus. Eur J Neurosci. 25:2081–2092.

Brown, H., and DiFrancesco, D. 1980. Voltage-clamp investigations of membrane currents underlying pace-maker activity in rabbit sino-atrial node. J Physiol. 308:331–51.

Brown, H.F., DiFrancesco, D., and Noble, S.J. 1979. How does adrenaline accelerate the heart?. Nature. 280:235–236.

Brünig, I., Sommer, M., Hatt, H., and Bormann, J. 1999. Dopamine receptor subtypes modulate olfactory bulb gamma-aminobutyric acid type A receptors. Proc Natl Acad Sci U S A. 96:2456–2460.

Bucchi, A., Baruscotti, M., and DiFrancesco, D. 2002. Current-dependent Block of Rabbit Sino-Atrial Node If Channels by Ivabradine. J Gen Physiol. 120:1–13.

Bucchi, A., Tognati, A., Milanesi, R., Baruscotti, M., and DiFrancesco, D. 2006. Properties of ivabradine-induced block of HCN1 and HCN4 pacemaker channels. J Physiol. 572:335–46.

Buck, L.B., and Axel, R. 1991. A novel multigene family may encode odorant receptors:a molecular basis for odor recognition. Cell. 65:175–187.

Cathala, L., and Paupardin-Tritsch, D. 1999. Effect of catecholamines on the hyperpolarization-activated cationic Ih and the inwardly rectifying potassium I(Kir) currents in the rat substantia nigra pars compacta. EurJ Neurosci. 11:398–406.

Cave, J.W., and Baker, H. 2009. Dopamine systems in the forebrain. Adv Exp Med Biol. 651:15–35.

Chan, C.S., Glajch, K.E., Gertler, T.S., Guzman, J.N., Mercer, J.N., Lewis, A.S., Goldberg, A.B., Tkatch, T., Shigemoto, R., Fleming, S.M., et al. 2011. HCN channelopathy in external globus pallidus neurons in models of Parkinson's disease. Nat Neurosci. 14:85–92.

Chao, T.I., Kasa, P., and Wolff, J.R. 1997. Distribution of astroglia in glomeruli of the rat main olfactory bulb: Exclusion from the sensory subcompartment of neuropil. J Comp Neurol. 388:191–210.

Chen, J., Mitcheson, J.S., Lin, M., and Sanguinetti, M.C. 2000. Functional roles of charged residues in the putative voltage sensor of the HCN2 pacemaker channel. J Biol Chem. 275:36465–36471.

Chen, S., Wang, J., and Siegelbaum, S.A. 2001. Properties of hyperpolarization-activated pacemaker current defined by coassembly of HCN1 and HCN2 subunits and basal modulation by cyclic nucleotide. J Gen Physiol. 117:491–504.

Cheng, L., Kinard, K., Rajamani, R., and Sanguinetti, M.C. 2007. Molecular mapping of the binding site for a blocker of hyperpolarization-activated, cyclic nucleotide-modulated pacemaker channels. J Pharmacol Exp Ther. 322:931–939.

Chow, S.S., Petegem, F. Van, and Accili, E.A. 2012. Energetics of cyclic AMP binding to HCN channel C terminus reveal negative cooperativity. J Biol Chem. 287:600–606.

Christel, C., Schaer, R., Wang, S., Henzi, T., Kreiner, L., Grabs, D., Schwaller, B., and Lee, A. 2012. Calretinin regulates Ca2+-dependent inactivation and facilitation of Ca(v)2.1 Ca2+ channels through a direct interaction with the α12.1 subunit. J Biol Chem. 287:39766–75.

Clapham, D.E. 1998. Not so funny anymore: pacing channels are cloned. Neuron. 21:5–7.

Craven, K.B., and Zagotta, W.N. 2006. CNG and HCN channels: two peas, one pod. Annu Rev Physiol. 68:375–401.

Day, H.E., Campeau, S., Watson, S.J., and Akil, H. 1997. Distribution of alpha 1a-, alpha 1b- and alpha 1d-adrenergic receptor mRNA in the rat brain and spinal cord. J Chem Neuroanat. 13:115–139.

Decher, N., Chen, J., and Sanguinetti, M.C. 2004. Voltage-dependent gating of hyperpolarization-activated, cyclic nucleotide-gated pacemaker channels: Molecular coupling between the S4-S5 and C-linkers. J Biol Chem. 279:13859–13865.

Demontis, G.C., Longoni, B., Barcaro, U., and Cervetto, L. 1999. Properties and functional roles of hyperpolarization-gated currents in guinea-pig retinal rods. J Physiol. 515 (Pt 3:813–28.

DiFrancesco, D. 1981a. A new interpretation of the pace-maker current in calf Purkinje fibres. J Physiol. 314:359–76.

DiFrancesco, D. 1981b. A study of the ionic nature of the pace-maker current in calf Purkinje fibres. J Physiol. 314:377–93.

DiFrancesco, D. 1982. Block and activation of the pace-maker channel in calf purkinje fibres: effects of potassium, caesium and rubidium. J Physiol. 329:485–507.

DiFrancesco, D., and Noble, D. 1985. A model of cardiac electrical activity incorporating ionic pumps and concentration changes. Philos Trans R Soc Lond B Biol Sci. 307:353–398.

DiFrancesco, D., and Ojeda, C. 1980. Properties of the current if in the sino-atrial node of the rabbit compared with those of the current iK, in Purkinje fibres. J Physiol. 308:353–367.

DiFrancesco, D., and Tortora, P. 1991. Direct activation of cardiac pacemaker channels by intracellular cyclic AMP. Nature. 351:145–147.

DiFrancesco, D., and Tromba, C. 1988. Muscarinic control of the hyperpolarization-activated current (if) in rabbit sino-atrial node myocytes. J Physiol. 405:493–510.

Doan, T.N., and Kunze, D.L. 1999. Contribution of the hyperpolarization-activated current to the resting membrane potential of rat nodose sensory neurons. J Physiol. 514:125–138.

Domyancic, A. V, and Morilak, D.A. 1997. Distribution of alpha1A adrenergic receptor mRNA in the rat brain visualized by in situ hybridization. J Comp Neurol. 386:358–378.

Doyle, D.A. 1998. The Structure of the Potassium Channel: Molecular Basis of K+ Conduction and Selectivity. Science (80-). 280:69–77.

Edman, A., Gestrelius, S., and Grampp, W. 1987. Current activation by membrane hyperpolarization in the slowly adapting lobster stretch receptor neurone. J Physiol. 384:671–690.

Elsaesser, R., Montani, G., Tirindelli, R., and Paysan, J. 2005. Phosphatidyl-inositide signalling proteins in a novel class of sensory cells in the mammalian olfactory epithelium. Eur J Neurosci. 21:2692–2700.

Ennis, M., Zhou, F.M., Ciombor, K.J., Aroniadou-Anderjaska, V., Hayar, A., Borrelli, E., Zimmer, L.A., Margolis, F., and Shipley, M.T. 2001. Dopamine D2 receptor-mediated presynaptic inhibition of olfactory nerve terminals. J Neurophysiol. 86:2986–2997.

Ennis, M., Zimmer, L.A., and Shipley, M.T. 1996. Olfactory nerve stimulation activates rat mitral cells via NMDA and non-NMDA receptors in vitro. Neuroreport. 7:989–992.

Faas, G.C., Schwaller, B., Vergara, J.L., and Mody, I. 2007. Resolving the fast kinetics of cooperative binding: Ca2+ buffering by calretinin. PLoS Biol. 5:e311.

Fain, G.L., Quandt, F.N., Bastian, B.L., and Gerschenfeld, H.M. 1978. Contribution of a caesium-sensitive conductance increase to the rod photoresponse. Nature. 272:466–469.

Farès, N., Bois, P., Lenfant, J., and Potreau, D. 1998. Characterization of a hyperpolarization-activated current in dedifferentiated adult rat ventricular cells in primary culture. J Physiol. 506 (Pt 1:73–82.

Feigenspan, A., Gustincich, S., Bean, B.P., and Raviola, E. 1998. Spontaneous activity of solitary dopaminergic cells of the retina. J Neurosci. 18:6776–6789.

Firestein, S. 2001. How the olfactory system makes sense of scents. Nature. 413:211–218.

Flynn, G.E., Black, K.D., Islas, L.D., Sankaran, B., and Zagotta, W.N. 2007. Structure and Rearrangements in the Carboxy-Terminal Region of SpIH Channels. Structure. 15:671–682.

Frace, A.M., Maruoka, F., and Noma, A. 1992. External K+ increases Na+ conductance of the hyperpolarization-activated current in rabbit cardiac pacemaker cells. Pflugers Arch. 421:94–96.

Freund, T.F., and Buzsáki, G. 1996. Interneurons of the hippocampus. Hippocampus. 6:347–470.

Fried, H.U., Kaupp, U.B., and Müller, F. 2010. Hyperpolarization-activated and cyclic nucleotide-gated channels are differentially expressed in juxtaglomerular cells in the olfactory bulb of mice. Cell Tissue Res. 339:463–479.

Gall, D., Roussel, C., Susa, I., D'Angelo, E., Rossi, P., Bearzatto, B., Galas, M.C., Blum, D., Schurmans, S., and Schiffmann, S.N. 2003. Altered neuronal excitability in cerebellar granule cells of mice lacking calretinin. J Neurosci. 23:9320–9327.

Garratt, J.C., Alreja, M., and Aghajanian, G.K. 1993. LSD has high efficacy relative to serotonin in enhancing the cationic current I(h): Intracellular studies in rat facial motoneurons. Synapse. 13:123–134.

Gauss, R., Seifert, R., and Kaupp, U.B. 1998. Molecular identification of a hyperpolarization-activated channel in sea urchin sperm. Nature. 393:583–7.

Gonchar, Y., and Burkhalter, A. 1999. Connectivity of GABAergic calretinin-immunoreactive neurons in rat primary visual cortex. Cereb Cortex. 9:683–96.

Gong, S., Zheng, C., Doughty, M.L., Losos, K., Didkovsky, N., Schambra, U.B., Nowak, N.J., Joyner, A., Leblanc, G., Hatten, M.E., et al. 2003. A gene expression atlas of the central nervous system based on bacterial artificial chromosomes. Nature. 425:917–925.

Grace, A.A., and Onn, S.P. 1989. Morphology and electrophysiological properties of immunocytochemically identified rat dopamine neurons recorded in vitro. J Neurosci. 9:3463–3481.

Gustincich, S., Feigenspan, A., Wu, D.K., Koopman, L.J., and Raviola, E. 1997. Control of dopamine release in the retina: A transgenic approach to neural networks. Neuron. 18:723–736.

Hainsworth, A.H., Roper, J., Kapoor, R., and Ashcroft, F.M. 1991. Identification and electrophysiology of isolated pars compacta neurons from guinea-pig substantia nigra. Neuroscience. 43:81–93.

Halász, N. 1990. The vertebrate olfactory system: chemical neuroanatomy, function and development. -.

Halliwell, J. V, and Adams, P.R. 1982. Voltage-clamp analysis of muscarinic excitation in hippocampal neurons. Brain Res. 250:71–92.

Hamill, O.P., Marty, A., Neher, E., Sakmann, B., and Sigworth, F.J. 1981. Improved patch-clamp techniques for high-resolution current recording from cells and cell-free membrane patches. Pflügers Arch Eur J Physiol. 391:85–100.

Hart, G. 1983. The kinetics and temperature dependence of the pace-maker current if in sheep Purkinje fibres. J Physiol. 337:401–416.

He, C., Chen, F., Li, B., and Hu, Z. 2014. Neurophysiology of HCN channels: from cellular functions to multiple regulations. Prog Neurobiol. 112:1–23.

Hibino, H., Inanobe, A., Furutani, K., Murakami, S., Findlay, I., and Kurachi, Y. 2010. Inwardly rectifying potassium channels: their structure, function, and physiological roles. Physiol Rev. 90:291–366.

Hille, B. 1992. Ionic channels of excitable membranes. Sunderland, MA, USA: Sinauer Associates Inc.

Hinds, J.W. 1968a. Autoradiographic study of histogenesis in the mouse olfactory bulb. I. Time of origin of neurons and neuroglia. J Comp Neurol. 134:287–304.

Hinds, J.W. 1968b. Autoradiographic study of histogenesis in the mouse olfactory bulb. II. Cell proliferation and migration. J Comp Neurol. 134:305–322.

Ho, W.-K., Brown, H.F., and Noble, D. 1994. High selectivity of the if channel to Na+ and K+ in rabbit isolated sinoatrial node cells. Pflügers Arch J Physiol Arch Eur J Physiol. 426:68–74.

Hodgkin, A.L., and Huxley, A.F. 1952. A Quantitative Description of Membrane Current and its Application to Conduction and Excitation in Nerves. J Physiol. 117:500–544.

Hsia, A.Y., Vincent, J.D., and Lledo, P.M. 1999. Dopamine depresses synaptic inputs into the olfactory bulb. J Neurophysiol. 82:1082–1085.

Huang, Z., Lujan, R., Kadurin, I., Uebele, V.N., Renger, J.J., Dolphin, A.C., and Shah, M.M. 2011. Presynaptic HCN1 channels regulate Cav3.2 activity and neurotransmission at select cortical synapses. Nat Neurosci. 14:478–486.

Huberman, A.D., Manu, M., Koch, S.M., Susman, M.W., Lutz, A.B., Ullian, E.M., Baccus, S.A., and Barres, B.A. 2008. Architecture and activity-mediated refinement of axonal projections from a mosaic of genetically identified retinal ganglion cells. Neuron. 59:425–38.

Inyushin, M.U., Arencibia-Albite, F., Vázquez-Torres, R., Vélez-Hernández, M.E., and Jiménez-Rivera, C.A. 2010. Alpha-2 noradrenergic receptor activation inhibits the hyperpolarization-activated cation current (Ih) in neurons of the ventral tegmental area. Neuroscience. 167:287–297.

Ishii, T.M., Takano, M., Xie, L.-H.H., Noma, A., and Ohmori, H. 1999. Molecular characterization of the hyperpolarization-activated cation channel in rabbit heart sinoatrial node. J Biol Chem. 274:12835–12839.

Jackowski, A., Parnavelas, J.G., Lieberman, A.R., and Jackwski, A. 1978. The reciprocal synapse in the external plexiform layer of the mammalian olfactory bulb. Brain Res. 195:17–28.

Jacobowitz, D.M., and Winsky, L. 1991. Immunocytochemical localization of calretinin in the forebrain of the rat. J Comp Neurol. 304:198–218.

Jahnsen, H., Llinas, R., and Llinás, R. 1984. Ionic basis for the electro-responsiveness and oscillatory properties of guinea-pig thalamic neurones in vitro. J Physiol. 349:227–247.

Joh, T.H., Geghman, C., and Reis, D. 1973. Immunochemical demonstration of increased accumulation of tyrosine hydroxylase protein in sympathetic ganglia and adrenal medulla elicited by reserpine. Proc Natl Acad Sci U S A. 70:2767–2771.

Jung, S., Bullis, J.B., Lau, I.H., Jones, T.D., Warner, L.N., and Poolos, N.P. 2010. Downregulation of dendritic HCN channel gating in epilepsy is mediated by altered phosphorylation signaling. J Neurosci. 30:6678–88.

Kamondi, A., and Reiner, P.B. 1991. Hyperpolarization-activated inward current in histaminergic tuberomammillary neurons of the rat hypothalamus. J Neurophysiol. 66:1902–1911.

Kasowski, H.J., Kim, H., and Greer, C.A. 1999. Compartmental organization of the olfactory bulb glomerulus. J Comp Neurol. 407:261–274.

Kiyokage, E., Pan, Y.-Z., Shao, Z., Kobayashi, K., Szabo, G., Yanagawa, Y., Obata, K., Okano, H., Toida, K., Puche, A.C., et al. 2010. Molecular identity of periglomerular and short axon cells. J Neurosci. 30:1185–1196.

Kobinger, W., Lillie, C., and Pichler, L. 1979. N-Allyl-derivative of clonidine, a substance with specific bradycardic action at a cardiac site. Naunyn Schmiedebergs Arch Pharmacol. 306:255–262.

Kocsis, B., and Li, S. 2004. In vivo contribution of h-channels in the septal pacemaker to theta rhythm generation. Eur J Neurosci. 20:2149–2158.

Kopp-Scheinpflug, C., Tozer, A.J.B., Robinson, S.W., Tempel, B.L., Hennig, M.H., and Forsythe, I.D. 2011. The sound of silence: Ionic mechanisms encoding sound termination. Neuron. 71:911–925.

Kosaka, K., and Kosaka, T. 2005. Synaptic organization of the glomerulus in the main olfactory bulb: compartments of the glomerulus and heterogeneity of the periglomerular cells. Anat Sci Int / Japanese Assoc Anat. 80:80–90.

Kosaka, K., and Kosaka, T. 2007. Chemical properties of type 1 and type 2 periglomerular cells in the mouse olfactory bulb are different from those in the rat olfactory bulb. Brain Res. 1167:42–55.

Kosaka, K., Toida, K., Aika, Y., and Kosaka, T. 1998. How simple is the organization of the olfactory glomerulus?: The heterogeneity of so-called periglomerular cells. Neurosci Res. 30:101–110.

Kosaka, K., Toida, K., Margolis, F.L., and Kosaka, T. 1997. Chemically defined neuron groups and their subpopulations in the glomerular layer of the rat main olfactory bulb .2. Prominent

differences in the intraglomerular dendritic arborization and their relationship to olfactory nerve terminals. Neuroscience. 76:775–786.

Kosaka, T., and Kosaka, K. 2008. Tyrosine hydroxylase-positive GABAergic juxtaglomerular neurons are the main source of the interglomerular connections in the mouse main olfactory bulb. Neurosci Res. 60:349–354.

Kosaka, T., and Kosaka, K. 2009. Olfactory Bulb Anatomy. In: Encyclopedia of Neuroscience. Oxford: Academic Press. pp. 59–69.

Kosaka, T., and Kosaka, K. 2011. “Interneurons” in the olfactory bulb revisited. Neurosci Res. 69:93–9.

Krieger, J., Strobel, J., Vogl, A., Hanke, W., and Breer, H. 1999. Identification of a cyclic nucleotide- and voltage-activated ion channel from insect antennae. Insect Biochem Mol Biol. 29:255–267.

Krosnowski, K., Ashby, S., Sathyanesan, A., Luo, W., Ogura, T., and Lin, W. 2012. Diverse populations of intrinsic cholinergic interneurons in the mouse olfactory bulb. Neuroscience. 213:161–178.

Larkman, P.M., and Kelly, J.S. 1997. Modulation of I(H) by 5-HT in neonatal rat motoneurones in vitro: Mediation through a phosphorylation independent action of cAMP. Neuropharmacology. 36:721–733.

Lee, S.C., and Ishida, A.T. 2007. Ih without kir in adult rat retinal ganglion cells. JNeurophysiol. 97:3790–3799.

Liberles, S.D., and Buck, L.B. 2006. A second class of chemosensory receptors in the olfactory epithelium. Nature. 442:645–650.

Lin, W., Margolskee, R., Donnert, G., Hell, S.W., and Restrepo, D. 2007. Olfactory neurons expressing transient receptor potential channel M5 (TRPM5) are involved in sensing semiochemicals. Proc Natl Acad Sci U S A. 104:2471–2476.

Linster, C., Nai, Q., and Ennis, M. 2011. Nonlinear effects of noradrenergic modulation of olfactory bulb function in adult rodents. J Neurophysiol. 105:1432–1443.

Lledo, P.-M.M., Merkle, F.T., Alvarez-Buylla, A., and varez-Buylla, A. 2008. Origin and function of olfactory bulb interneuron diversity. Trends Neurosci. 31:392–400.

Ludwig, A., Budde, T., Stieber, J., Moosmang, S., Wahl, C., Holthoff, K., Langebartels, A., Wotjak, C., Munsch, T., Zong, X., et al. 2003. Absence epilepsy and sinus dysrhythmia in mice lacking the pacemaker channel HCN2. EMBO J. 22:216–224.

Ludwig, A., Zong, X., Jeglitsch, M., Hofmann, F., and Biel, M. 1998. A family of hyperpolarization-activated mammalian cation channels. Nature. 393:587–591.

Lupica, C.R., Bell, J.A., Hoffman, A.F., and Watson, P.L. 2001. Contribution of the hyperpolarization-activated current (I(h)) to membrane potential and GABA release in hippocampal interneurons. J Neurophysiol. 86:261–8.

Maccaferri, G., Mangoni, M., Lazzari, A., and DiFrancesco, D. 1993. Properties of the hyperpolarization-activated current in rat hippocampal CA1 pyramidal cells. J Neurophysiol. 69:2129–36.

Maccaferri, G., and McBain, C.J. 1996. The hyperpolarization-activated current (Ih) and its contribution to pacemaker activity in rat CA1 hippocampal stratum oriens-alveus interneurones. J Physiol. 497 (Pt 1:119–130.

Macri, V., and Accili, E.A. 2004. Structural Elements of Instantaneous and Slow Gating in Hyperpolarization-activated Cyclic Nucleotide-gated Channels. J Biol Chem. 279:16832–16846.

Macri, V., Angoli, D., and Accili, E.A. 2012. Architecture of the HCN selectivity filter and control of cation permeation. Sci Rep. 2:894.

Macrides, F., and Schneider, S.P. 1982. Laminar organization of mitral and tufted cells in the main olfactory bulb of the adult hamster. J Comp Neurol. 208:419–430.

Macrides, F., Schoenfeld, T.A., Marchand, J.E., and Clancy, A.N. 1985. Evidence for morphologically, neurochemically and functionally heterogeneous classes of mitral and tufted cells in the olfactory bulb. Chem Senses. 10:175–202.

Magee, J.C. 1998. Dendritic hyperpolarization-activated currents modify the integrative properties of hippocampal CA1 pyramidal neurons. J Neurosci. 18:7613–7624.

Magee, J.C. 1999. Dendritic Ih normalizes temporal summation in hippocampal CA1 neurons. Nat Neurosci. 2:508–514.

Maher, B.J., and Westbrook, G.L. 2008. Co-transmission of dopamine and GABA in periglomerular cells. J Neurophysiol. 99:1559–1564.

Männikkö, R., Elinder, F., and Larsson, H.P. 2002. Voltage-sensing mechanism is conserved among ion channels gated by opposite voltages. Nature. 419:837–841.

Marchis, S. De, Bovetti, S., Carletti, B., Hsieh, Y.-C., Garzotto, D., Peretto, P., Fasolo, A., Puche, A.C., and Rossi, F. 2007. Generation of distinct types of periglomerular olfactory bulb interneurons during development and in adult mice: implication for intrinsic properties of the subventricular zone progenitor population. J Neurosci. 27:657–664.

Marx, T., Gisselmann, G., Störtkuhl, K.F., Hovemann, B.T., and Hatt, H. 1999. Molecular cloning of a putative voltage- and cyclic nucleotide-gated ion channel present in the antennae and eyes of Drosophila melanogaster. Invert Neurosci. 4:55–63.

Matsushita, N., Okada, H., Yasoshima, Y., Takahashi, K., Kiuchi, K., and Kobayashi, K. 2002. Dynamics of tyrosine hydroxylase promoter activity during midbrain dopaminergic neuron development. J Neurochem. 82:295–304.

McCleskey, E.W., Fox, A.P., Feldman, D., and Tsien, R.W. 1986. Different types of calcium channels. J Exp Biol. 124:177–190.

McCormick, D.A., and Pape, H.C. 1990a. Noradrenergic and serotonergic modulation of a hyperpolarization-activated cation current in thalamic relay neurones. J Physiol. 431:319–342.

McCormick, D.A., and Pape, H.C. 1990b. Properties of a hyperpolarization-activated cation current and its role in rhythmic oscillation in thalamic relay neurones. J Physiol. 431:291–318.

McLean, J.H., Shipley, M.T., Nickell, W.T., Aston-Jones, G., and Reyher, C.K. 1989. Chemoanatomical organization of the noradrenergic input from locus coeruleus to the olfactory bulb of the adult rat. J Comp Neurol. 285:339–349.

Mercuri, N.B., Bonci, A., Calabresi, P., Stefani, A., and Bernardi, G. 1995. Properties of the hyperpolarization-activated cation current I(h) in rat midbrain dopaminergic neurons. Eur J Neurosci. 7:462–469.

Miettinen, R., Gulyas, A.I., Baimbridge, K.G., Jacobowitz, D.M., and Freund, T.F. 1992. Calretinin is present in non-pyramidal cells of the rat hippocampus-- II. Co-existence with other calcium binding proteins and GABA. Neuroscience. 48:29–43.

Mistrik, P., Mader, R., Michalakis, S., Weidinger, M., Pfeifer, A., and Biel, M. 2005. The murine HCN3 gene encodes a hyperpolarization-activated cation channel with slow kinetics and unique response to cyclic nucleotides. J Biol Chem. 280:27056–27061.

Mombaerts, P. 1996. Targeting olfaction. Curr Opin Neurobiol. 6:481–486.

Mombaerts, P. 1999. Seven-transmembrane proteins as odorant and chemosensory receptors. Science. 286:707–711.

Mombaerts, P. 2004. Genes and ligands for odorant, vomeronasal and taste receptors. Nat Rev Neurosci. 5:263–278.

Monteggia, L.M., Eisch, A.J., Tang, M.D., Kaczmarek, L.K., and Nestler, E.J. 2000. Cloning and localization of the hyperpolarization-activated cyclic nucleotide-gated channel family in rat brain. Mol Brain Res. 81:129–139.

Moosmang, S., Biel, M., Hofmann, F., and Ludwig, A. 1999. Differential distribution of four hyperpolarization-activated cation channels in mouse brain. Biol Chem. 380:975–980.

Mori, K., Kishi, K., and Ojima, H. 1983. Distribution of dendrites of mitral, displaced mitral, tufted and granule cells in the rabbit olfactory bulb. JCompNeurol. 219:339–355.

Mori, K., and Sakano, H. 2011. How is the olfactory map formed and interpreted in the mammalian brain?. Annu Rev Neurosci. 34:467–499.

Much, B., Wahl-Schott, C., Zong, X., Schneider, A., Baumann, L., Moosmang, S., Ludwig, A., and Biel, M. 2003. Role of subunit heteromerization and N-linked glycosylation in the formation of functional hyperpolarization-activated cyclic nucleotide-gated channels. J Biol Chem. 278:43781–6.

Nagatsu, T., Levitt, M., and Udenfriend, S. 1964. Tyrosine hydroxylase. The initial step in norepinephrine biosynthesis. J Biol Chem. 239:2910–2917.

Nagayama, S., Homma, R., and Imamura, F. 2014. Neuronal organization of olfactory bulb circuits. Front Neural Circuits. 8:98.

Nagayama, S., Takahashi, Y.K., Yoshihara, Y., and Mori, K. 2004. Mitral and tufted cells differ in the decoding manner of odor maps in the rat olfactory bulb. J Neurophysiol. 91:2532–2540.

Neher, E., and Sakmann, B. 1976. Single-channel currents recorded from membrane of denervated frog muscle fibres. Nature. 260:799–802.

Neuhoff, H., Neu, A., Liss, B., and Roeper, J. 2002. I(h) channels contribute to the different functional properties of identified dopaminergic subpopulations in the midbrain. J Neurosci. 22:1290–1302.

Niimura, Y., and Nei, M. 2003. Evolution of olfactory receptor genes in the human genome. Proc Natl Acad Sci U S A. 100:12235–12240.

Niimura, Y., and Nei, M. 2005. Comparative evolutionary analysis of olfactory receptor gene clusters between humans and mice. Gene. 346:13–21.

Niimura, Y., and Nei, M. 2007. Extensive gains and losses of olfactory receptor genes in mammalian evolution. PLoS One. 2:e708.

Nolan, M.F., Dudman, J.T., Dodson, P.D., and Santoro, B. 2007. HCN1 channels control resting and active integrative properties of stellate cells from layer II of the entorhinal cortex. J Neurosci. 27:12440–12451.

Noma, A., and Irisawa, H. 1976. Membrane currents in the rabbit sinoatrial node cell as studied by the double microelectrode method. Pflugers Arch. 364:45–52.

Notomi, T., and Shigemoto, R. 2004. Immunohistochemical Localization of Ih Channel Subunits, HCN1-4, in the Rat Brain. J Comp Neurol. 471:241–276.

Orona, E., Rainer, E.C., and Scott, J.W. 1984. Dendritic and axonal organisation of mitral and tufted cells in the rat olfactory bulb. JCompNeurol. 226:346–356.

Palczewska, M., Groves, P., Batta, G., Heise, B., and Kuźnicki, J. 2003. Calretinin and calbindin D28k have different domain organizations. Protein Sci. 12:180–184.

Panzanelli, P., Fritschy, J.M., Yanagawa, Y., Obata, K., and Sassoè-Pognetto, M. 2007. GABAergic phenotype of periglomerular cells in the rodent olfactory bulb. J Comp Neurol. 502:990–1002.

Pape, H.C. 1996. Queer current and pacemaker: the hyperpolarization-activated cation current in neurons. AnnuRevPhysiol. 58:299–327.

Pape, H.C., and McCormick, D.A. 1989. Noradrenaline and serotonin selectively modulate thalamic burst firing by enhancing a hyperpolarization-activated cation current. Nature. 340:715–718.

Parrish-Aungst, S., Shipley, M.T., Erdelyi, F., Szabo, G., and Puche, A.C. 2007. Quantitative analysis of neuronal diversity in the mouse olfactory bulb. J Comp Neurol. 501:825–836.

Pena, F., Amuzescu, B., Neaga, E., and Flonta, M.L. 2006. Thermodynamic properties of hyperpolarization-activated current (Ih) in a subgroup of primary sensory neurons. In: Experimental Brain Research. pp. 282–290.

Pignatelli, A., Ackman, J.B., Vigetti, D., Beltrami, A.P., Zucchini, S., and Belluzzi, O. 2009. A potential reservoir of immature dopaminergic replacement neurons in the adult mammalian olfactory bulb. Pflugers Arch Eur J Physiol. 457:899–915.

Pignatelli, A., Borin, M., Fogli Iseppe, A., Gambardella, C., and Belluzzi, O. 2013. The h-current in periglomerular dopaminergic neurons of the mouse olfactory bulb. PLoS One. 8:e56571.

Pignatelli, A., Kobayashi, K., Okano, H., and Belluzzi, O. 2005. Functional properties of dopaminergic neurones in the mouse olfactory bulb. J Physiol. 564:501–514.

Pinching, A.J., and Powell, T.P. 1971a. The neuron types of the glomerular layer of the olfactory bulb. J Cell Sci. 9:305–345.

Pinching, A.J., and Powell, T.P. 1971b. The neuropil of the glomeruli of the olfactory bulb. J Cell Sci. 9:347–377.

Pinching, A.J., and Powell, T.P. 1971c. The neuropil of the periglomerular region of the olfactory bulb. J Cell Sci. 9:379–409.

Price, J.L., and Powell, T.P. 1970a. The mitral and short axon cells of the olfactory bulb. J Cell Sci. 7:631–651.

Price, J.L., and Powell, T.P. 1970b. The morphology of the granule cells of the olfactory bulb. J Cell Sci. 7:91–123.

Price, J.L., and Powell, T.P. 1970c. The synaptology of the granule cells of the olfactory bulb. J Cell Sci. 7:125–155.

Proenza, C., Angoli, D., Agranovich, E., Macri, V., and Accili, E.A. 2002. Pacemaker channels produce an instantaneous current. J Biol Chem. 277:5101–5109.

Prole, D.L., and Yellen, G. 2006. Reversal of HCN channel voltage dependence via bridging of the S4-S5 linker and Post-S6. J Gen Physiol. 128:273–282.

Puopolo, M., Bean, B.P., and Raviola, E. 2005. Spontaneous activity of isolated dopaminergic periglomerular cells of the main olfactory bulb. J Neurophysiol. 94:3618–3627.

Purves, D. 2004. Neuroscience Third Edition.

Ramon y Cajal, S. 1890. Origen y terminacion de las fibras nerviosas olfatorias. 1–21.

Ramon y Cajal, S. 1901. Textura del lóbulo olfativo accesorio. In: Trab Lab Invest Biol. pp. 141–149.

Ramon y Cajal, S. 1911. Histologie du Sistème Nerveux de l'Homme et des Vertébrés. -.

Resibois, A., and Rogers, J.H. 1992. Calretinin in rat brain: An immunohistochemical study. Neuroscience. 46:101–134.

Robinson, R.B., and Siegelbaum, S.A. 2003. Hyperpolarization-activated cation currents: from molecules to physiological function. Annu Rev Physiol. 65:453–80.

Rodrigues, A.R.A., and Oertel, D. 2006. Hyperpolarization-activated currents regulate excitability in stellate cells of the mammalian ventral cochlear nucleus. J Neurophysiol. 95:76–87.

Rodríguez, B.M., Sigg, D., and Bezanilla, F. 1998. Voltage gating of Shaker K+ channels. The effect of temperature on ionic and gating currents. J Gen Physiol. 112:223–242.

Rogers, J.H., and Résibois, A. 1992. Calretinin and calbindin-D28k in rat brain: patterns of partial co-localization. Neuroscience. 51:843–865.

Ronnett, G. V, and Moon, C. 2002. G proteins and olfactory signal transduction. Annu Rev Physiol. 64:189–222.

Saino-Saito, S., Sasaki, H., Volpe, B.T., Kobayashi, K., Berlin, R., and Baker, H. 2004. Differentiation of the dopaminergic phenotype in the olfactory system of neonatal and adult mice. J Comp Neurol. 479:389–398.

Sakano, H. 2010. Neural map formation in the mouse olfactory system. Neuron. 67:530–42.

Sánchez-Alonso, J.L., Halliwell, J. V, and Colino, A. 2008. ZD 7288 inhibits T-type calcium current in rat hippocampal pyramidal cells. Neurosci Lett. 439:275–280.

Santoro, B., Chen, S., Luthi, A., Pavlidis, P., Shumyatsky, G.P., Tibbs, G.R., and Siegelbaum, S.A. 2000. Molecular and functional heterogeneity of hyperpolarization-activated pacemaker channels in the mouse CNS. J Neurosci. 20:5264–5275.

Santoro, B., Liu, D.T., Yao, H., Bartsch, D., Kandel, E.R., Siegelbaum, S.A., and Tibbs, G.R. 1998. Identification of a gene encoding a hyperpolarization-activated pacemaker channel of brain. Cell. 93:717–729.

Sawamoto, K., Nakao, N., Kobayashi, K., Matsushita, N., Takahashi, H., Kakishita, K., Yamamoto, A., Yoshizaki, T., Terashima, T., Murakami, F., et al. 2001. Visualization, direct isolation, and transplantation of midbrain dopaminergic neurons. Proc Natl Acad Sci U S A. 98:6423–6428.

Schild, D., and Restrepo, D. 1998. Transduction mechanisms in vertebrate olfactory receptor cells. PhysiolRev. 78:429–466.

Schneider, S.P., and Macrides, F. 1978. Laminar distributions of interneurons in the main olfactory bulb of the adult hamster. Brain Res Bull. 3:73–82.

Schoenfeld, T.A., Marchand, J.E., and Macrides, F. 1985. Topographic organization of tufted cell axonal projections in the hamster main olfactory bulb: an intrabulbar associational system. J Comp Neurol. 235:503–518.

Schurmans, S., Schiffmann, S.N., Gurden, H., Lemaire, M., Lipp, H.-P., Schwam, V., Pochet, R., Imperato, A., Bohme, G.A., and Parmentier, M. 1997. Impaired long-term potentiation induction in dentate gyrus of calretinin-deficient mice. Proc Natl Acad Sci. 94:10415–10420.

Schwaller, B. 2014. Calretinin: from a “simple” Ca(2+) buffer to a multifunctional protein implicated in many biological processes. Front Neuroanat. 8:3.

Schwaller, B., Durussel, I., Jermann, D., Herrmann, B., and Cox, J.A. 1997. Comparison of the Ca2+-binding properties of human recombinant calretinin-22k and calretinin. J Biol Chem. 272:29663–29671.

Seamon, K.B., and Daly, J.W. 1981. Forskolin: a unique diterpene activator of cyclic AMP-generating systems. J Cyclic Nucleotide Res. 7:201–224.

Shealy, R.T., Murphy, A.D., Ramarathnam, R., Jakobsson, E., and Subramaniam, S. 2003. Sequence-function analysis of the K+-selective family of ion channels using a comprehensive alignment and the KcsA channel structure. Biophys J. 84:2929–42.

Shin, K.S., Rothberg, B.S., and Yellen, G. 2001. Blocker state dependence and trapping in hyperpolarization-activated cation channels: evidence for an intracellular activation gate. J Gen Physiol. 117:91–101.

Shin, M., Brager, D., Jaramillo, T.C., Johnston, D., and Chetkovich, D.M. 2008. Mislocalization of h channel subunits underlies h channelopathy in temporal lobe epilepsy. Neurobiol Dis. 32:26–36.

Shipley, M.T., and Ennis, M. 1996. Functional organization of olfactory system. J Neurobiol. 30:123–176.

Solomon, J.S., and Nerbonne, J.M. 1993. Hyperpolarization-activated currents in isolated superior colliculus-projecting neurons from rat visual cortex. J Physiol. 462:393–420.

Soltesz, I., Lightowler, S., Leresche, N., Jassik-Gerschenfeld, D., Pollard, C.E., and Crunelli, V. 1991. Two inward currents and the transformation of low-frequency oscillations of rat and cat thalamocortical cells. J Physiol. 441:175–97.

Stevens, J., and Rogers, J.H. 1997. Chick calretinin: purification, composition, and metal binding activity of native and recombinant forms. Protein Expr Purif. 9:171–181.

Takeuchi, H., and Sakano, H. 2014. Neural map formation in the mouse olfactory system. Cell Mol Life Sci. 71:3049–3057.

Thollon, C., Bedut, S., Villeneuve, N., Cogé, F., Piffard, L., Guillaumin, J.-P., Brunel-Jacquemin, C., Chomarat, P., Boutin, J.-A., Peglion, J.-L., et al. 2007. Use-dependent inhibition of hHCN4 by ivabradine and relationship with reduction in pacemaker activity. Br J Pharmacol. 150:37–46.

Thollon, C., Cambarrat, C., Vian, J., Prost, J.F., Peglion, J.L., and Vilaine, J.P. 1994. Electrophysiological effects of S 16257, a novel sino-atrial node modulator, on rabbit and guinea-pig cardiac preparations: comparison with UL-FS 49. Br J Pharmacol. 112:37–42.

Traunecker, W., and Walland, A. 1980. Haemodynamic and electrophysiologic actions of alinidine in the dog. Arch Int Pharmacodyn Ther. 244:58–72.

Travagli, R.A., and Gillis, R.A. 1994. Hyperpolarization-activated currents, IH and IKIR, in rat dorsal motor nucleus of the vagus neurons in vitro. J Neurophysiol. 71:1308–1317.

Ulens, C., and Tytgat, J. 2001. Functional heteromerization of HCN1 and HCN2 pacemaker channels. J Biol Chem. 276:6069–72.

Ulrich, D. 2002. Dendritic resonance in rat neocortical pyramidal cells. J Neurophysiol. 87:2753–2759.

Voets, T., Droogmans, G., Wissenbach, U., Janssens, A., Flockerzi, V., and Nilius, B. 2004. The principle of temperature-dependent gating in cold- and heat-sensitive TRP channels. Nature. 430:748–754.

Wahl-Schott, C., and Biel, M. 2009. HCN channels: structure, cellular regulation and physiological function. Cell Mol Life Sci. 66:470–94.

Wainger, B.J., DeGennaro, M., Santoro, B., Siegelbaum, S.A., and Tibbs, G.R. 2001. Molecular mechanism of cAMP modulation of HCN pacemaker channels. Nature. 411:805–810.

Whitaker, G.M., Angoli, D., Nazzari, H., Shigemoto, R., and Accili, E.A. 2007. HCN2 and HCN4 isoforms self-assemble and co-assemble with equal preference to form functional pacemaker channels. J Biol Chem. 282:22900–9.

Whitman, M.C., and Greer, C.A. 2007. Adult-generated neurons exhibit diverse developmental fates. Dev Neurobiol. 67:1079–1093.

Wicks, N.L., Wong, T., Sun, J., Madden, Z., and Young, E.C. 2011. Cytoplasmic cAMP-sensing domain of hyperpolarization-activated cation (HCN) channels uses two structurally distinct mechanisms to regulate voltage gating. Proc Natl Acad Sci U S A. 108:609–614.

Williams, S.R., Christensen, S.R., Stuart, G.J., Häusser, M., and Hausser, M. 2002. Membrane potential bistability is controlled by the hyperpolarization-activated current I(H) in rat cerebellar Purkinje neurons in vitro. JPhysiol. 539:469–483.

Williams, S.R., and Stuart, G.J. 2000. Site independence of EPSP time course is mediated by dendritic I(h) in neocortical pyramidal neurons. J Neurophysiol. 83:3177–3182.

Winzer-Serhan, U.H., Raymon, H.K., Broide, R.S., Chen, Y., and Leslie, F.M. 1997. Expression of alpha 2 adrenoceptors during rat brain development--I. Alpha 2A messenger RNA expression. Neuroscience. 76:241–260.

Wollmuth, L.P., and Hille, B. 1992. Ionic selectivity of Ih channels of rod photoreceptors in tiger salamanders. J Gen Physiol. 100:749–765.

Yagi, J., and Sumino, R. 1998. Inhibition of a hyperpolarization-activated current by clonidine in rat dorsal root ganglion neurons. J Neurophysiol. 80:1094–1104.

Yanagida, H., Inoue, R., Tanaka, M., and Ito, Y. 2000. Temperature-sensitive gating of cation current in guinea pig ileal muscle activated by hyperpolarization. Am J Physiol Cell Physiol. 278:C40–C48.

Yanagihara, K., and Irisawa, H. 1980. Inward current activated during hyperpolarization in the rabbit sinoatrial node cell. Pflügers Arch J Physiol. 385:11–19.

Young, J.M., Friedman, C., Williams, E.M., Ross, J.A., Tonnes-Priddy, L., and Trask, B.J. 2002. Different evolutionary processes shaped the mouse and human olfactory receptor gene families. Hum Mol Genet. 11:535–546.

Young, W.S., and Kuhar, M.J. 1980. Noradrenergic alpha 1 and alpha 2 receptors: light microscopic autoradiographic localization. Proc Natl Acad Sci U S A. 77:1696–1700.

Yu, C.R., Power, J., Barnea, G., O'Donnell, S., Brown, H.E. V, Osborne, J., Axel, R., and Gogos, J.A. 2004a. Spontaneous neural activity is required for the establishment and maintenance of the olfactory sensory map. Neuron. 42:553–566.

Yu, F.H., and Catterall, W.A. 2003. Overview of the voltage-gated sodium channel family. Genome Biol. 4:207.

Yu, F.H., and Catterall, W.A. 2004. The VGL-chanome: a protein superfamily specialized for electrical signaling and ionic homeostasis. Sci STKE. 2004:re15.

Yu, F.H., Yarov-Yarovoy, V., Gutman, G.A., and Catterall, W.A. 2005. Overview of molecular relationships in the voltage-gated ion channel superfamily. Pharmacol Rev. 57:387–395.

Yu, X., Chen, X.-W., Zhou, P., Yao, L., Liu, T., Zhang, B., Li, Y., Zheng, H., Zheng, L.-H., Zhang, C.X., et al. 2007. Calcium influx through If channels in rat ventricular myocytes. Am J Physiol Cell Physiol. 292:C1147–C1155.

Yu, X., Duan, K.-L., Shang, C.-F., Yu, H.-G., and Zhou, Z. 2004b. Calcium influx through hyperpolarization-activated cation channels (I(h) channels) contributes to activity-evoked neuronal secretion. Proc Natl Acad Sci U S A. 101:1051–1056.

Yung, W.H., Häusser, M.A., and Jack, J.J. 1991. Electrophysiology of dopaminergic and non-dopaminergic neurones of the guinea-pig substantia nigra pars compacta in vitro. J Physiol. 436:643–667.

Záborszky, L., Carlsen, J., Brashear, H.R., and Heimer, L. 1986. Cholinergic and GABAergic afferents to the olfactory bulb in the rat with special emphasis on the projection neurons in the nucleus of the horizontal limb of the diagonal band. J Comp Neurol. 243:488–509.

Zagotta, W.N., Olivier, N.B., Black, K.D., Young, E.C., Olson, R., and Gouaux, E. 2003. Structural basis for modulation and agonist specificity of HCN pacemaker channels. Nature. 425:200–205.

Zhang, X., and Firestein, S. 2002. The olfactory receptor gene superfamily of the mouse. Nat Neurosci. 5:124–133.

Zhou, L., and Siegelbaum, S.A. 2007. Gating of HCN channels by cyclic nucleotides: residue contacts that underlie ligand binding, selectivity, and efficacy. Structure. 15:655–670.

Zhou, L., and Siegelbaum, S.A. 2008. Pathway and endpoint free energy calculations for cyclic nucleotide binding to HCN channels. Biophys J. 94:L90–L92.